Doctoral Dissertation

Design of High-Throughput Experiments for Three-Way Catalysis

Thuy Phuong Nhat Tran

Supervisor: Assoc. Prof. Toshiaki Taniike

Graduate School of Advanced Science and Technology

Japan Advanced Institute of Science and Technology

[Materials Science]

September 2020

Referee-in-chief: Associate Professor Toshiaki Taniike
Japan Advanced Institute of Science and Technology

Referees: Associate Professor Yuki Nagao
Japan Advanced Institute of Science and Technology

Associate Professor Shun Nishimura
Japan Advanced Institute of Science and Technology

Associate Professor Dam Hieu Chi
Japan Advanced Institute of Science and Technology

Associate Professor Keisuke Takahashi
Hokkaido University

Design of High-Throughput Experiments for Three-Way Catalysis

Tran Phuong Nhat Thuy

1720416

To meet the increasingly stringent legislation for the gasoline engine exhaust emission, the exhaust aftertreatment systems need a breakthrough in the research and development of three-way catalysts (TWCs). While the catalysis society has made enormous efforts focusing on materials aspects for seeking the best or novel catalyst formulations, the development in methodology aspects, especially high-throughput (HTP) approaches, has just emerged to hold a great promise in that regard. Even though HTP catalyst screening techniques have become a mature and well-established tools in many catalytic systems, their applications in the TWCs have been hardly reported due to both technical and material constraints. The diversity and complexity of the catalytic system and reaction conditions necessitate a primary screening technique to quickly and broadly screen a huge parametric space. This catalytic system also requires highly accurate screening tools to distinguish the activity in a one-digit difference, signifying the essential of implementing secondary screening with higher precision. Therefore, the aim of this thesis is to design an integrated HTP screening protocol for the development of the TWCs.

The upstream of the hierarchical HTP workflow is the primary catalyst screening, which typically requires a fast and non-intrusive technique being capable of truly parallelized screening, preferably based on an optical method. For that, a novel chemiluminescence (CL) method was developed with special emphasis on high-temperature gaseous catalysis. In **Chapter 2**, the proof of concept of the CL method was formulated by thoroughly studying the CL behavior of the catalytic oxidation of CO and C_3H_6 by of O_2 and/or NO, which are the major processes in a catalytic converter, under both stoichiometric and non-stoichiometric conditions. In this stage, a CL instrument was developed based on the cooperation among a gas mixer, a custom-made CL analyzer using a photonmultiplier as a detector, and an on-line gas chromatography (GC) for simultaneous analysis of the effluent mixture from the CL reactor. The CL activity of these oxidation reactions was confirmed by temperature-ramping measurements, where the CL intensity showed an exponential behavior against the temperature irrespective of catalysts. Steady-state measurements demonstrated a linear relationship between the CL intensity and reactions rate regardless of stoichiometry, thus the CL intensity is a good measure of the reaction rate. The capability of the CL method in rapid catalyst screening was confirmed by a good linear correspondence between the CL intensity and the catalytic activity in C_3H_6 oxidation by O_2 for a series of Rh-based catalysts In **Chapter 3**, a CL imaging instrument was designed for achieving primary screening of the TWCs. The CL imaging instrument was equipped a reactor cell for gaseous catalysis and electron multiplying charged-coupled device camera for single photon detection in the form of images. The CL imaging technique exhibited the feasibility of a simple, straightforward, and rapid evaluation of catalytic activity based on a good correlation between the CL intensity and the C_3H_6 conversion. In addition, the one-to-one correspondence of the CL intensity obtained from the single and parallel measurement signified the great potential of the CL imaging technique in HTP catalyst screening. **Chapter 4** describes the HTP secondary screening of a simulated lead TWCs library based on a HTP screening instrument featured with fully-automated catalytic evaluation of 20 reactor channels in a wide range of conditions with the aid of a quadruple mass spectrometer. The instrument allowed generation of a large

process-relevant dataset at high accuracy, which is satisfactory for the secondary screening. Three-way catalytic reactions were conducted in 49 conditions over 20 catalyst samples, affording 980 data points in one operation. The obtained dataset is of high quality and accuracy, and the catalyst performance (in terms of light-off temperature and width of stoichiometric window) were found consistent with literature data. The reaction conditions cover a wide range of temperature and air/fuel equivalence ratio λ, allowing the multi-aspect comparison of the TWCs.

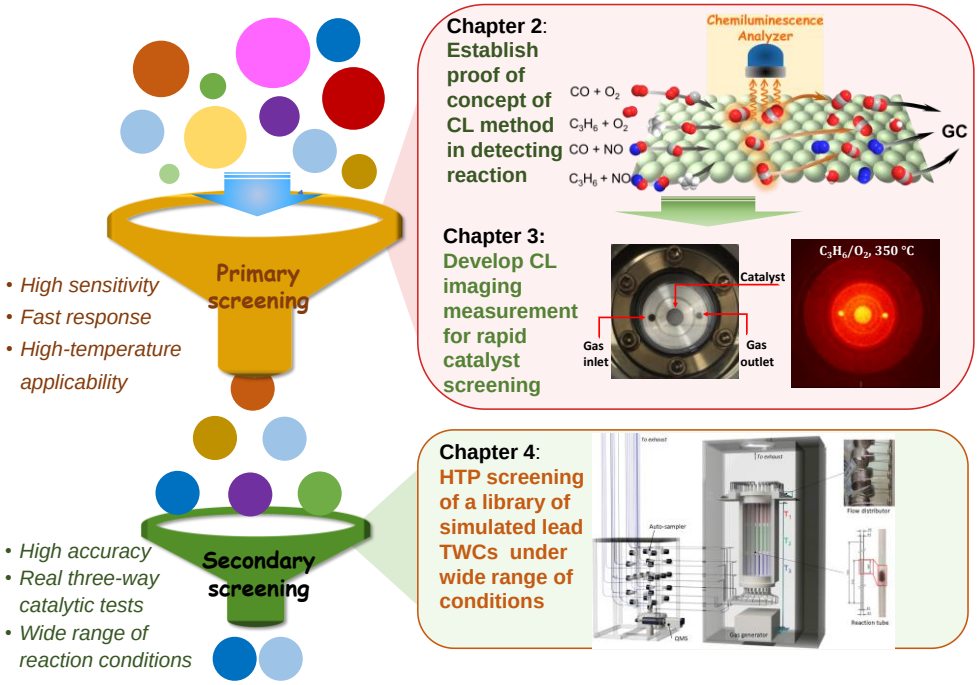

Figure 1. The developed high-throughput approach for three-way catalyst.

Keywords: Three-way catalysts, high-throughput catalyst screening, chemiluminescence imaging, high-throughput screening instruments.

Preface

The present thesis is submitted for the Degree of Doctor of Philosophy at Japan Advanced Institute of Science and Technology, Japan. The thesis is consolidation of results of the research work on the topic “Design of High-Throughput Experiments for Three-Way Catalysis” and implemented during October 2017–September 2020 under the supervision of Assoc. Prof. Toshiaki Taniike at Graduate School of Advanced Science and Technology, Japan Advanced Institute of Science and Technology.

Chapter 1 is a general introduction, which explains fundamental as well as specific background of the research field, followed by the objective of this thesis. **Chapter 2** provides comprehensive understanding about the chemiluminescence behavior of the catalytic oxidation of CO and hydrocarbon, then demonstrating the potential of the chemiluminescence method on rapid catalyst evaluation. **Chapter 3** reports the development of a chemiluminescence imaging instrument and its feasibility in primary catalyst screening for high-temperature gaseous catalysis. **Chapter 4** describes a high-throughput screening protocol for a library of three-way catalysts under wide range of reaction conditions. Finally, **Chapter 5** summarizes the important findings and conclusions of this thesis. To the best of my knowledge, this work is original, and no part of this thesis has been plagiarized.

Tran Phuong Nhat Thuy

Graduate School of Advanced Science and Technology

Japan Advanced Institute of Science and Technology

September 2020

Acknowledgements

I wish to express my sincere gratitude and deepest appreciation to my supervisor, Associate Professor Dr. Toshiaki Taniike for his mentorship, encouragement, and guidance during the past five years. His endless enthusiasm, passion in science and working attitude has inspired me a lot in doing research. This work would never have been completed without his great help and advisor.

To the members of my review committee: Assoc. Prof. Yuki Nagao (JAIST), Assoc. Prof. Shun Nishimura (JAIST), Assoc. Prof. Dam Hieu Chi (JAIST), and Assoc. Prof. Keisuke Takahashi (Hokkaido University), I would like express my grateful appreciation for their valuable time to read this thesis, their insightful comments and remarks to enhance the quality of this thesis from various perspectives.

I would also take an opportunity to express my sincere gratitude to Associate Professor Shun Nishimura for his enthusiastic guidance and valuable advices in my minor research project.

My special thanks also go to Senior Lecturer Patchanee Chammingkwan, Dr. Ashutosh Thakur, and Dr. Toru Wada for their enthusiastic supports and advices.

I am heartily grateful to all members in Taniike laboratory for their kindness, great help and accompany not only in research but also in daily life.

I also show my heartiest thanks for Toyota Motor Corporation for their collaboration in doing the research.

I would like to thank the Ministry of Education, Cultures, Sports, Science and Technology of Japan for their scholarship during my stay in Japan.

I would like to express my sincere thanks to Japan Advance Institute of Science and Technology (JAIST) for giving me an excellence chance to join and do the most advanced research here. I deeply appreciate JAIST officials and JAIST staffs for their kind support all the time.

Lastly, I express my heartfelt gratitude to my family members for their unconditional love, taking care and encouraging me all the time.

TRAN PHUONG NHAT THUY

Table of contents

Chapter 1

General introduction

1.1. Exhaust emission and regulation

After the World War II, the motor vehicle manufacturing industry has witnessed a steady growth, amounting up to 98 million units produced worldwide in 2018 [1]. According the data reported in the first half of 2019, approximately 90% of global vehicles sale is internal combustion engine vehicles, which are mainly powered by gasoline [2]. Air quality deterioration caused by engine exhaust emission has then occurred as an inevitable consequence. In principle, the energy for the internal combustion engine vehicles is generated through the controlled combustion of gasoline, which is predominantly comprising hydrocarbons (HCs) such as paraffins, cycloalkane, olefins, and aromatics. The process yields complete combustion products of CO_2, water as well as incomplete combustion products of CO (1–2 vol.%), unburned HCs (500–1000 vppm), and low level of partially combusted oxygenates such as carboxylic acids, aldehydes or ketones [3]. During the combustion, NO_x (100–3000 vppm) was also formed as a result of thermal fixation of N_2 in the atmosphere at high temperature [4]. Three major pollutants contained in the gasoline engine exhaust are therefore CO, HCs, and NO_x. CO has been best known for its toxicity to human health as just a few thousands ppm is lethal [5]. The toxicity level of HCs varies depending on the type of HCs. Benzene, for example, has been well-known as a carcinogen, and 80% of benzene in the atmosphere comes from the gasoline engine exhaust [6]. Alkenes can react with NO_x to generate secondary pollution such as tropospheric ozone and photochemical smog [7]. Among NO_x, NO_2 is the most toxic as it can damage lung tissues and interfere with oxygen transport in blood via reaction with hemoglobin [8]. The interaction between HCs and NO_x in the gasoline engine exhaust promoted by sunlight is primarily responsible for the photochemical smog, which is severe air pollution in many urban areas [9,10].

Legislation requirement

The first global action to raise the environmental awareness on the control of gasoline engine exhaust emission was initiated in 1970, when the US congress passed the comprehensive federal law called Clean Air Act (CAA) to regulate exhaust emission from the internal combustion engines. The CAA required the reduction of 90% of CO and unburned HCs by 1975 and 50% NO_x by 1976 [11]. Initially, the automotive industry adopted this legislation by means of implementing several modifications in engine design and control technology to lower the exhaust emission. Despite some achieved emission improvements, these efforts could not alone satisfy the 1975 US Federal and Californian emission limits. As a result, a catalytic converter, which converts the pollutants in gasoline engine exhaust into less harmful compounds by catalyzing their redox reactions, was considered as the most efficient way forwards.

Since then to now, the continuing growth of the number of vehicles as well as the advancement of catalyst and engine technology has resulted in more and more stringent emission regulations. Figure 1.1 illustrates the annual changes in the emission standards for non-methane HCs and NO_x in the US, implying that the exhaust emission control is one of the most rapidly developing technologies. The most updated standards are the California low-emission vehicle (LEVIII) and the Federal US Tier 3, which are described as the cumulative amount of non-methane HCs and NO_x per km with the automotive catalyst durability of 150000 miles or 15 years. The Tier 3 regulation requests a decrease on the emission of these gases to 0.018 g/km by 2025, corresponding to over 99.5% reduction of CO, HCs, and NO_x [12,13].

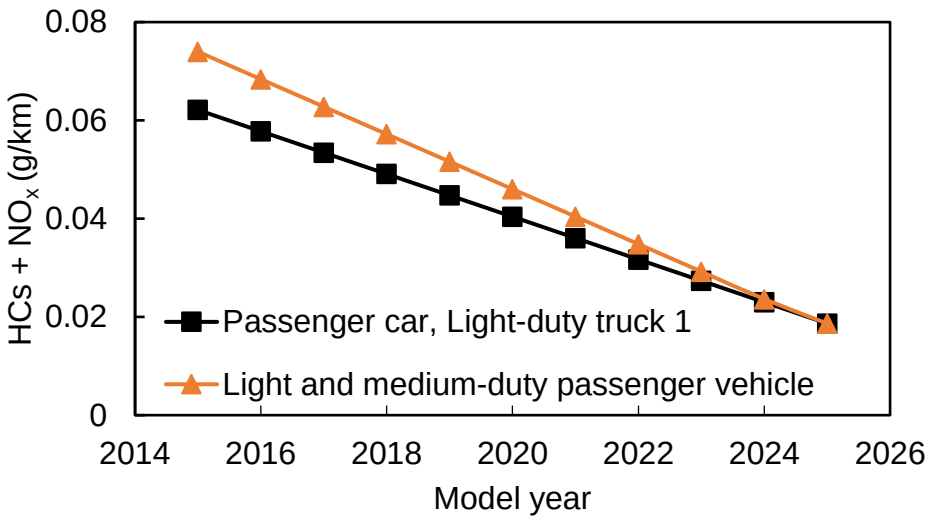

Figure 1.1. Fleet average non-methane hydrocarbons and NO_x emission standard in the low-emission vehicles (LEV III) and Tier 3. The graph is plotted based on the data from Ref. [13].

The legislation requirement for automotive emission has become stricter also in other continents. The United Nations Economic Commission for Europe (ECE) instituted the Urban Driving Cycle ECE-15 in 1970 to describe the typical usage of vehicles in European cities [14]. At that time, the first base directive 70/220/EEC was introduced to set the emission standards for CO and HCs. The directive was then consolidated as 91/441/EEC in 1991, forming the EURO I, which was the first mandatory European vehicle emission standard [15]. In 1997, the New European Driving Cycle (NEDC) was updated and consisted of four repeated ECE-15 urban driving cycles and one Extra-Urban driving cycle, resulting in the EURO II standard. Most recently, the NEDC was replaced by EURO 6 in 2014, in which vehicular CO, none-methane HCs, and NO_x emission targets were set as 1.000, 0.068, and 0.060 g/km, respectively. The overview of EURO standards is given in Table 1.1 [15,16].

Table 1.1. European standards for gasoline fueled vehicles (g/km) [15].

	Year	CO	HCs	HCs + NO_x	NO_x
EURO 1	1991	2.72	-	0.97	-
EURO 2	1996	2.2		0.5	
EURO 3	2000	2.3	0.2	-	0.15
EURO 4	2005	1.0	0.1	-	0.08
EURO 5	2009	1.0	0.1	-	0.06
EURO 6	2014	1.0	0.1	-	0.06

In China, the China's Ministry of Environmental Protection released the final China 6 light-duty vehicle regulations in 2016, phasing over two steps: China 6a regulations enforced in 2020, which was based on the EURO 6, and China 6b enforced in 2023. China 6a sets CO, non-methane HCs, and NO_x emission targets of 0.700, 0.068 and 0.060 g/km, respectively. The regulation is much more tightened in China 6b, where the CO and HCs emission limits lower by 50% and NO_x lower by 40%. Furthermore, China 6b also limits the N_2O emission level of 0.020 g/km [11,17]. In 2020, the Government of India has finalized their decision on the emission regulation to leapfrog from EURO 4-equivalent directly to EURO 6-equivalent standards. In the last updated regulation, the exhaust emission from light-duty gasoline automobiles is targeted using the modified NEDC as CO of 0.100 g/km, non-methane HCs of 0.068 g/km and NO_x of 0.060 g/km [14,17]. These targets are very challenging and certainly require significant improvement in automotive catalysis technology.

From the overview of the legislation requirements for vehicle exhaust emission in different continents, it is clear that the regulations became globally more stringent in dealing with the rising levels of hazardous atmospheric pollutants due to rapid growth

of global vehicle sales, while the worldwide efforts to lower the emission is advancing. In order to meet the newest regulations, it is required for the reduction of more than 99.5% of pollutants in tail pipe emission. This challenging task would emphasize the significance of continuous development of novel and highly durable automotive catalyst materials for the catalytic converter.

1.2. Early automotive catalysts

The motor vehicle manufacturing industry started to consider the development of an exhaust aftertreatment system in order to meet the increasingly stringent emission legislation, which could not be satisfied only with the engine modifications. During the adoption of the first CAA in 1970s, the main target of the catalytic converter was to achieve complete combustion of CO and HCs. On the other hand, the engine manufacturers employed a non-catalytic exhaust gas recirculation technique for NO_x removal: A certain amount of the exhaust containing N_2, CO_2, and H_2O was recycled into a combustion chamber. This strategy helps improve the heat capacity and thus reduce the combustion temperature, leading to less thermal NO_x formation [11]. For CO and HCs oxidation in the catalytic converter, base metal oxides and platinum group metals (PGMs) were proposed as two good candidates. Base metal oxide catalysts, basically containing nickel, cobalt or copper, are cost-effective and readily available; however, they were found very sensitive to lead- and sulfur- poisoning and exhibited insufficient thermal durability [18,19]. The PGMs were attractive due to their excellent oxidation activity, despite their high cost and limited availability. According to a study of Kummer group in 1975 on the comparison of these two candidates for automotive catalysts, the PGMs were much more active in CO and HCs oxidation compared to the

base metal oxides [20]. Even though the low activity of the base metal oxides could be compensated by increasing their amount with a larger reactor volume, this solution would cause a space issue for the engine exhaust underfloor piping. During that period, considerable efforts were made to enhance the oxidation activity of base metal oxide systems, especially Cu-based catalysts; however, their usage as primary automotive catalysts for vehicle emission control has been hardly commercialized so far.

In the case of the PGMs, their mechanical and catalytic deterioration during the operation necessitated the use of supports and an immobilization method thereon. For this, γ-Al_2O_3 was employed to disperse the active metal species due to its high surface area and relatively good thermal stability. However, the sintering of γ- Al_2O_3 to a lower surface area was noticed after aging at high temperature (typically 900 °C), leading to the burial of the active species and preventing the access of the exhaust to them. These naturally resulted in a loss of catalytic activity [3]. Enormous research had been conducted toward minimizing the sintering of γ-Al_2O_3 and understanding its mechanism. It was found that proper incorporation of oxides such as La_2O_3, CeO_2 or BaO during the preparation process exhibits an outstanding stabilizing effect on γ-Al_2O_3 and significantly slows down the sintering [21,22].

In parallel with the studies on the choice and combination of catalytic components as well as the suppression of deactivation, another important issue that the engine manufacturers had to address was how to position the catalyst in the exhaust. The most conventional method was to use the beaded catalysts where stabilizing oxides and active species were loaded on γ-Al_2O_3 support. At that time, this conventional reactor design worked to attain sufficient CO and HCs removal efficiency. One considerable concern was the attrition of the beads induced by their motion against each

other under the gas flow and vibration of the vehicles. The occurrence of gas bypass also led to poor performance [3,19]. This issue was addressed by using a ceramic honeycomb monolith with a multi-channel structure (Figures 1.2a,b) [23]. A thin layer of γ-Al_2O_3 containing well-dispersed active metal species and stabilizers is deposited onto the channel walls, that is referred as a washcoat layer (Figure 1.2c). The high surface area of the washcoat enables high conversion despite low residence time. The monoliths are basically made of cordierite ($2MgO{\cdot}5SiO_2{\cdot}2Al_2O_3$), a low thermal expansion ceramic material, which is able to provide sufficient mechanical strength and cracking resistance under thermally stressed conditions. This honeycomb design exhibits several advantages, including improved heat and mass transfer rates, low-pressure drop, increased flexibility in reactor design, and high adaptability to an exhaust manifold. Thus, the honeycomb monolith configuration was recognized as the optimal physical structure for the catalytic converters.

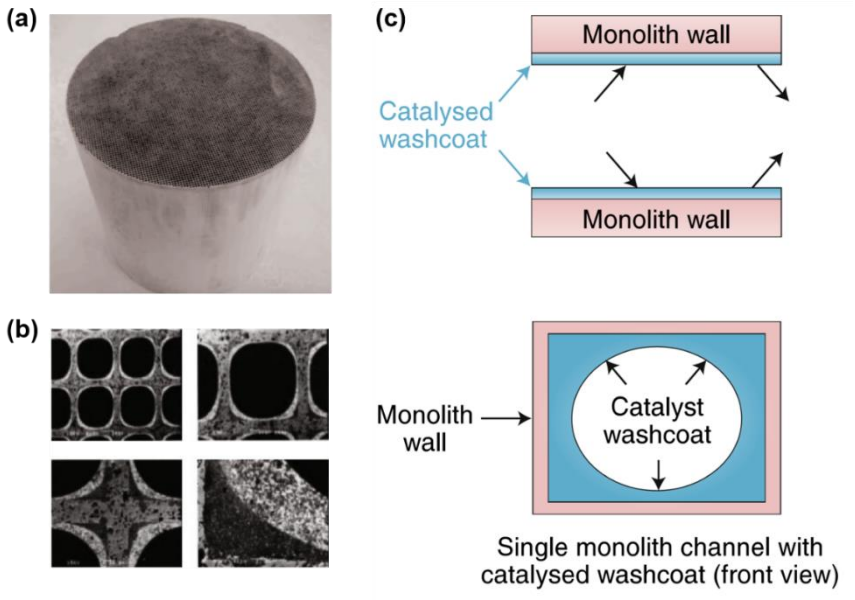

Figure 1.2. Catalytic converters with a honeycomb monolith configuration: (a) Cordierite honeycomb monolith, (b) SEM micrographs of a wash coated monolith, and

(c) schematic images of a wash coated monolith. The figure is reproduced from Ref. [17].

In summary, the first-generation automotive catalysts were composed of Pt and Pd as catalytic active components, γ-Al_2O_3 as the support, CeO_2, La_2O_3 or BaO as the stabilizer for the support. A ceramic honeycomb monolith was washcoated by the catalysts.

1.3. Three-way catalysts

1.3.1. Working principle

In the early 1980s, the emission regulations for NO_x became more tightened and it became obvious that the non-catalytic exhaust gas recirculation system itself would not meet the demand of over 90% NO_x conversion. At that time, Rh was recognized as an excellent catalyst for NO/NO_2 reduction [24–27]. A bimetallic Pt/Rh catalyst then became predominated in automotive catalyst formulations, and a double-catalyst bed design was employed for the conversion of all three pollutants. The engine operated under slightly fuel rich condition, creating reducing atmosphere for NO_x reduction by CO and HCs in the first Pt/Rh-containing bed. Subsequently, the second bed was supplied to oxidize the residual CO and HCs by air [28,29]. During practical operation of the double-catalyst bed, NH_3 was formed as a by-product of NO reduction in the first bed, then the re-oxidation of NH_3 occurred in the second bed, eventually leading to lower NO conversion at the end of the pipe [25]. This issue prompted the automotive industry to develop a single-catalyst bed capable of simultaneous removal of all three pollutants, so-called “three-way catalysts” (TWCs). A typical automotive catalyst design is schematically demonstrated in Figure 1.3.

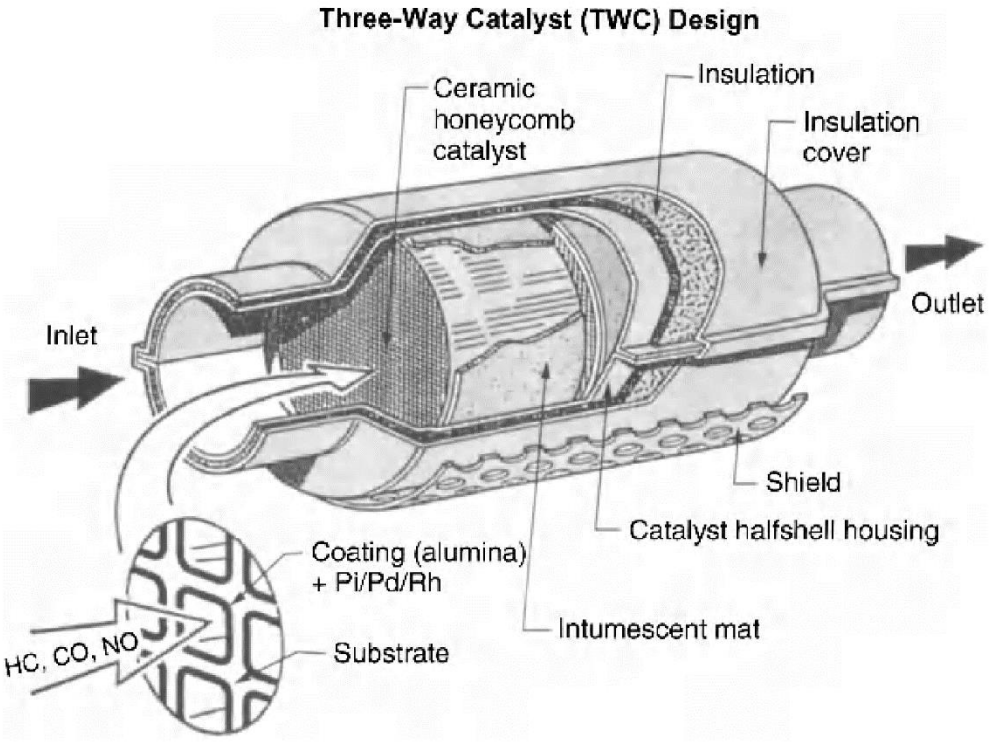

Figure 1.3. Schematico cut away of a three-way catalytic conventer. The figure is reproduced from Ref. [3].

The uniqueness of the TWCs is that it works mainly around stoichiometric air/fuel (A/F) ratio that is suitable for the oxidation of CO and HCs and the reduction of NO_x. The three-way catalytic converters require three major components [19]:

i) Electronic fuel injection

ii) Two O_2 sensors placed at the inlet and outlet of the catalytic converter to measure the O_2 content of the feed and the effluent.

iii) A feedback control loop to adjust the amount of fuel entering in the catalytic converter to keep the exhaust composition around the stoichiometric point. The signal from the O_2 sensors is used for the feedback.

The stoichiometric value of the A/F ratio ($(A/F)_{stoich.}$) is determined as follows: Octane (C_8H_{18}) is selected as a representative species for gasoline, its complete combustion by air is described by the following equation:.

$$C_8H_{18} + 12.5\ O_2 \rightarrow 8CO_2 + 9H_2O$$

The $(A/F)_{stoich.}$ is then defined as:

$$(A/F)_{stoich.} = \frac{Mass\ of\ air}{Mass\ of\ fuel} \approx 14.7$$

The ratio between the real feed and the stoichiometric feed is called the A/F equivalence ratio or lambda (λ):

$$\lambda = \frac{(A/F)}{(A/F)_{stoich.}}$$

Figure 1.4 describes typical performance of the TWCs at different A/F ratios as well as λ values: At λ < 1 (A/F < 14.7), the exhaust is fuel rich or O_2 deficient, then the NO_x reduction by HCs and CO readily occurs, whereas the CO and HCs oxidation are not completed due to the lack of O_2. At λ > 1 (A/F > 14.7), the exhaust is fuel lean or O_2 excess, then the oxidation reactions are predominant while the NO_x reduction is sacrificed.

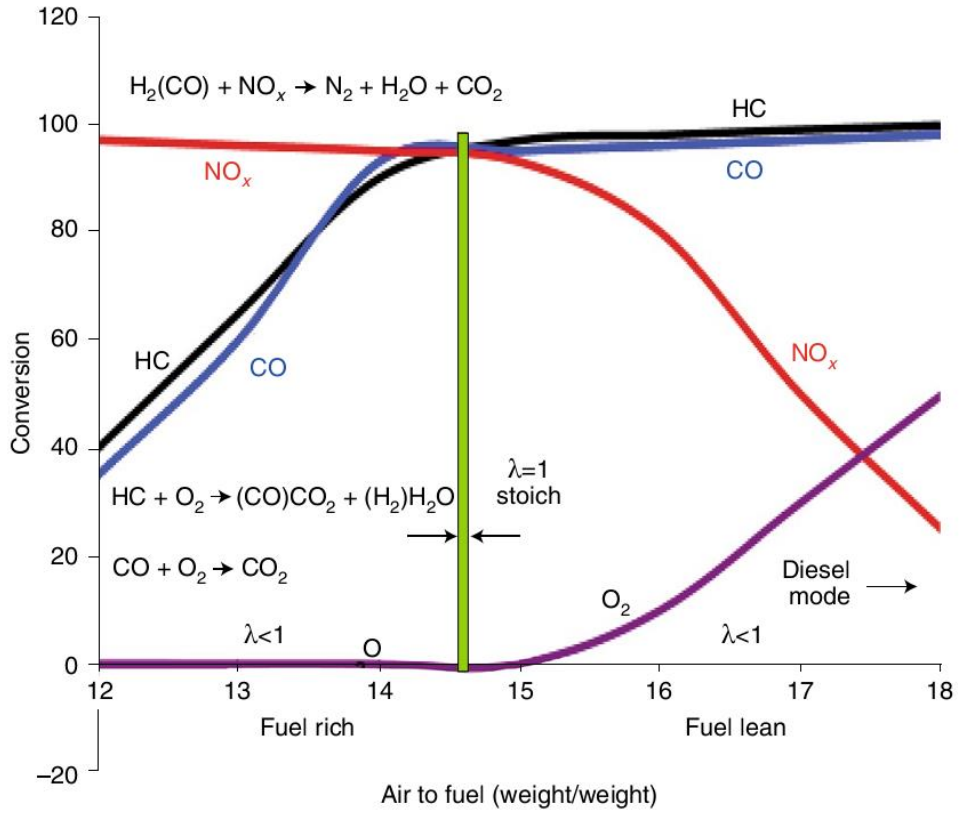

Figure 1.4. Typical performance of a three-way catalyst as a function of A/F ratio as well as λ value (A/F equivalence ratio). Green line demonstrates the stoichiometric condition, correponding to A/F = 14.7 and λ =1. The figure is reproduced from Ref. [17].

1.3.2. Formulation

The chemistry on the TWCs has been acknowledged as one of the important subjects in the field of environmental catalysis [30]. Today the TWCs typically consist of: i) a honeycomb monolithic substrate made of a cordierite ($2MgO{\cdot}5SiO_2{\cdot}2Al_2O_3$) or stainless-steel, ii) high-surface-area γ-Al_2O_3 as the support, iii) an oxygen storage material, iv) catalytic components (Pt, Pd and Rh), and/or v) a promoter. As the detailed description on the substrate, support and active species were provided in former parts,

this section will focus on a unique component of the TWCs, that is the oxygen storage material.

The A/F ratio adjustment in gasoline vehicles is essential as the operation of the TWCs is only performed in close proximity to the stoichiometric point. The O_2 sensor and the feedback control loop themselves are not sufficient as a slight oscillation of the exhaust composition around the stochiometric point is frequently observed. This is mainly due to the response time of the O_2 sensor and a time lag in the feedback system. Therefore, it is necessary to auxiliarily supply a small amount of O_2 to complete the oxidation of the unreacted CO and HCs under fuel-rich conditions. Conversely, it was also essential to consume O_2 when the exhaust goes slightly oxidizing. This was accomplished by the development of an O_2 buffer material, which was so-called an oxygen storage component (OSC) to buffer the gas composition perturbations [31,32]. CeO_2 was found to have a proper redox response and has been the most commonly used OSCs in the modern three-way catalytic converters. CeO_2 is able to store/release O_2 with respect to the oxidizing/reducing conditions due to the Ce^{4+}/Ce^{3+} redox cycle. Under the shortage of O_2 ($\lambda < 1$), CeO_2 is reduced to Ce_2O_3. This in turn supplies O_2 to oxidize CO and HCs. When O_2 becomes excess due to the perturbation, Ce_2O_3 is recovered to CeO_2. The whole process is described in Figure 1.5.

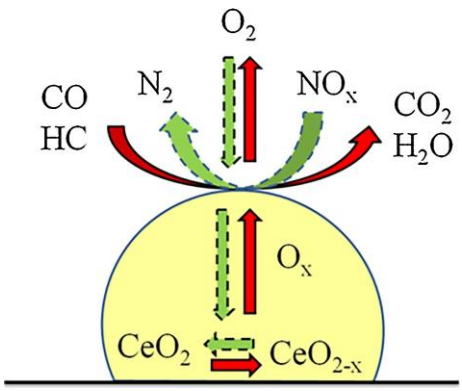

Fuel rich (oxygen lean)

$CO + CeO_2 \rightarrow Ce_2O_3 + CO_2$

$C_xH_y + CeO_2 \rightarrow Ce_2O_3 + CO_2 + H_2O$

Fuel lean (oxygen rich)

$Ce_2O_3 + O_2 \rightarrow CeO_2$

$Ce_2O_3 + NO_x \rightarrow CeO_2 + N_2$

Figure 1.5. The function of CeO_2 as an oxygen storage component under a redox condition in the automotive exhaust application. The figure is reproduced from Ref. [33].

The early implementation of the CeO_2-containing TWCs showed that the interaction between noble metal and CeO_2 is lost during the thermal ageing and this triggers the catalyst deactivation [34]. The catalyst deactivation was associated with the two different phenomena: i) sintering of noble metal particles resulting in a loss of metal surface area, and ii) sintering of CeO_2 resulting in a deterioration in the oxygen storage capacity [35]. To address this issue, extensive efforts have been made to enhance the thermal stability of CeO_2 based on finding stabilizers/promoters, and ZrO_2 appeared to be the most efficient [35,36]. The presence of ZrO_2 prevents the occurrence of undesirable reactions between CeO_2 and Al_2O_3, avoiding the deterioration of Ce^{4+}/Ce^{3+} redox couple due to the formation of the undesired $CeAl_2O_3$ mixed oxide [35–37]. Moreover, the incorporation of the smaller isovalent Zr^{4+} (ionic radius of 0.84 Å) into the CeO_2 lattice (ionic radius of Ce^{4+} is 0.97 Å) generates defective sites which greatly

promote the mobility of O_2 from the bulk to the surface of CeO_2. The diffusion rate of O_2 was consequently improved, leading to the enhanced reducibility of Ce^{4+}. Therefore, the oxygen storage capacity of CeO_2-ZrO_2 mixed oxide is much higher than those of pure CeO_2 [37–39].

Besides the most important role as an O_2 buffer, CeO_2-based oxides also offer various benefits for the TWCs, such as i) promoting the metal dispersion, ii) improving the thermal stability of the γ-Al_2O_3 support by preventing its sintering, and iii) promoting the CO removal via oxidation with lattice O_2.

1.3.3. Future perspectives

Nowadays, the stringent level of the emission regulations has been continuously rising due to the rapid increase in the number of vehicles. Therefore, the advancement of the automotive catalyst technology is further required to meet developing legislation worldwide. This fact makes the research on the TWCs remains a hot topic, as evidenced by hundreds of publications and patents released annually. The research on the TWCs not only provides significant contribution to the automotive industry, which is one of the largest economic sectors by revenue in the world, but also brings enormous benefits in the science of catalysis. It also carries out a great mission of environmental protection via catalysis. The methodology and strategies of catalyst tailoring, promoting, and stabilizing could be applied not only for the improvement of the TWCs but also for other catalyst systems, thus it helps to broaden the horizon of the catalytic research. Major future targets of this hot research topic could be summarized as follows [22,29]:

i) Widening the operating window to provide more working space for the TWCs, and make the catalyst more tolerant to the oxygen perturbation in the exhaust during vehicle operation.

ii) Reducing or even replacing the loading of PGMs while maintaining the performance based on the usage of promoter.

iii) Reducing or replacing the usage of rare and expensive Rh in the TWC formulations by improving the catalytic performance of Pt or Pd in the NO_x reduction. The development and enhancement of Pd-only TWCs were also proposed [40,41].

iv) Improving the thermal stability as well as the lifespan of the catalysts.

v) Enhancing the selectivity of NO_x reduction toward N_2 as the only product. This target is based on the observation that a considerable amount of N_2O as a by-product was formed during the NO_x reduction in the TWCs system.

1.4. High-throughput experiments in heterogeneous catalysis

1.4.1. Impact of high-throughput screening on catalysis

In 1970, industrial chemist Joseph J. Hanak, who is best-known for the successful synthesis and application of composition spreads or gradient libraries at the RCA-Laboratories Princeton [42], raised a controversial question about the real efficiency of the conventional approaches for the discoveries of new materials. One of his most famous quotes was that [42]: "…*the present approach to the search for new materials suffers from a chronic ailment, that of handling one sample at a time in the processes of synthesis, analysis and testing of properties. It is an expensive and time-*

consuming approach, which prevents highly-trained personnel from taking full advantage of its talents and keeps the tempo of discovery of new materials at a low level." His statement is also critical in the field of heterogeneous catalysis, where the efficiency and speed of conventional approaches for catalyst preparation and evaluation are not satisfactory. While the knowledge could help scientists in experimental designs or objective identification, the parameter space to be explored is large even in the most well-understood catalytic reactions. Thus, in order to make discoveries, the scientists must navigate these unpredictable complex and diverse space to a limited database. This action could probably work for the optimization of known systems, where the synthesis-structure-property relationships were well-established. However, it would be inefficient for the optimization of systems where such relationships were not established due to the complexity of the relationships and simply due to the novelty of the systems. The latter scenario is far more dominant in the field of heterogeneous catalysis.

The research and development of the chemical and refinery industry have been facing the raising economic pressures of higher efficiency and productivity in an environmentally responsible manner. For that, the implementation of combinatorial or high-throughput (HTP) catalyst screening (these two terminology can be used interchangeably) becomes indispensable. HTP catalyst screening is a methodology that large and diverse catalyst libraries are parallelly produced, processed and evaluated for their performance in a HTP fashion. This approach was first addressed by Hanak in 1970, when he questioned about the above-mentioned issues of the traditional approaches. At that time, Hanak also introduced an integrated workflow for materials development with the following four major aspects: i) finish the preparation of an entire multicomponent system in just one experiment, ii) employ a simple, rapid, non-destructive and all-inclusive method for chemical analysis, iii) properties testing using

a scanning device, and iv) computer data processing. This workflow is a root for many research and development works for HTP catalyst screening today. However, his works went unnoticed for 25 years until a famous publication of Schultz *et al.* in 1995 reinitiated the HTP approach to materials discovery, including heterogeneous catalysts [43]. The concept of HTP catalyst screening had then started to broadly spread in the field of catalysis. In 1999, Jandeleit *et al.* published the first comprehensive review on the combinatorial approach in catalysis [44]. This review covered 207 publications on the developments and applications of a broad variety of HTP technologies, thus documenting the explosive growth of HTP catalyst screening as a new paradigm of the chemical and refinery industry.

Nowadays, HTP catalyst screening has been recognized as an indispensable tool for the catalysis research to accelerate the discovery of novel catalyst materials while optimizing the reaction conditions with minimal cost operation, time, and human intervention. HTP catalyst screening could also help better understanding about science of catalysis in several ways: The significant acceleration of the catalyst research could enhance the chance for the discovery of new or even unexpected catalysts, which possibly provide a breakthrough in our knowledge on that catalytic system. In addition, recently HTP catalyst screening techniques have been coupled with data science to explore trends and patterns hidden in big data, thus offering valuable strategy for the development of catalysts.

The workflow of the research and development in HTP catalyst screening (toward commercialization) generally consist of three distinct stages, which are illustrated as a hierarchical workflow in Figure 1.6.

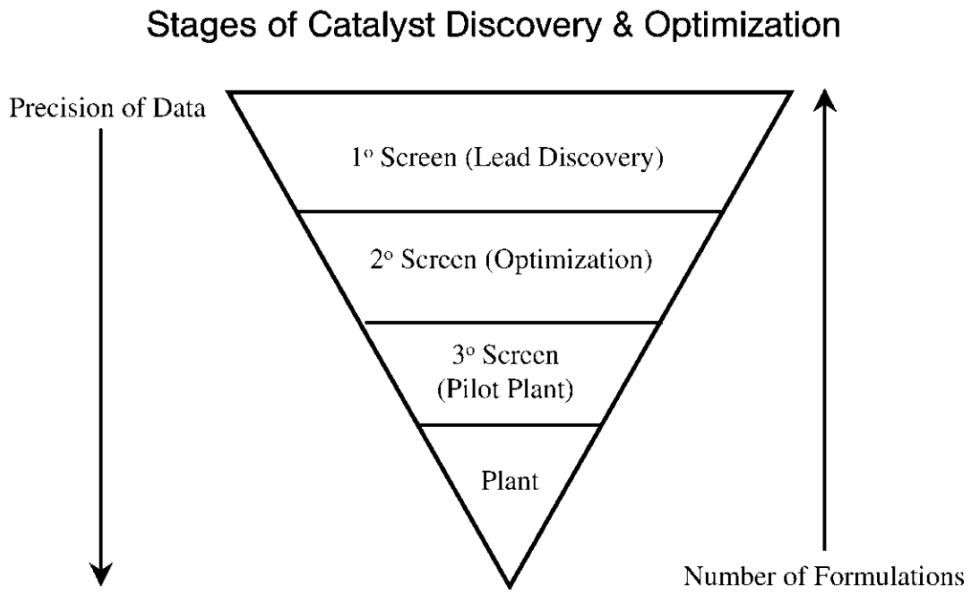

Figure 1.6. Hierarchical workflow of high-throughput catalyst screening. The figure is reproduced from Ref. [45].

1.4.2. Primary screening

The first stage is known as primary screening. This stage is dedicated for the broad screening of a large and wide-ranging parameter space of the catalysis. The ultimate target of this stage is to discover truly novel and promising catalysts (so called "leads"). While HTP researchers pursue to maximize the quality of the data and minimize the simplification of the catalytic conditions in primary screening, the substantial amounts of performed experiments make it challenging to acquire quality data at the conventional laboratory level. However, in some circumstances, to attain a sufficient throughput, one does not screen for the exact targeted properties, but rather screen for properties that are easier to achieve in HTP fashion instead [46,47]. The accuracy and throughput are balanced in a reasonable way so as to enhance the chance of success while reducing the risk of false negatives or positives. Qualitative trends

within the data are acquired in primary screening to remove some classes of catalysts from diverse libraries and to recognize potential leads to grow to a catalyst champion.

Optical screening techniques have been extensively employed in primary screening of heterogeneous catalysts due to their broad applicability, high speed, simple instrumentation, ability for in-situ analysis, non-invasive feature, and no requirement of sampling [48–51]. Typical examples of optical screening techniques for catalysts include infrared (IR) thermography [48,49,52–54] and laser-induced fluorescence imaging (LIFI) [48,55,56].

IR thermography is a truly parallel screening method applied for the rapid evaluation of the catalytic activity in exothermic reactions, where the temperature of the catalyst surface correlated with the reaction rate. The working principle of the IR thermography is based on the relationship between the radiation energy and the temperature of the catalyst surface, which is described in the following modified Stefan-Boltzmann equation [48]:

$$q = e\sigma T^4$$

where q is the radiation energy emitted on the catalyst surface, T is the absolute temperature, e is the temperature- and composition-dependent emissivity of the catalyst surface, and σ is the Stefan-Boltzmann constant. The Stefan-Boltzmann equation shows that the radiation energy is extremely sensitive to the catalyst temperature, thus IR thermography can detect a very small temperature deviations. Olong *et al.* have employed emissivity-corrected IR-thermography (ecIRT) for the HTP screening of 207 catalyst in low-temperature soot oxidation [52]. The reliability of the obtained results was confirmed by a conventional thermal gravimetric analysis as both two techniques showed that the combination of Cu, Ce, Ag, and Co catalysts exhibited the best

performance for low-temperature soot oxidation. Weidenhof *et al.* utilized ecIRT for the rapid parallel screening of a library of HCs/NO oxidation catalysts [57]. One critical fact of the IR thermography as a tool of catalyst screening is that the visualization of reaction heats by IR thermography normally gives no information about the chemical composition of the product mixture.

Laser-induced fluorescence imaging (LIFI) is a powerful screening technique featured great sensitivity and high spatial and temporal resolutions [55,56,58]. The LIFI works based on the destruction or formation of chemical bonds that cause the modification of fluorescence properties of molecules. The region above the catalyst surface is irritated with an external laser source, allowing the detection of the fluorescence intensity of products and/or reactants by a charge-coupled device (CCD) camera, thus florescence imaging could be simultaneously acquired. Su and Yeung made pioneering works on the development of the LIFI as a HTP catalyst screening technique by taking the selective oxidation of naphthalene as an example [55,56]. They demonstrated that the LIFI technique can allow the in-situ screening of 15 binary vanadia-based catalysts in just 15 seconds. An obvious pitfall of the LIFI lies on its working principle that it requires a change of the fluorescence properties of molecules during catalytic reactions. Indeed, such reactions are limited especially in term of practical catalysis [48,49,59].

Chemiluminescence imaging

Chemiluminescence imaging has been recently emerged as a promising HTP optical screening technique in analytical-related fields. CL is the light emission, mainly in the visible or near-IR region, during the relaxation of excited molecular species

produced in the course of a redox reaction [59–61]. The first application of the CL method in heterogeneous catalysis was reported by Breysse *et al.* in 1976 [59]. The authors found that the catalytic oxidation of CO on ThO_2 surface was accompanied by a specific luminescence, and the luminous intensity was proportional to the reaction rate. At that time, this important finding was mainly applied to fabricate sensors for gas detection [62,63]. This is because the CL-based optical sensing system has many advantages, such as high sensitivity, fast response, low natural background, no external excitation source, and simple instrumentation [64,65]. In spite of such advantages, the CL method had not been used as a catalyst screening technique until 2007, when Zhang *et al.* established a proof of concept for a CL imaging screening method. They used CL imaging for rapid evaluation of the activity of five supported gold catalysts in low-temperature CO oxidation [66]. They found that the brightness of the spots in the CL image was well correlated with the catalytic activities of the corresponding catalysts. This work is acknowledged as a pioneering study on the application of the CL method in HTP catalyst screening.

Figure 1.7 illustrates a typical catalyzed oxidation process taking place on a solid surface, which could be divided into five steps:

(1) Diffusion of reactant (R) and oxidant (O) gases to the catalyst surface.

(2) Chemisorption of R and O (denoted as R_{ad} and O_{ad}).

(3) Interaction between R_{ad} and O_{ad} to generate RO_{ad}.

(4) Desorption of RO_{ad} from the catalyst surface.

(5) Diffusion of product RO to the gas phase.

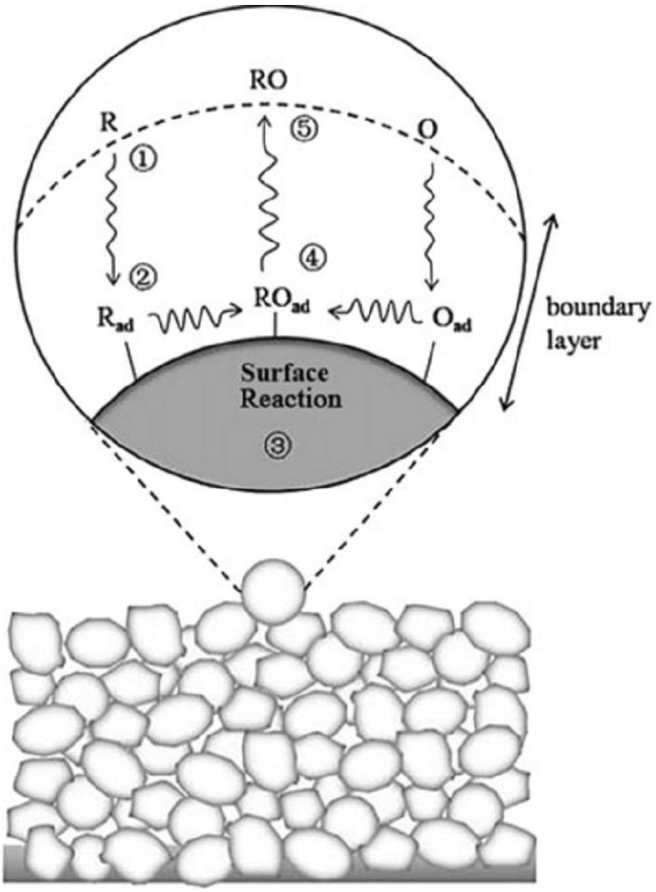

Figure 1.7. Oxidation reaction on a catalyst surface. The figure is reproduced from Ref. [62]

The CL emission is then generated through two basic mechanisms: i) Radiation from excited species (luminescence is generated during the produced excited species decaying to the ground state; and ii) recombination radiation (the desorption of RO_{ad} is combined with annihilation of excitons, then the recombination of electrons and holes results in luminescence).

The choice of catalytic reactions is important to apply the CL method for catalyst screening. The key requirements for a reaction to produce light are described as follows:

i) The reactions must be exothermic to generate sufficient energy for the formation of an electronically excited state.

ii) The reaction exotherm needs to be efficiently transferred for the formation of an electronically excited state. If the energy is dissipated in a form of heat via vibration and rotational energy, the CL will not be emitted.

iii) Deactivation process of the excited species must be favorable to the photon emission rather than other competitive non-radiative processes (e.g. molecules dissociation, intramolecular energy transfer, intermolecular energy transfer, and so on). The different routes for losing energy of an excited species are summarized in Figure 1.8.

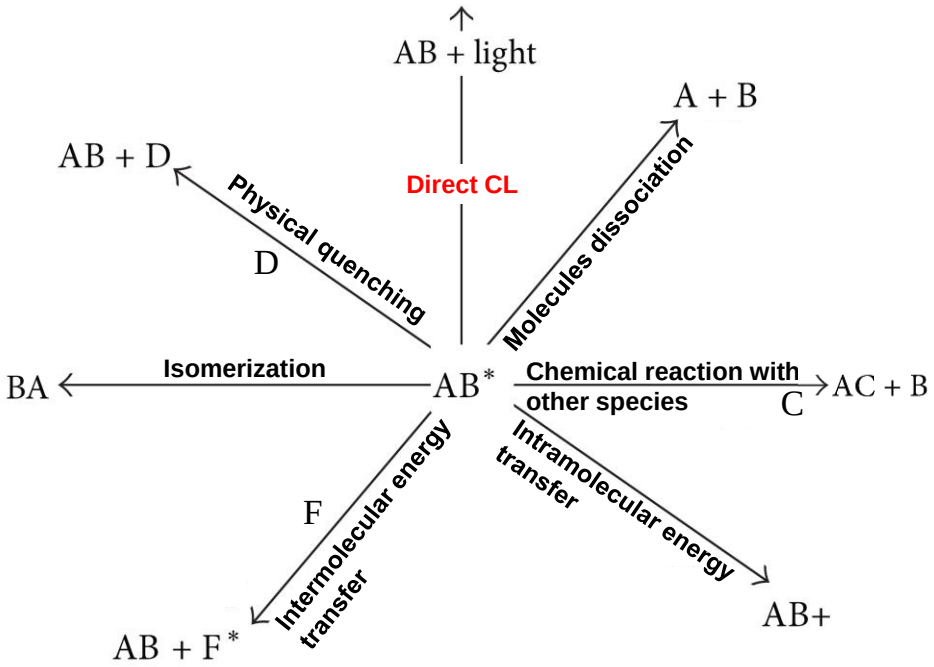

Figure 1.8. Different excited-state decay processes. The figure is reproduced from Ref. [67].

As demonstrated by the work of Breysse [59], the CL intensity exhibits a linear correlation with the reaction rate. On the other hand, the reaction rate is a function of the reactant concentration, thus the CL method is applicable for quantitative analysis. The advantages of the CL method that makes it promising in HTP primary catalyst screening can be summarized below:

i) High sensitivity: The detection limit of the CL method in the gas phase could reach the level of picomoles if the efficiency of the chemiluminescence reaction is sufficiently high.

ii) Truly parallel, non-invasive, and able for in-situ measurement.

iii) Simple instrumentation: To develop a HTP-CL screening measurement, the only requirement for the instrument is a transparent window of the reaction cell. The CL signal could be easily imaged by a CCD camera.

iv) Free from external radiation sources, scattering and background luminescence.

v) Able to identify a product mixture and provide selectivity information based on spectroscopic separation of reactions: The CL efficiencies and spectral shapes of the CL depend on the kinds of reactants, chemical processes and even catalysts.

To date, Zhang *et al.* has been only the group who attempted to employ the CL method in relation to catalyst screening. In fact, their conscious choice of the catalyst library (gold-based catalysts) and reaction (low-temperature CO oxidation) could significantly minimize challenges: CO oxidation is one of the most extensively used model reactions in gas-phase catalysis without any by-products and without multistep processes. The catalysis occurred in the temperature range of 140–180°C, which is regarded as relatively low in the field of catalytic gas-phase reactions. Moreover, in the

low-temperature conditions, the CL emission is not contaminated by the thermal radiations from the catalysts or even from reactor substances (so-called black-body radiation). Therefore, the CL method as an optical technique in HTP primary catalyst screening remained largely unexplored.

1.4.3. Secondary screening

The main tasks of the secondary screening are optimization and/or validation, rather than discovery, to generate reliable trends within the data as well as champion catalysts. The accuracy level of screening techniques employed in this stage should be at least as high as conventional methods. The significance of more realistic reaction test and precise catalyst synthetic protocols is also noticed in this stage. The demand of highly accurate and qualified data is often met by slowing down the screening and reducing the number of tested catalysts. Based on these requirements, the development of HTP secondary screening is often oriented to automated or parallel synthetic techniques at a laboratory scale and parallel reactor systems applicable for various reactions.

It must be noted that the input of secondary screening is either the leads obtained from primary screening process or others. The latter can be seen in some circumstance, where one can go directly to secondary catalyst screening when precision and quality of the data are more critical than the amount and broadness. When the secondary screening is connected with the leads generated from primary screening, its main purposes will be the validation of these leads and/or optimization to create champion catalysts.

Gas chromatography (GC) and mass spectrometry (MS) are often the choice of screening techniques in this stage. MS is a mature and widely employed methodology for HTP screening of a complex gas mixture in a sequential manner. Cong *et al.* successfully demonstrated the potential of MS as a HTP screening technique in CO oxidation by O_2/NO using a library containing 120 metal catalysts [68]. Reactants and products were sampled directly above the catalysts and injected to the mass spectrometer, where the sequential analysis took a minute per sample. Wang *et al.* developed a HTP screening system for catalyst libraries that were produced by primary screening in aldol condensation of acetone by incorporation of an 80-pass reactor and a multistream mass spectrometer containing an automated 80-way valve [69]. Each reactor was connected to a capillary and the effluent gas mixture was individually transferred for analysis via the 80-way valve with a sampling time of 1−10 s. The HTP-MS screening system allowed sequential analysis of 80 reactors in 80 seconds to 13 mins. The requirement of sampling and sample withdrawal process could be regarded as the main drawback of MS toward HTP screening.

GC has also been acknowledged as a versatile screening technique in heterogeneous catalysis [70–76]. Hoffmann *et al.* developed a 49-channel parallel reactor for HTP screening of methane oxidation catalysts under conditions close to conventional ones [76]. A two-GC setup with a hot column and a cold column was connected to a three-way valve via capillaries attached to the outlet of each channel, allowing sequential analysis of 42 different catalysts at two different temperatures. A fast serial GC detection as a HTP secondary catalyst screening technique in the direct amination of benzene to aniline was demonstrated by Desrosiers group, allowing the screening of around 25000 catalyst samples per year [70]. A considerable challenge in

the application of GC to HTP catalyst screening is the long sampling time, which will be an obstacle for kinetic as well as catalyst deactivation studies.

1.4.4. High-throughput screening in automotive catalysts

As described in section 1.1, the increasingly stringent regulation on the automotive emission has served as one of the major impulses for the engine manufacturers and automobile researchers to keep searching for more efficient TWCs, especially better low-temperature activity and higher thermal durability. These goals have been pursued for a long period of time by many research groups worldwide with diverse strategies and directions, typically including: i) Optimization of the washcoat formulation by variation of different parameters (the choice of catalyst supports, the type and loading of noble metals, the type and loading of a promoter, and etc.); ii) appropriate synthesis methods (co-precipitation, impregnation, sol-gel, micro-emulsion, and so on); and iii) optimization of process conditions (calcination temperature, aging condition, and etc.) [77–80]. Likewise, it is obvious that the research and development of the TWCs needs to deal with a huge parametric space. In most of literature, the evaluation of newly generated catalysts is done successively from one catalyst to another, and the evaluation itself for each catalyst is time-consuming. This is because in laboratory scale, the performance of TWCs is often analyzed based on its light-off temperature (*i.e.* the temperature of 50% or 80% of reactants conversion) and the width of the operation window. The experiments to acquire these information need to be done separately. Considering these backgrounds, it is undoubtedly true that the HTP screening is indispensable in the research and development of the TWCs.

Despite the explosive growth of HTP catalyst screening techniques, attempts of applying a HTP approach in the research and development of TWCs has been relatively scarce. Some possible reasons could be: i) costs; ii) the requirement of online and time-resolved analytical techniques for all reactants and products; and iii) the lack of data acquisition in an automated sequence of process conditions.

To date, hte Aktiengesellschaft, one German company, has been the only group, who successfully applied a HTP approach in automotive catalyst screening [80-82]. Their testing unit consisted of a reactor block consisting of identical 48 channels and operated at isothermal conditions with the temperature range from 100 to 575 °C. The unit works in a way that reactant gas mixture is supplied to one channel selected at a time, and then the gas effluent is switched to a line for MS analysis. The same protocol is applied for other channels in a sequential mode.

1.5. Purpose of the thesis

The research and development of automotive catalysts need a breakthrough to meet the current and future emission targets. Enormous efforts have been devoted for a long period of time and worldwide in the materials aspect, especially for the optimization of the washcoat formulation via systematic variation of individual parameters in a huge parametric material space. The exploration in the materials aspect is moving forward when grouping these parameters and viewing them as a single page, but the whole picture of materials design for automotive catalysts is seemingly approaching saturation.

The ultimate purpose of this thesis is to develop a new approach for the research and development of automotive catalysts, more specifically the TWCs based on a

methodology aspect. Witnessed by the impressive growth of HTP catalyst screening techniques with substantial contributions in acceleration of catalyst discovery and optimization, I believe that similar achievements could be acquired when applying HTP catalyst screening in the field of three-way catalysis. Considering the large and diverse parametric space, the implementation of primary screening is essential to narrow down the library. Furthermore, since considerable endeavors have been made to enhance the catalyst performance at the level of one digit, the more detailed investigation in the secondary screening is also essential. Therefore, I aimed at designing and proposing HTP techniques and protocols for primary and secondary screening of the TWCs for the first time.

Major qualifications associated with the development of techniques in primary screening are fast, non-invasive, reliable, and truly parallel. Primary screening based on optical techniques exhibited a great potential in this regard, but it has just started and still remain an interesting field of the research. As reviewed in previous sections, even though already-established optical screening techniques are elegant, there is still a need for more straightforward, sensitive, simple, and in-situ screening techniques. I aimed to solve this challenge by the development of a novel HTP chemiluminescence (CL) imaging technique for oxidative catalyst screening with special emphasis on the application for high-temperature reactions. Since all elemental reactions occurring in the TWCs are sufficiently exothermic, the CL method is found relevant for detecting these reactions at the best time resolution of 1 s. To conduct secondary screening, a HTP screening instrument which consists of 20 parallel fixed bed reactors coupled with mass spectrometer was employed.

References

[1] I. Wagner, Worldwide automobile production through 2019 (2020) http://www.statista.com/statistics/262747/worldwide-automobile-production-since-2000/

[2] F. Munoz, Internal Combustion Engines (ICE) counted for over 90% of global car sales in H1 2019, 2019. http://www.jato.com/internal-combustion-engines-ice-counted-for-over-90-of-global-car-sales-in-h1-2019/

[3] R.M. Heck, R.J. Farrauto, S.T. Gulati, Catalytic air pollution control: commercial technology, John Wiley & Sons, 2016.

[4] Y.B. Zeldovich, Acta Physicochimica U.S.S.R 21 (1946) 577–628.

[5] J.A. Guzman, Critical Care Clinics 28 (2012) 537–548.

[6] A. Yardley-Jones, D. Anderson, D.V. Parke, Br. J. Ind. Med. 48 (1991) 437–444.

[7] P.S. Monks, A.T. Archibald, A. Colette, O. Cooper, M. Coyle, R. Derwent, D. Fowler, C. Granier, K.S. Law, G.E. Mills, D.S. Stevenson, O. Tarasova, V. Thouret, E. von Schneidemesser, R. Sommariva, O. Wild, M.L. Williams, Atmos. Chem. Phys. 15 (2015) 8889–8973.

[8] N.M. Elsayed, Toxicology 89 (1994) 161–174.

[9] A.J. Haagen-Smit, C. Bradley, M. Fox, Ind. Eng. Chem. Res. 45 (1953) 2086–2089.

[10] R.P. Wayne, Chemistry of atmospheres. I - An introduction to the chemistry of the atmospheres of earth, the planets, and their satellites, 1985.

[11] B.I. Bertelsen, Platinum Met. Rev. 45 (2001) 50–58.

[12] California Air Resources Board (2017) http://www.arb.ca.gov/html/lawsregs

[13] Regulatory Background on the US Mobile Source Emission Control Program, MECA, 2019.

[14] T. Johnson, A. Joshi, SAE Int. J. Engines 11 (2018) 1307–1330.

[15] P. Greening, Top. Catal. 16 (2001) 5–13.

[16] R. Searles, Stud. Surf. Sc. Catal 116 (1998) 23–32.

[17] R.J. Farrauto, M. Deeba, S. Alerasool, Nat. Catal. 2 (2019) 603–613.

[18] M.V. Twigg, Catal. Today 163 (2011) 33–41.

[19] M.V. Twigg, Appl. Catal. B 70 (2007) 2–15.

[20] J.T. Kummer, Catalysts for the Control of Automotive Pollutants, American Chemical Society, 1975, 178–192.

[21] J. Kašpar, P. Fornasiero, N. Hickey, Catal. Today 77 (2003) 419–449.

[22] S. Rood, S. Eslava, A. Manigrasso, C. Bannister, Proc. Inst. Mech. Eng. D 234 (2020) 936–949.

[23] J.G. Cohn, Environ. Health Perspect. 10 (1975) 159–164.

[24] L. Hegedus, J.C. Summers, Platinum-rhodium catalyst for automotive emission control, Google Patents, 1978.

[25] M. Shelef, Catal. Rev. 11 (1975) 1–40.

[26] Z. Hu, Chem. Commun. (1996) 879–880.

[27] M. Shelef, G.W. Graham, Catal. Rev. 36 (1994) 433–457.

[28] A.M. Efstathiou, V.N. Stathopoulos, in Perovskites and Related Mixed Oxides (eds P. Granger, V.I. Parvulescu, V.I. Parvulescu and W. Prellier), 2015, doi:10.1002/9783527686605.ch26

[29] M. Konsolakis,. I.V. Yentekakis, in Perovskites and Related Mixed Oxides (eds P. Granger, V.I. Parvulescu, V.I. Parvulescu and W. Prellier), 2015 doi:10.1002/9783527686605.ch25

[30] J.N. Armor, Appl. Catal. B 1 (1992) 221–256.

[31] B. Harrison, A. Diwell, C. Hallett, Platinum Met. Rev. 32 (1988) 73–83.

[32] G.B. Fisher, J.R. Theis, M.V. Casarella, S.T. Mahan, The Role of Ceria in Automotive Exhaust Catalysis and OBD-II Catalyst Monitoring, SAE International, 1993.

[33] P. Li, X. Chen, Y. Li, J.W. Schwank, Catal. Today 327 (2019) 90–115.

[34] H. Permana, D.N. Belton, K.M. Rahmoeller, S.J. Schmieg, C.E. Hori, K.Y.S. Ng, A. Brenner, SAE Transactions 106 (1997) 104–114.

[35] J. Kašpar, P. Fornasiero, M. Graziani, Catal. Today 50 (1999) 285–298.

[36] A. Trovarelli, Catal. Rev. 38 (1996) 439–520.

[37] P. Fornasiero, R. Dimonte, G.R. Rao, J. Kaspar, S. Meriani, A. Trovarelli, M. Graziani, J. Catal. 151 (1995) 168–177.

[38] H.S. Gandhi, G.W. Graham, R.W. McCabe, J. Catal. 216 (2003) 433–442.

[39] N. Guillén-Hurtado, V. Rico-Pérez, A. Garcia-Garcia, D. Lozano-Castelló, A. Bueno-López, Dyna 79 (2012) 114–121.

[40] S. Li, H. Zhang, Y. Dan, J. Deng, J. Wang, L. Xiong, Y. Chen, Mol. Catal. 482 (2020) 110696–110707.

[41] S. Matsuura, A. Hirai, K. Arimura, H. Shinjoh, Development of Three-Way Catalyst with Using Only Pd as Activator, SAE International, 1995.

[42] J.J. Hanak, J. Mater. Sci. 5 (1970) 964–971.

[43] X.-D. Xiang, X. Sun, G. Briceño, Y. Lou, K.-A. Wang, H. Chang, W.G. Wallace-Freedman, S.-W. Chen, P.G. Schultz, Science 268 (1995) 1738–1740.

[44] B. Jandeleit, D.J. Schaefer, T.S. Powers, H.W. Turner, W.H. Weinberg, Angew. Chem. Int. Ed. 38 (1999) 2494–2532.

[45] W.H. Weinberg, H.W. Turner, in High-Throughput Screening in Heterogeneous Catalysis (eds A. Hagmeyer, P. Strasser and A.F. Volpe), 2005 doi:10.1002/3527604103.ch1

[46] T.R. Boussie, G.M. Diamond, C. Goh, K.A. Hall, A.M. LaPointe, M. Leclerc, C. Lund, V. Murphy, J.A.W. Shoemaker, U. Tracht, H. Turner, J. Zhang, T. Uno, R.K. Rosen, J.C. Stevens, J. Am. Chem. Soc. 125 (2003) 4306–4317.

[47] H.W. Turner, A.F. Volpe, W.H. Weinberg, Surf. Sci. 603 (2009) 1763–1769.

[48] S. Senkan, Angew. Chem. Int. Ed. 40 (2001) 312–329.

[49] E. Sasmaz, K. Mingle, J. Lauterbach, Engineering 1 (2015) 234–242.

[50] S.A. Schunk, D. Demuth, A. Cross, O. Gerlach, A. Haas, J. Klein, J.M. Newsam, A. Sundermann, W. Stichert, W. Strehlau, U. Vietze, T. Zech, in High-Throughput Screening in Heterogeneous Catalysis (eds A. Hagmeyer, P. Strasser and A.F. Volpe), 2005. doi:10.1002/3527604103.ch2

[51] W.F. Maier, K. Stöwe, S. Sieg, Angew. Chem. Int. Ed. 46 (2007) 6016–6067.

[52] N.E. Olong, K. Stöwe, W.F. Maier, Appl. Catal. B 74 (2007) 19–25.

[53] F.C. Moates, M. Somani, J. Annamalai, J.T. Richardson, D. Luss, R.C. Willson, Ind. Eng. Chem. Res. 35 (1996) 4801–4803.

[54] M.T. Reetz, M.H. Becker, K.M. Kühling, A. Holzwarth, Angew. Chem. Int. Ed. 37 (1998) 2647–2650.

[55] H. Su, E.S. Yeung, J. Am. Chem. Soc. 122 (2000) 7422–7423.

[56] H. Su, Y. Hou, R.S. Houk, G.L. Schrader, E.S. Yeung, Anal. Chem. 73 (2001) 4434–4440.

[57] B. Weidenhof, M. Reiser, K. Stöwe, W.F. Maier, M. Kim, J. Azurdia, E. Gulari, E. Seker, A. Barks, R.M. Laine, J. Am. Chem. Soc. 131 (2009) 9207–9219.

[58] J. Zetterberg, S. Blomberg, J. Gustafson, J. Evertsson, J. Zhou, E.C. Adams, P.-A. Carlsson, M. Aldén, E. Lundgren, Nat. Commun 6 (2015) 7076.

[59] M. Breysse, B. Claudel, L. Faure, M. Guenin, R.J.J. Williams, T. Wolkenstein, J. Catal. 45 (1976) 137–144.

[60] M.M. Rauhut, Acc. Chem. Res. 2 (1969) 80–87.

[61] N. Siraj, B. El–Zahab, S. Hamdan, T.E. Karam, L.H. Haber, M. Li, S.O. Fakayode, S. Das, B. Valle, R.M. Strongin, Anal. Chem. 88 (2015) 170–202.

[62] Z. Long, H. Ren, Y. Yang, J. Ouyang, N. Na, Anal. Bioanal. Chem 408 (2016) 2839–2859.

[63] S. Wang, Z. Yuan, L. Zhang, Y. Lin, C. Lu, Analyst 142 (2017) 1415–1428.

[64] K. Aslan, S.N. Malyn, C.D. Geddes, J. Am. Chem. Soc. 128 (2006) 13372–13373.

[65] X. Liu, R. Freeman, E. Golub, I. Willner, ACS Nano 5 (2011) 7648–7655.

[66] X. Wang, Na, S. Zhang, Y. Wu, X. Zhang, J. Am. Chem. Soc. 129 (2007) 6062–6063.

[67] T.H. Fereja, A. Hymete, T. Gunasekaran, ISRN Spectroscopy 2013 (2013) 1–12.

[68] P. Cong, R.D. Doolen, Q. Fan, D.M. Giaquinta, S. Guan, E.W. McFarland, D.M. Poojary, K. Self, H.W. Turner, W.H. Weinberg, Angew. Chem. Int. Ed. 38 (1999) 483–488.

[69] H. Wang, Z. Liu, J. Shen, J. Comb. Chem. 5 (2003) 802–808.

[70] P. Desrosiers, S. Guan, A. Hagemeyer, D.M. Lowe, C. Lugmair, D.M. Poojary, H. Turner, H. Weinberg, X. Zhou, R. Armbrust, G. Fengler, U. Notheis, Catal. Today 81 (2003) 319–328.

[71] S. Gomez, J.A. Peters, J.C.v.d. Waal, T. Maschmeyer, Appl. Catal. 254 (2003) 77–84.

[72] M. Lucas, P. Claus, Appl. Catal. 254 (2003) 35–43.

[73] J.E. Bedenbaugh, S. Kim, E. Sasmaz, J. Lauterbach, ACS Comb. Sci. 15 (2013) 491–497.

[74] O. Trapp, J. Chromatogr. A 1184 (2008) 160–190.

[75] O. Trapp, Angew. Chem. Int. Ed. 46 (2007) 5609–5613.

[76] C. Hoffmann, H.-W. Schmidt, F. Schüth, J. Catal. 198 (2001) 348–354.

[77] D.C. Montgomery, Design and analysis of experiments, 8th ed., John Wiley & Sons, 2012.

[78] E. George, J.S. Hunter, W.G. Hunter, R. Bins, K. Kirlin IV, D. Carroll, Statistics for experimenters: design, innovation, and discovery, 2nd ed., Wiley, 2005.

[79] A. Sundermann, O. Gerlach, Catalysts 6 (2016) 23–39.

[80] A. Sundermann, M. Kögel, O. Gerlach, Catalysts 9 (2019) 776–795.

[81] A. Sundermann, O. Gerlach, 86 (2014) 1941–1947.

Chapter 2

Understanding chemiluminescence in catalytic oxidation of CO and hydrocarbons

Abstract

A chemiluminescence (CL) instrument was developed to understand the CL behavior of catalytic oxidation of CO and hydrocarbons, which are major processes occurring in catalytic converters. The instrument is based on the cooperation among a gas mixer, a custom-made CL analyzer, and an on-line gas chromatography. The concept of the CL method was formulated by thoroughly investigating the CL emission during the catalytic oxidation of CO and C_3H_6 in the presence of O_2 and/or NO under both stoichiometric and non-stoichiometric conditions. All the oxidation reactions were found to be CL-active, where the CL intensity increased exponentially with the temperature. The steady-state measurements showed good linearity between the CL intensity and the reaction rates, suggesting that the CL emission is a direct product of the reactions. It was also found that the CL intensity per CO_2 production was different among the reactions, most plausibly due to both/either the presence of multiple CL processes and/or the difference in the heat of the reactions. Based on the linear correlation between the CL intensity and the reaction rate, a feasibility study was successfully demonstrated for rapid catalyst evaluation in C_3H_6 oxidation.

Keywords: Chemiluminescence method, catalytic oxidation of CO and hydrocarbons, reaction monitoring, catalyst screening.

2.1. Introduction

Environmental concerns due to automobile exhaust emission have become increasingly serious and widespread in the modern society [1,2]. The automobile exhaust gas is predominantly composed of CO, hydrocarbons (HCs), and NO_x, which are difficult to be simultaneously eliminated as the oxidation of CO and HCs favors fuel-lean operation conditions, while the removal of NO_x prefers fuel-rich atmosphere [3]. A great deal of efforts have been made to promote the abatement of CO, HCs, and NO_x, among which a three-way catalysts (TWCs) is one of the most extensively employed techniques owing to its ability to synchronously convert these pollutants to less harmful compounds via catalytic oxidation of CO and HCs by O_2 and/or NO_x [2,4–6]. Since regulations of automobile emission are getting increasingly stringent, the development of more efficient catalysts is highly desired with special emphasis on low-temperature activity and high-temperature stability. This purpose needs to be greatly aided by various screening techniques designed for rapid evaluation of the performance of catalysts. They are exemplified by infrared (IR) thermography [7–14], Fourier transform IR imaging [15–19], laser-induced fluorescence imaging [20–22], and mass spectrometry [23–25], while few techniques are applicable for the catalytic converters. Further efforts have to be put forward not only for the acceleration of the discovery of novel catalyst materials but also for the diversification of the toolbox.

Recently, a chemiluminescence (CL) detection method has acquired great attention in materials screening [26–29]. CL is the emission of electromagnetic radiation by the relaxation of excited molecular species in the course of a redox reaction [30–32]. The detection of the CL emission from redox reactions taking place on the surface of a solid catalyst has been recognized as a promising technique for rapid screening of heterogeneous catalysts due to its high sensitivity to low reagent

concentrations and other advantageous characteristics: The CL method is potentially applicable to a wide variety of catalytic reactions without any external irradiation source as only the reaction mediates the light emission. Moreover, the CL method can provide spectroscopic separation of reactions based on the fact that the CL spectrum depends on the kind of reactants, chemical processes, and even catalysts [33]. In addition, the CL instrument requires only a transparent window for the reaction cell, thus a large number of catalysts arranged in an array could be simultaneously and in-situ evaluated through parallel imaging at the best time resolution of 0.1 to few seconds. The utilization of the CL method in the heterogeneous catalysis was pioneered by Breysse *et al.*, then followed by Wang *et al.* for the detection of the CL emission during the catalytic oxidation of CO on thoria (ThO_2) and titania (TiO_2)-supported gold nanoparticles [27,30]. The former group found that the luminescence was ascribed to the light emission by the catalytic oxidation, and the latter group reported that the CL intensity was linearly correlated with the catalytic oxidation rate of CO. The group of Lu reported the evaluation of solid base-catalyzed aldol condensation reactions based on a direct correlation between the number of specific basic sites and the CL intensity [34]. Later, they also discovered that the intensity of the CL emission in diethyl ether oxidation on the surface of TiO_2 nanoparticles was proportional to the concentration of oxygen vacancies of TiO_2. Based on this finding, they proposed the CL method as a simple and facile alternative to conventional X-ray photoelectron spectroscopy for quantifying the concentration of oxygen vacancies [35].

In Chapter 2, I attempted to understand the CL behavior of the catalytic oxidation of CO and HCs in relation to the catalytic converters. The concept of the CL method was established by correlating the CL emission with the reaction rate for CO and C_3H_6 oxidation in the presence of O_2 and/or NO under both stoichiometric and non-

stoichiometric conditions. Then, a feasibility study was demonstrated for rapid catalyst evaluation based on the CL intensity. These were achieved by a custom-made CL instrument equipped with a reaction cell for gaseous catalysis and synchronized with a gas mixer and a gas chromatograph (GC).

2.2. Experimental

2.2.1. Materials

Catalyst samples were prepared by wet impregnation. γ-Al_2O_3 (PURALOX SCFa100, SASOL, BET surface area of 106 m^2/g), CeO_2 (HSA-20, RODIA, BET surface area of 133 m^2/g), monoclinic ZrO_2 (RC-100, Daiichi Kigenso Kagaku Kogyo, BET surface area of 99 m^2/g), SiO_2 (Aerosil 50, EVONIK, BET surface area of 61 m^2/g), and TiO_2 (Aeroxide P25, EVONIK, BET surface area of 55 m^2/g) were used as support materials. A specified amount of support powder was impregnated with an aqueous solution of $Rh(NO_3)_2$, followed by evaporation to remove the solvent. The solid was dried at 120 °C for 15 h, and calcined in air at 500 °C for 2 h. The Rh loading of the catalysts was fixed at 1 wt%. Catalyst powder of *ca.* 80 mg was pressed into a self-supporting disk of 10 mm in the diameter, and then used for CL measurements.

2.2.2. Instrumental

A schematic layout of the developed CL instrument is shown in Figure 2.1. The system consists of three major components: A gas mixer (MU-3200, HORIBA, Ltd.), a custom-made CL analyzer (Tohoku Electronic Industrial Co., Ltd.), and a GC apparatus (GAS100, J-SCIENCE LAB Co., Ltd.) equipped with a thermal conductivity detector (TCD).

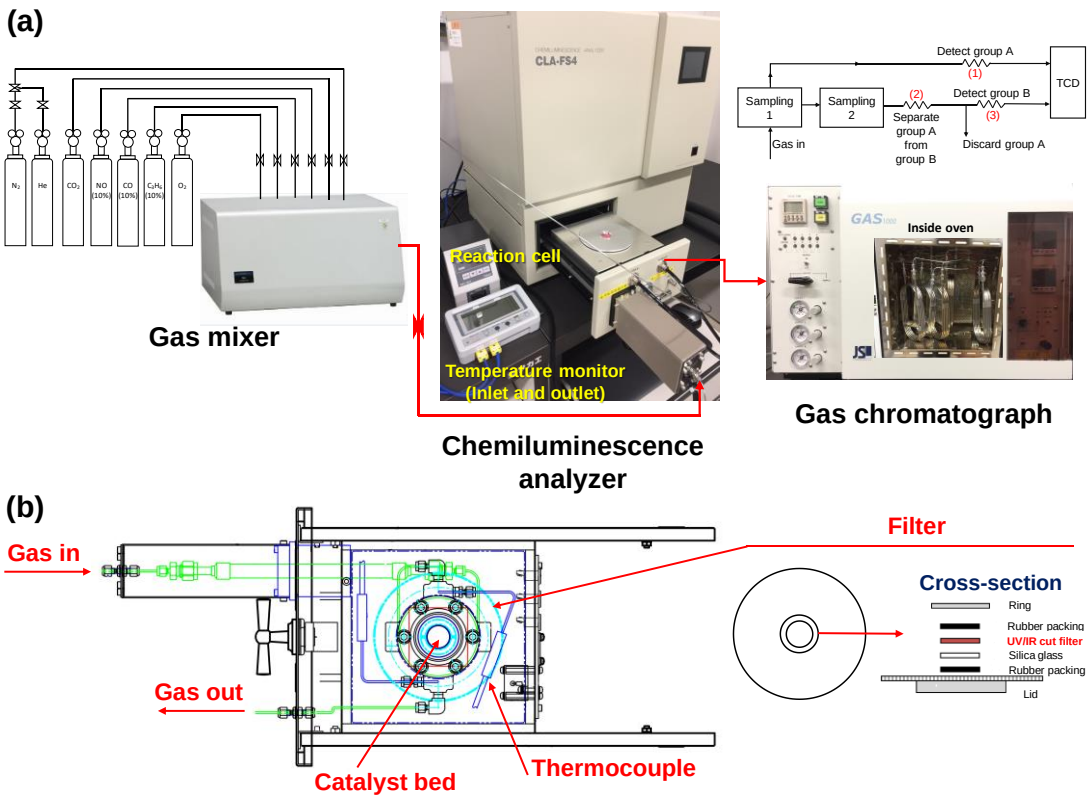

Figure 2.1. Schematic representation of the chemiluminescence instrument: (a) The whole system, and (b) the reaction cell unit.

The composition of the reaction gas mixture and its flow rate are controlled by the gas mixer and continuously supplied to the reactor cell. The gas mixer contains six mass flow controllers corresponding to six gases: C_3H_6, NO, CO, CO_2, O_2, and N_2/He. The specific flow volume of each gas can be regulated by setting its volume percentage over the whole flow volume of the gas mixture. He was used as the balance and carrier gas.

The CL analyzer consists of two major units: a detection unit and a reaction cell unit. The detection is performed using a photon multiplier based on single photon counting in the detection range of 300–850 nm at a time resolution of 0.1 to 10 s. To minimize the thermal noise, the photon multiplier is thermoelectrically cooled using

Peltier cooling elements. The cooling elements can be considered as a heat sink, where the heat produced by these elements is dissipated by circulating cold water. The reaction cell unit is basically made of stainless steel, and comprised of a viewport, a cell body with gas ports, an electrical plate heater, and an optical filter. A catalyst in the pellet form is placed in the center of the cell and closed with a quartz viewport (inner diameter of 38 mm, outer diameter of 70 mm) sealed with a nickel gasket. The detectable CL emission is supposed to happen mainly from exposed surfaces of the pellet. The use of the pellet form aimed to restrict the gas diffusion into the bulk, thus providing a consistent situation for the CL and GC-TCD measurements. The viewport is covered with a UV/IR cut filter (ϕ = 110 mm, cutoff wavelengths of 400 and 650 nm) to prevent the over exposure of the photon multiplier and to cutoff infrared thermal radiation, which becomes evident when the measurement is carried out over 250 °C. The heating is done using the electrical heater fixed under the cell body, and the cell temperature is programmable in the range of 50–400 °C. A thermocouple is placed beneath the cell body to control the temperature. The gas temperature at the inlet and outlet of the reaction cell is recorded through two in-line thermocouples.

The composition of the effluent gas is analyzed by the on-line GC, which contains three main columns. Column 1 (Porapak QS 170 °C) is used for the CO_2, N_2O, C_3H_6, H_2O (group A) detection; column 2 (Porapak Q 170 °C) is used to separate group A gases from O_2, N_2, CO (group B), and column 3 (MS-13X 300 °C) is used for the detection of group B gases. The concentration of each gas was calibrated using a standard gas mixture (N_2, CO, O_2, C_3H_6, N_2O, CO_2), containing individual gases at 1000 ppm and balanced with He. The NO conversion was derived based on the total yield of N_2 and N_2O.

The CL instrument also equips a safety management system to prevent potential accidents during operation. The CO and NO gas cylinders are placed in a cabinet, whereas the gas mixer, CL analyzer, and GC-TCD are placed inside a fume-hood. Gas detectors, whose detection limits are 50 and 25 ppm for CO and NO, respectively, are attached to the cabinet and the fume-hood. When the leakage happens, the gas supply and the operation of the gas mixer are automatically shut down, while the cabinet and hood are blown by N_2 until reaching the safety level. Similar automatic suspension acts by electric loss, earthquake, and so on.

2.2.3. Catalytic test

The CL behavior of four elemental reactions was investigated under stoichiometric conditions. These reactions are shown in Scheme 2.1 together with the corresponding heat of reactions [36,37]. Table 2.1 summarizes the feed compositions for these four reactions. The reactions were carried out based on a temperature program, which is illustrated in Figure 2.2. A catalyst pellet was first calcined at 400 °C under dry air in the reaction cell, followed by cooling to 50 °C. A reaction gas mixture at a specific composition was introduced in the cell at 100 mL/min, and the temperature was ramped from 50 °C to 400 °C at 16 °C/min, during which the CL intensity was monitored. Following this, steady-state measurements were performed at 400 °C and 350 °C, where the CL and GC data were acquired at individual feed compositions. The feed program was fully synchronized with the temperature program to realize full automation.

$2CO + O_2 \rightarrow 2CO_2$ $\Delta H = -588$ kJ/mol (1)

$2C_3H_6 + 9O_2 \rightarrow 6CO_2 + 6H_2O$ $\Delta H = -2058$ kJ/mol (2)

$2NO + 2CO \rightarrow N_2 + 2CO_2$ $\Delta H = -769$ kJ/mol (3)

$18NO + 2C_3H_6 \rightarrow 9N_2 + 6CO_2 + 6H_2O$ $\Delta H = -3684$ kJ/mol (4)

Scheme 2.1. Elemental reactions which were examined in this study.

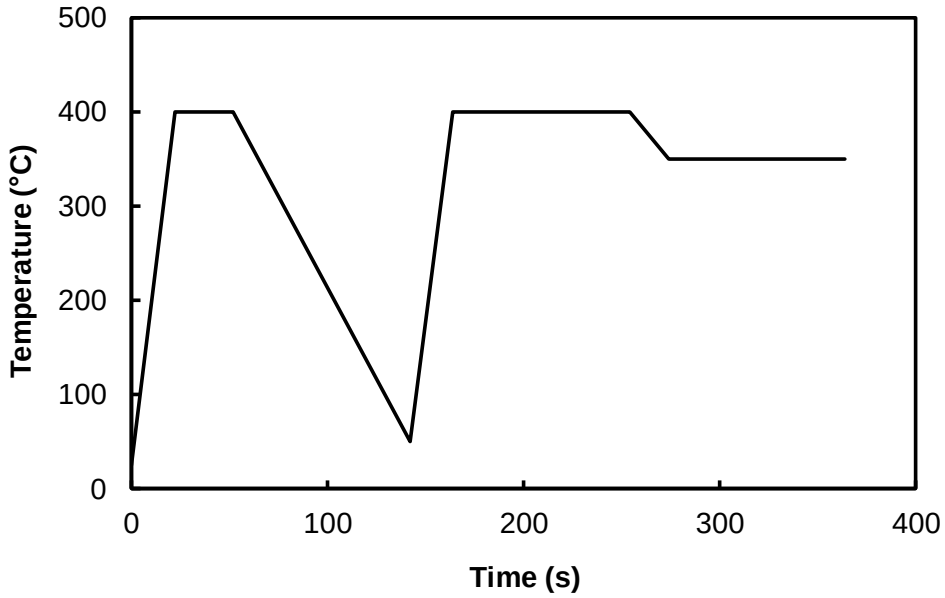

Figure 2.2. Employed temperature program.

Table 2.1. Feed stream composition for elemental reactions[a].

	Run[a]	CO (ppm)	O_2 (ppm)	C_3H_6 (ppm)	NO (ppm)
CO oxidation by O_2	1	8000	4000	-	-
	2	12000	6000	-	-
	3	18000	9000	-	-
C_3H_6 oxidation by O_2	4	-	9000	2000	-
	5	-	18000	4000	-
	6	-	27000	6000	-
CO oxidation by NO	7	2000	-	-	2000
	8	4000	-	-	4000
	9	8000	-	-	8000
C_3H_6 oxidation by NO	10	-	-	500	4500
	11	-	-	700	6300
	12	-	-	800	7200

[a] *The steady-state measurements were performed in all of the conditions. The ramping experiments were performed using conditions 3,4,9,12 for the individual elemental reactions.*

The CL measurements were also performed when elemental reactions were combined on the basis of the stoichiometric mixture. They are termed two-way conditions when three reaction gases are mixed (Runs 13–21, Table 2.2) and three-way conditions when four gases are mixed (Runs 22–24). For example, Runs 13–15 correspond to the combination of CO and C_3H_6 oxidation, Runs 16–18 correspond to the combination of CO oxidation and NO reduction, and etc. The effect of the air/fuel equivalence ratio (λ) on the CL response was also examined, where the O_2 concentration was varied while the concentrations of the other gases were fixed constant (Runs 25–29). It must be noted that all the reactions were performed in a dry condition to minimize excessive complications. The presence of water vapor needs to be considered in the future for more practical operation.

Table 2.2. Feed stream composition for combined reactions.

Run	CO (ppm)	O_2 (ppm)	C_3H_6 (ppm)	NO (ppm)	CO_2 (ppm)[a]	λ[b]
13	8000	13000	2000	-	-	1.0
14	12000	24000	4000	-	-	1.0
15	18000	36000	6000	-	-	1.0
16	10000	4000	-	2000	-	1.0
17	16000	6000	-	4000	-	1.0
18	26000	9000	-	8000	-	1.0
19	-	9000	2500	4500	-	1.0
20	-	18000	4700	6300	-	1.0
21	-	27000	6800	7200	-	1.0
22[a]	3250	3500	500	750	5000	1.0
23[a]	6500	7000	1000	1500	10000	1.0
24[a]	13000	14000	2000	3000	20000	1.0
25[a]	13000	7000	2000	3000	20000	0.5
26[a]	13000	10000	2000	3000	20000	0.7
27[a]	13000	16000	2000	3000	20000	1.1
28[a]	13000	18000	2000	3000	20000	1.3
29[a]	13000	21000	2000	3000	20000	1.5

[a] *CO_2 was also introduced as an environmental gas for more practical operation.*
[b] *Air/fuel equivalence ratio*

2.3. Results and discussion

In previous studies, the CL method was mostly employed for reactions which occur at moderate temperatures, whereas its characteristics at higher temperatures (typically over 250 °C) have been hardly reported. Thus, prior to the CL measurement, the background radiation was recorded in a ramping mode in the absence of a catalyst under dry air or pure N_2. The corresponding intensity curves are represented in Figure 2.3a. It was found that the background radiation was negligible when the measurement temperature was below 300 °C, while it increased exponentially with the temperature from 300 to 400 °C. Importantly, the presence or absence of O_2 never affected the intensity of the background radiation, which was evidenced by the intensity ratio in the two distinct atmospheres (Figure 2.3a). This fact revealed that the radiation was neither based on the luminescence from O_2 (*e.g.* $^1O_2 \rightarrow {}^3O_2$) nor the oxidative combustion of contaminants on the substance. Rather, it is attributed to the thermal radiation emitted from the stainless-steel substance (the thermal radiation from the substance more or less exists at a lower temperature, but its wavelength is longer than the cutoff wavelength of the filter below 300 °C).

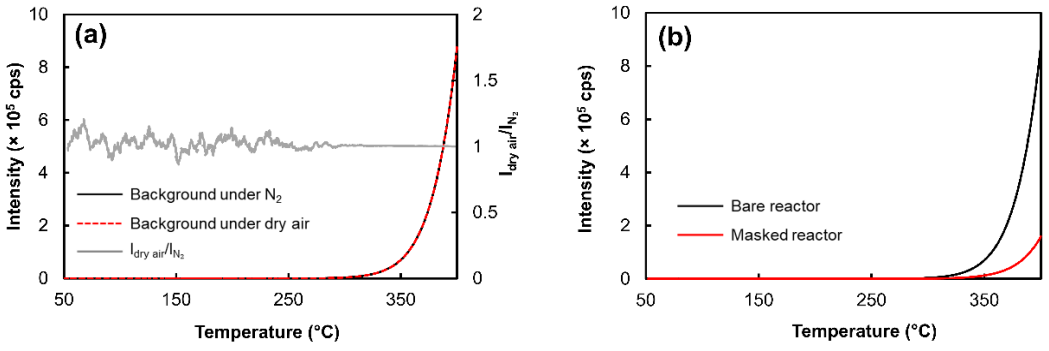

Figure 2.3. Background radiation: (a) Under different atmospheres, and (b) after masking the reactor cell with an aluminum plate (under N_2).

In order to suppress the thermal radiation, the stainless-steel substance of the reactor cell was masked by an aluminum plate. The radiation was compared before and after this modification under N_2 (Figure 2.3b). Since the emissivity of aluminum (0.032–0.15) is much less compared to that of stainless steel (0.80–0.87) [38,39], the introduction of the aluminum mask successfully reduced the intensity of the background radiation. The level of the reduction was roughly five times at 400 °C, and this was close to the ratio of the emissivity between the two substances. Thus, the thermal radiation as the main source of the background radiation was confirmed.

The CL behavior of the four elemental redox reactions was first investigated in a ramping mode. The temperature was increased at 16 °C/min while the gate time was set to 1 s, *i.e.* 3.75 times acquisition at each °C. The background was separately acquired using the same catalyst under He, and it was subtracted from the raw CL intensity. Thus acquired CL curves for the Rh/CeO_2 catalyst are represented in Figure 2.4. All the reactions were found to be CL-active. The CL intensity showed an exponential behavior against the temperature for the four elemental reactions, and this was similar for the other catalysts. The exponential dependence of the CL efficiency on the temperature was analyzed based on the Arrhenius plot and expressed in the form of the activation energy (Figure 2.5). It was around 38–42 kcal/mol irrespective of the elemental reactions, whereas the activation energy of CO oxidation by O_2, for instance, was reported in the range of 22–37 kcal/mol [40,41]. It was considered that the temperature dependence of the CL intensity arises from the combination of the temperature dependence of the reaction rate and that of the CL efficiency. The CL efficiency denotes the combined efficiency of generating a molecule in an excited state and its transition to the ground state through light emission [42]. When the CO oxidation by O_2 was taken as an example, the CL intensity increased from 100 count per second (cps) at 300 °C to

2×10^4 cps at 400 °C, while the CO conversion was improved only by *ca.* 30 % in this temperature range. This fact clearly indicated that the CL efficiency played a major role in the exponential increase of the CL intensity: The CL method becomes more sensitive at a higher temperature.

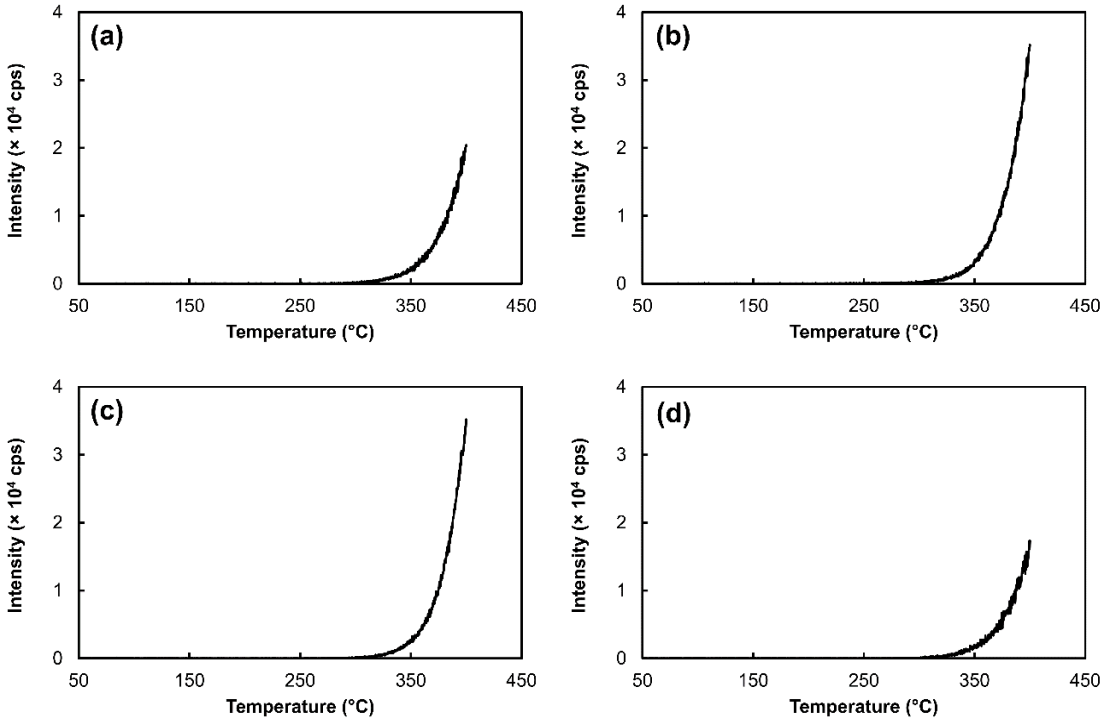

Figure 2.4. Chemiluminescence of four elemental reactions in the ramping mode: (a) CO oxidation by O_2, (b) C_3H_6 oxidation by O_2, (c) CO oxidation by NO, and (d) C_3H_6 oxidation by NO. A Rh/CeO_2 pellet (*ca.* 80 mg) was used in all the reactions.

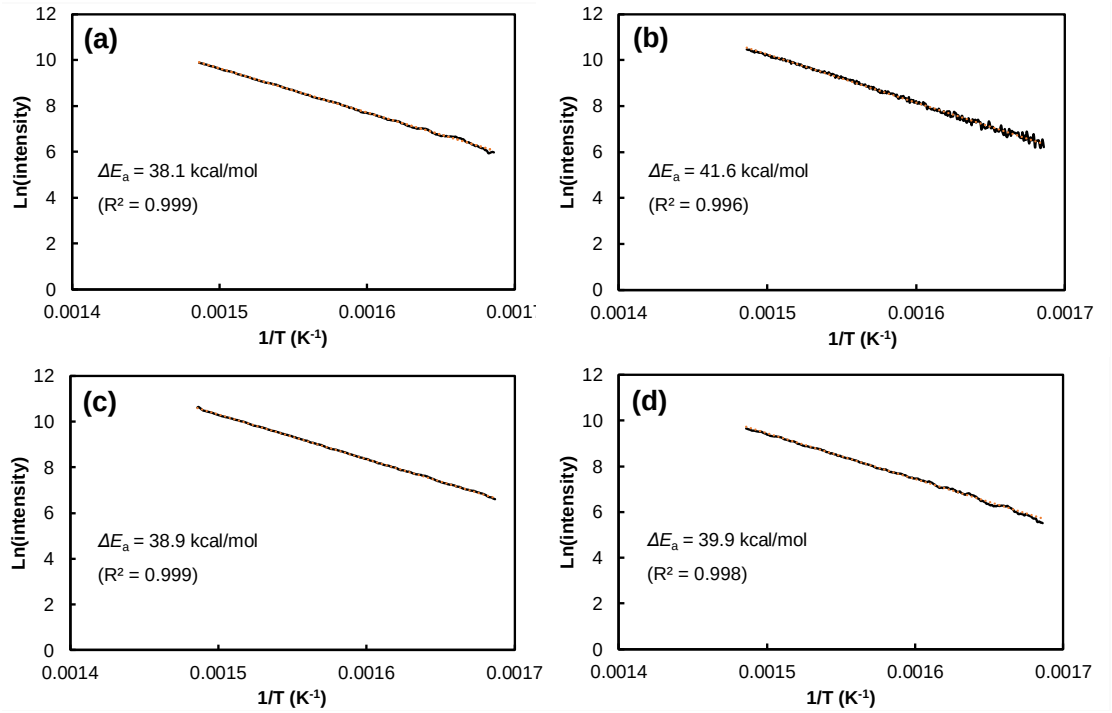

Figure 2.5. Arrhenius plot of the CL intensity: (a) CO oxidation by O_2, (b) C_3H_6 oxidation by O_2, (c) CO oxidation by NO, and (d) C_3H_6 oxidation by NO. A Rh/CeO_2 pellet (*ca.* 80 mg) was used in all the reactions.

Next, the CL measurements were performed in the steady-state mode, where the CL intensity of the four elemental reactions was recorded and compared with the reactant conversion and the CO_2 yield, which were determined by the online GC measurement. The reactant concentrations were altered at individual stoichiometric conditions, while the feed volume was fixed at constant. Figures 2.6 and 2.7 summarize the results obtained at 350 °C and 400 °C for Rh/CeO_2. It was found that the conversion and yield were nearly constant at different reactant concentrations for all the elemental reactions: The reaction rate was proportional to the reactant concentration. To be important, the CL intensity increased linearly through the origin against the reactant concentration. The consistency between the CL intensity and the reaction rate suggested

that the CL emission is a direct product of the elemental reactions, and the detection of the CL emission could be considered as equal to detecting the reactions. In order to further validate this hypothesis, the possibility of an indirect CL process was excluded by conducting additional experiments, where extra O_2, CO_2, and NO were added to the reaction feed and the CL intensity was observed. In Figure 2.8, the CL intensity is shown as a function of the extra concentration of O_2, CO_2, and NO in the CO oxidation by O_2. It became clear that the CL emission was never promoted by the presence of the extra gases in the feed, which excluded the indirect emission *via* energy transfer, and validated that the CL emission in these reactions is a direct process.

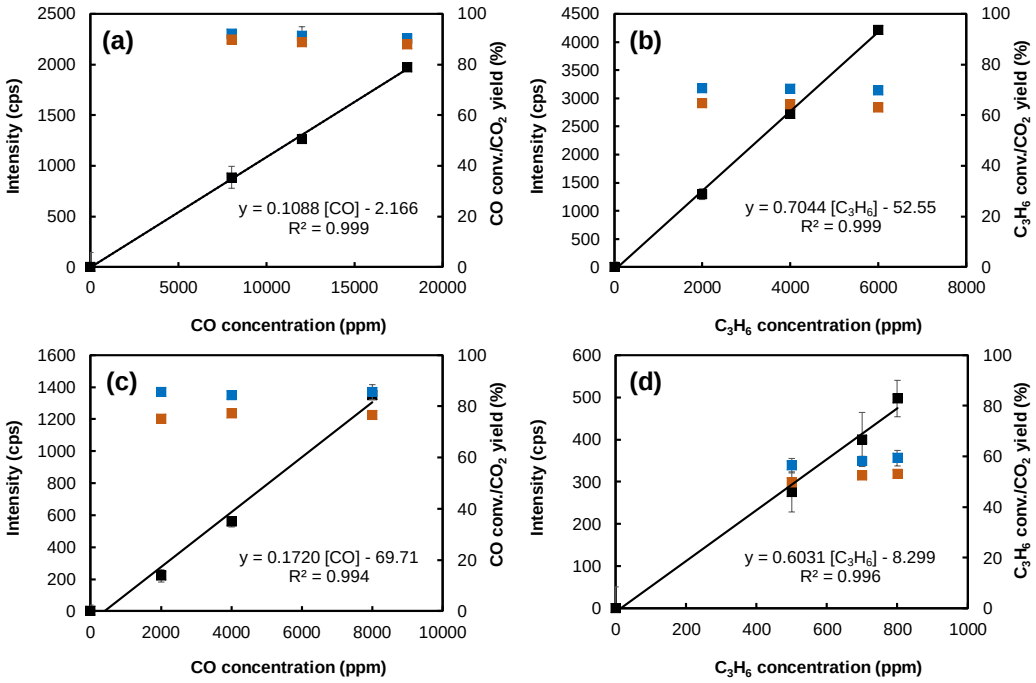

Figure 2.6. Results of the chemiluminescence measurements in the steady-state mode at 350 °C: a) CO oxidation by O_2, b) C_3H_6 oxidation by O_2, c) CO oxidation by NO, and d) C_3H_6 oxidation by NO. Chemiluminescence intensity (■), reagent conversion (■), and product yield (■). A Rh/CeO_2 pellet (*ca.* 80 mg) was used in all the reactions.

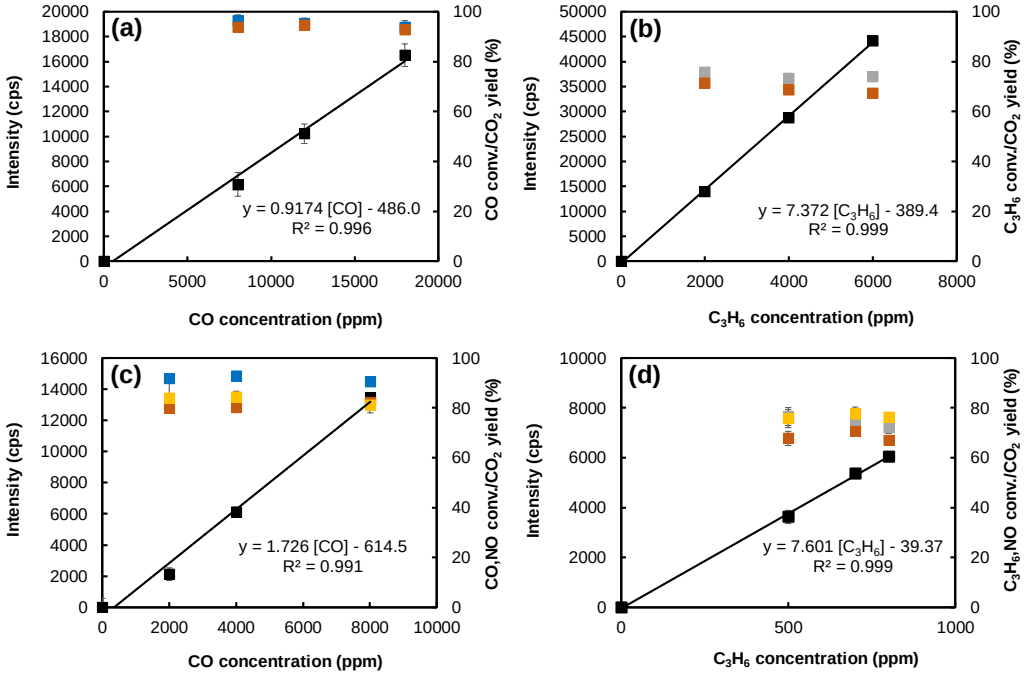

Figure 2.7. Results of the chemiluminescence measurements in the steady-state mode at 400 °C: (a) CO oxidation by O_2, (b) C_3H_6 oxidation by O_2, (c) CO oxidation by NO, and (d) C_3H_6 oxidation by NO. Chemiluminescence intensity (■), CO conversion (■), C_3H_6 conversion (■), NO conversion (■), and CO_2 yield (■). A Rh/CeO_2 pellet (*ca.* 80 mg) was used for all the reactions.

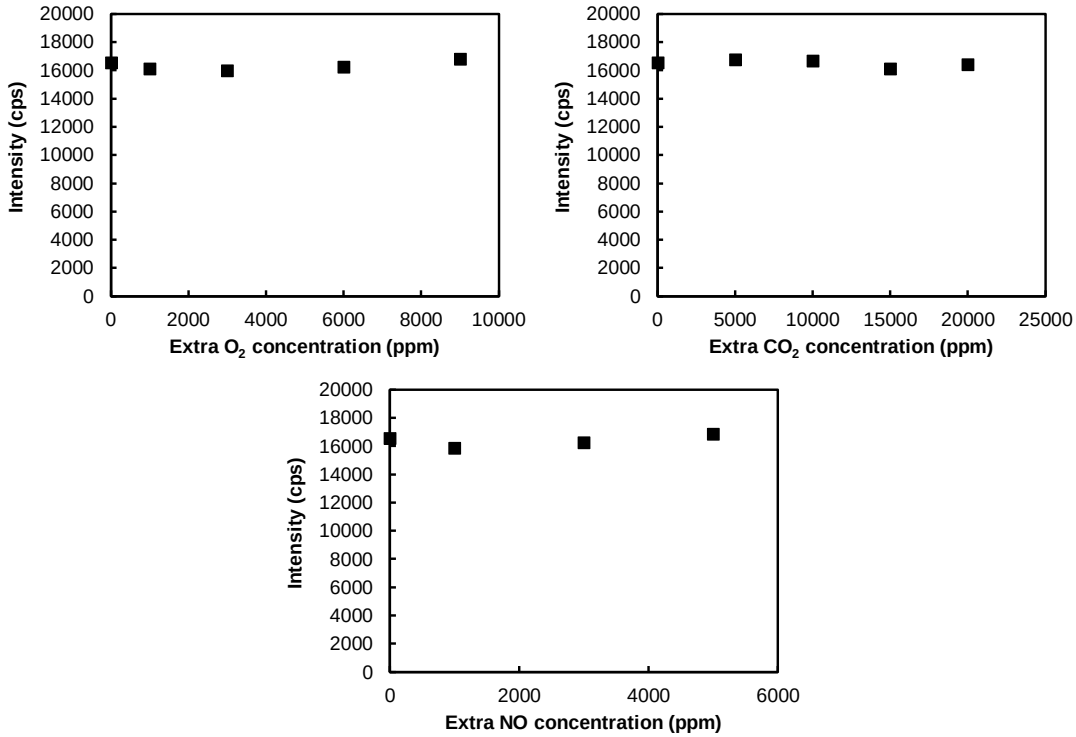

Figure 2.8. Effect of the O_2, CO_2 and NO addition on the chemiluminescence intensity in the CO oxidation by O_2. To the stoichiometric feed (CO = 18000 ppm and O_2 = 9000 ppm), an extra oxidant (O_2/NO) or CO_2 was supplied. The chemiluminescence intensity was recorded in a steady state at 400 °C using a Rh/CeO_2 pellet (*ca.* 80 mg).

In Figures 2.6 and 2.7, the slope of the linear dependence corresponds to the CL emission per reactant concentration. It is interesting that the slope was different among the four elemental reactions, following the order of CO/O_2 < CO/NO < C_3H_6/O_2 ≈ C_3H_6/NO. Considering that the CL emission is production-based, the CL efficiency of the individual elemental reactions was estimated by the normalized CL intensity in term of the CO_2 yield rate at 400 °C (expressed as photon per CO_2 molecule in Table 2.3). The CL efficiency would become identical among the four reactions only when the process of the CL emission was identical (actually not). It was found that the order of

the photon emitted per CO_2 molecule was consistent with the order of the slope values in Figure 2.7. It is known that the CO oxidation by O_2 occurs in the order of i) CO adsorption on catalyst surfaces, ii) O_2 dissociation into O adatoms, and iii) $CO + O \rightarrow CO_2$ [43]. The CL emission must be attributed to the step iii). In the case of the CO oxidation by NO, by-production of N_2O was confirmed by GC. Besides, the heat of reaction in CO/NO was greater than that in CO/O_2. Accordingly, the higher CL efficiency in CO/NO compared to that in CO/O_2 was likely explained by the presence of multiple CL processes and/or the greater heat of reaction in CO/NO. Similar explanation must hold for the far greater CL efficiency in C_3H_6/O_2 and C_3H_6/NO.

Table 2.3. CL efficiency of the four elemental reactions.

Reaction	Photon per CO_2 molecule[a]	Sensitivity[b] (nmol)
CO oxidation by O_2	$2.3 \times 10^{-14} \pm 6.5$ %	72
C_3H_6 oxidation by O_2	$8.7 \times 10^{-14} \pm 3.1$ %	19
CO oxidation by NO	$4.8 \times 10^{-14} \pm 4.7$ %	35
C_3H_6 oxidation by NO	$9.0 \times 10^{-14} \pm 2.9$ %	19

[a] *Estimated based on the CL intensity (in cps) and the corresponding CO_2 yield rate (molecule/s).*
[b] *Estimated based on the CL efficiency and the noise level.*

The detection limit of the CL method was also estimated. Figure 2.9 illustrates the raw steady-state data of CO oxidation by O_2 at 400 °C, where the noise of the CL signal at was observed as around 1000 cps. Based on the photon per CO_2 molecule, the amount of the reaction to overcome the noise level was calculated based on the following equation:

$$Sensitivity = \frac{1000\ counts}{2.3 \times \frac{10^{-14} counts}{molecule} \times 6 \times \frac{10^{23} molecule}{mol}} = 72\ \times 10^{9} mol = 72\ nmol$$

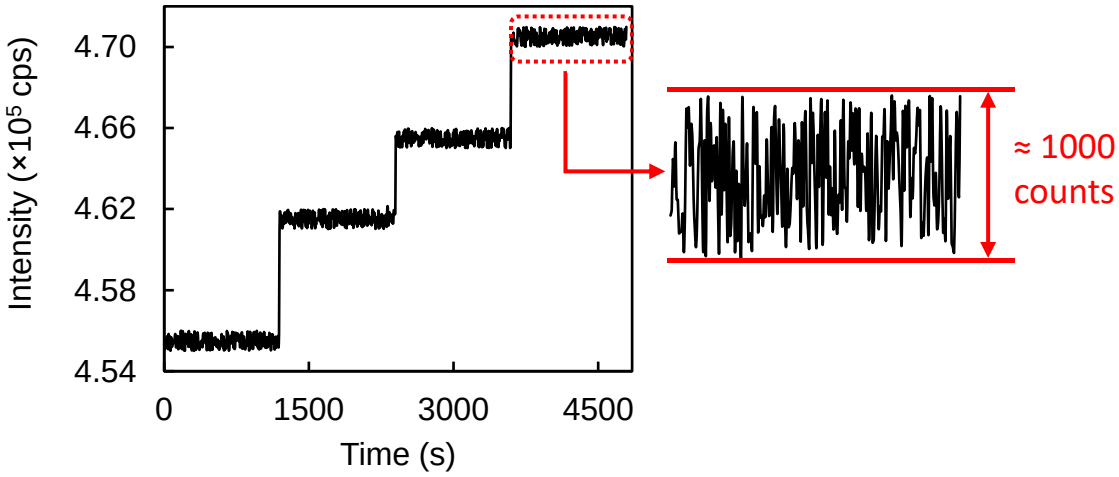

Figure 2.9. Raw CL intensity curve of the steady-state measurement for CO/O_2 at 400 °C.

The sensitivity of the CL method in detecting other reactions was similarly calculated based on their corresponding CL efficiency and the noise level. The results are summarized in Table 2.3, where the obtained sensitivity is in the range of 19–72 nmol. This high sensitivity and in-situ detection without sampling dictated a great potential of the CL method in catalysis sensing.

Followed by the understanding of the CL behavior for the individual elemental reactions, the CL measurement was applied to more complicated reaction systems (termed two-way and three-way conditions, Table 2.2). The CL behavior was examined in two-way stoichiometric conditions, where the CL intensity was measured in the steady-state mode at 400 °C for Rh/CeO_2 while varying the reactant concentrations. Figure 2.10 summarizes the CL intensity for the three types of the two-way systems: i) CO and C_3H_6 oxidation by O_2, ii) CO oxidation by O_2 and NO, and iii) C_3H_6 oxidation by O_2 and NO. In order to consider potential interference among different elemental reactions, the CL intensity was estimated as the sum of the CL intensities of two

elemental reactions. Quantitative agreement was found between the measured and estimated CL intensities, suggesting that the CL emission was still a direct process of individual elemental reactions even when they were combined. From this fact, it was considered that the performance of a catalyst can be estimated by comparing the CL intensity with the theoretical maximum intensity that is calculated based on the full conversion of all gases. The CL measurements were then performed in the three-way conditions. Figure 2.11a plots the CL intensity when the reactant concentrations were scaled, keeping the stoichiometric ratio ($\lambda = 1$). Similar to the two-way conditions, the CL intensity linearly increased along the reactant concentrations. The CL behavior was also investigated in the three-way conditions under rich/lean atmosphere. Figure 2.11b depicts a relationship between the CL intensity and reactant conversion as a function of λ. It was found that the CL intensity decreased in a rich condition ($\lambda < 1$), while kept almost constant in a lean condition ($\lambda > 1$). This result is reasonable in a sense that the oxidation (or more roughly saying, CO_2 production) is the main cause of the CL emission: In a lean condition, the conversion of CO and C_3H_6 was nearly constant so that further addition of O_2 did not add the CL emission. In other words, the CL method is not suitable to detect NO reduction in a lean condition.

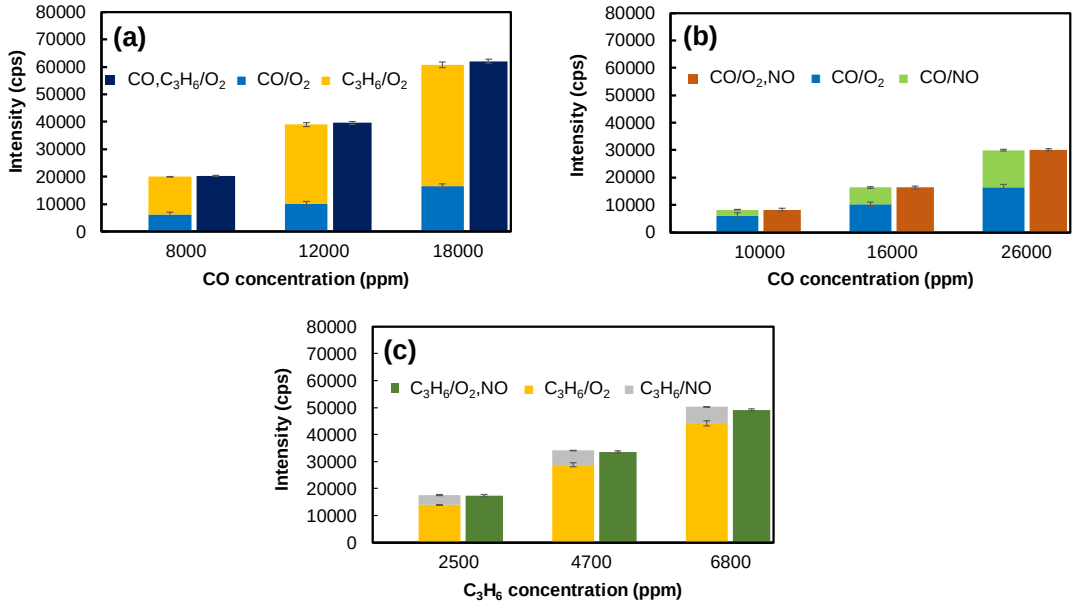

Figure 2.10. CL intensity in two-way conditions: (a) CO and C_3H_6 oxidation by O_2, (b) CO oxidation by O_2 and NO, and (c) C_3H_6 oxidation by O_2 and NO. The measurements were performed at 400 °C using Rh/CeO_2 pellet (*ca.* 80 mg). The stacked columns correspond to the estimated CL intensity as a sum of the CL intensities of two elemental reactions.

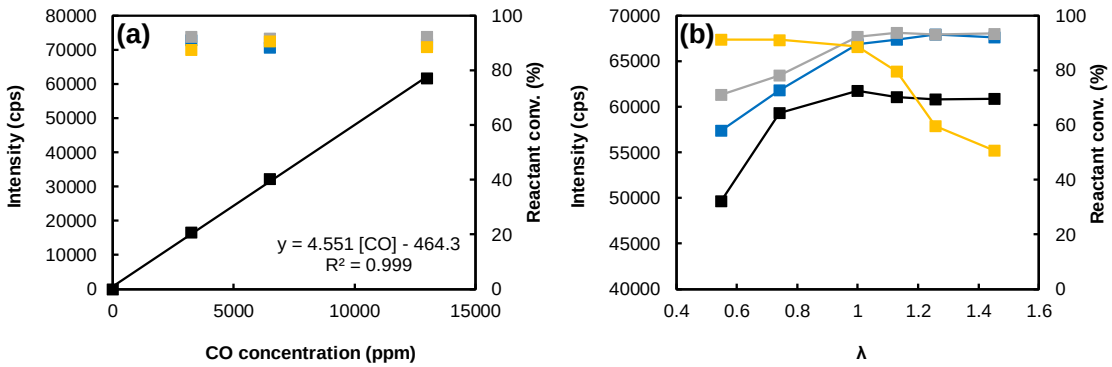

Figure 2.11. Results of the chemiluminescence measurements in three-way conditions at 400 °C: (a) The reactant concentration were scaled at λ =1, and (b) the air/fuel equivalence ratio (λ) was altered at a fixed fuel concentration. Chemiluminescence intensity (■), CO conversion (■), C_3H_6 conversion (■), and NO conversion (■). A Rh/CeO_2 pellet (*ca.* 80 mg) was used.

Lastly, the utilization of the CL method was demonstrated for rapid catalyst screening. Employing a series of Rh catalysts with different support materials (SiO_2, CeO_2, ZrO_2, Al_2O_3, TiO_2) and pristine SiO_2 as an inactive reference, the CL intensity after background subtraction was compared in the oxidation of C_3H_6 by O_2 at 400 °C where $[C_3H_6]$ = 6000 ppm (Figure 2.12). A good correlation was found between the CL intensity and the C_3H_6 conversion: The CL intensity increased according to the catalyst activity in the order of Rh/SiO_2 > Rh/Al_2O_3 > Rh/CeO_2 > Rh/ZrO_2 > Rh/TiO_2 > SiO_2. These results further supported the CL as a promising technique for rapid catalyst screening.

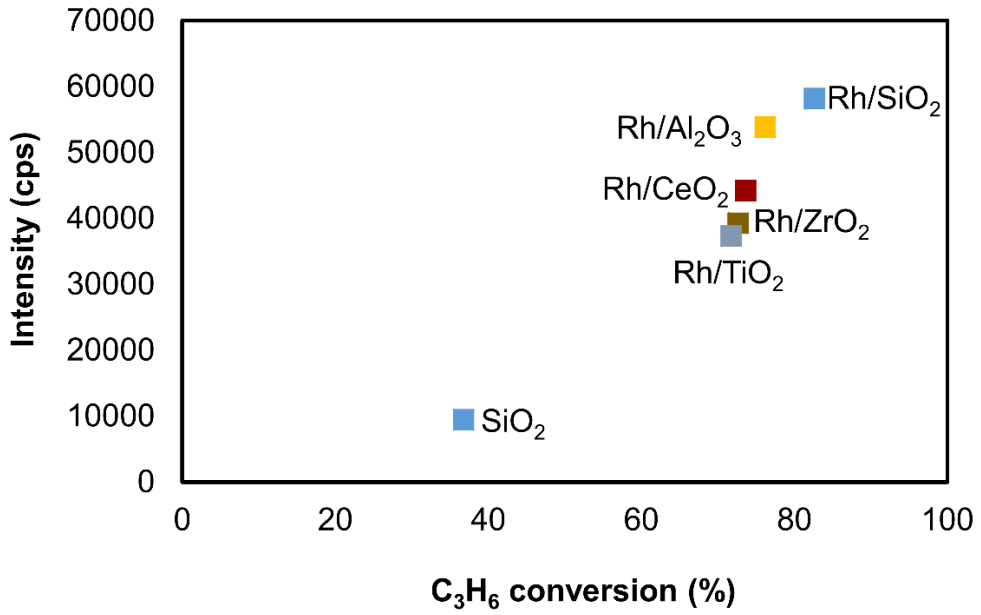

Figure 2.12. Correlation between the chemiluminescence intensity and the performance of different Rh catalysts in C_3H_6 oxidation by O_2 at 400 °C.

2.4. Conclusions

In order to explore chemiluminescence (CL) as a potential technique for rapid catalyst screening in catalytic converters, the CL behavior of catalytic oxidation of CO and C_3H_6 by O_2 and/or NO under both stoichiometric and non-stoichiometric conditions was thoroughly studied. It was found that the CL emission became more intensive at a higher temperature due to the exponential temperature dependence of the CL efficiency. The linear correlation between the CL intensity and the reaction rate in a steady state revealed that the CL emission is a production-based process; therefore, the detection of the CL emission could be regarded as equal to the detection of the reaction. This was true even when elemental reactions were combined for more practical two-way and three-way conditions. The feasibility of the CL method for rapid catalyst screening was successfully demonstrated in the C_3H_6 oxidation by O_2 using a series of Rh-based catalysts, where a good linear correlation between the CL intensity and the C_3H_6 conversion was observed.

References

[1] S. Matsumoto, Recent advances in automobile exhaust catalysts, Catal. Today, 90 (2004), 183–190.

[2] J. Kašpar, P. Fornasiero, N. Hickey, Catal. Today, 77 (2003), 419–449.

[3] L. Lan, S. Chen, M. Zhao, M. Gong, Y. Chen, J. Mol. Catal. A: Chem., 394 (2014), 10–21.

[4] M. Shelef, Catal. Rev., 11 (1975), 1–40.

[5] H.S. Gandhi, A.G. Piken, M. Shelef, R.G. Delosh, Laboratory Evaluation of Three-Way Catalysts, SAE Technical Paper 760201, 1976.

[6] H. He, H.X. Dai, L.H. Ng, K.W. Wong, C.T. Au, J. Catal., 206 (2002), 1–13.

[7] F.C. Moates, M. Somani, J. Annamalai, J.T. Richardson, D. Luss, R.C. Willson, Ind. Eng. Chem. Res., 35 (1996), 4801–4803.

[8] S. Senkan, Angew. Chem. Int. Ed., 40 (2001), 312–329.

[9] N.E. Olong, K. Stowe, W.F. Maier, Appl. Catal. B: Environ., 74 (2007), 19–25.

[10] M.T. Reetz, M.H. Becker, K.M. Kühling, A. Holzwarth, Angew. Chem. Int. Ed., 37 (1998), 2647–2650.

[11] A. Holzwarth, H.W. Schmidt, W.F. Maier, Angew. Chem. Int. Ed., 19 (1998), 2644–2647.

[12] J. Klein, W. Stichert, W. Strehlau, A. Brenner, D. Demuth, S.A. Schunk, H. Hibst, S. Storck, Catal. Today, 81 (2003), 329–335.

[13] J. Loskyll, K. Stoewe, W.F. Maier, ACS Comb. Sci., 14 (2012), 295–303.

[14] B. Weidenhof, M. Reiser, K. Stöwe, W.F. Maier, M. Kim, J. Azurdia, E. Gulari, E. Seker, A. Barks, R.M. Laine, J. Am. Chem. Soc., 131 (2009), 9207–9219.

[15] E.N. Lewis, P.J. Treado, R.C. Reeder, G.M. Story, A.E. Dowrey, C. Marcott, I.W. Levin, Anal. Chem., 67 (1995), 3377–3381.

[16] C.M. Snively, S. Katzenberger, G. Oskarsdottir, J. Lauterbach, Opt. Lett., 24 (1999), 1841–1843.

[17] C.M. Snively, G. Oskarsdottir, J. Lauterbach, Angew. Chem. Int. Ed., 40 (2001), 3028–3030.

[18] P. Kubanek, O. Busch, S. Thomson, H.W. Schmidt, F. Schüth, J. Comb. Chem., 6 (2004), 420–425.

[19] G. Li, D. Hu, G. Xia, J.M. White, C. Zhang, Rev. Sci. Instrum., 79 (2008), 074101.

[20] H. Su, E.S. Yeung, J. Am. Chem. Soc., 122 (2000), 7422–7423.

[21] H. Su, Y. Hou, R.S. Houk, G.L. Schrader, E.S. Yeung, Anal. Chem., 73 (2001), 4434–4440.

[22] J. Zetterberg, S. Blomberg, J. Gustafson, J. Evertsson, J. Zhou, E.C. Adams, P.-A. Carlsson, M. Aldén, E. Lundgren, Nat. Commun., 6 (2015), 7076.

[23] P. Cong, R.D. Doolen, Q. Fan, D.M. Giaquinta, S. Guan, E.W. McFarland, D.M. Poojary, K. Self, H.W. Turner, W.H. Weinberg, Angew. Chem. Int. Ed., 38 (1999), 483–488.

[24] H. Wang, Z. Liu, J. Shen, J. Comb. Chem., 5 (2003), 802–808.

[25] M. Richter, M. Langpape, S. Kolf, G. Grubert, R. Eckelt, J. Radnik, M. Schneider, M.M. Pohl, R. Fricke, Appl. Catal. B: Environ., 36 (2002), 261–277.

[26] N. Aratani, I. Katada, K. Nakayama, M. Terano, T. Taniike, Polym. Degrad. Stab., 121 (2015), 340–347.

[27] X. Wang, N. Na, S.C. Zhang, Y.Y. Wu, X.R. Zhang, J. Am. Chem. Soc., 129 (2007), 6062–6063.

[28] F. Teng, W.Q. Yao, Y.F. Zhu, M.D. Chen, R.H. Wang, S.I. Mho, D.D. Meng, J. Phys. Chem. C, 113 (2009), 3089–3095.

[29] N. Na, S. Zhang, X. Wang, X. Zhang, Anal. Chem., 81 (2009), 2092–2097.

[30] M. Breysse, B. Claudel, L. Faure, M. Guenin, R.J.J. Williams, T. Wolkenstein, J. Catal., 45 (1976), 137–144.

[31] M.M. Rauhut, Acc. Chem. Res., 2 (1969), 80–87.

[32] N. Siraj, B. El-Zahab, S. Hamdan, T.E. Karam, L.H. Haber, M. Li, S.O. Fakayode, S. Das, B. Valle, R.M. Strongin, G. Patonay, H.O. Sintim, G.A. Baker, A. Powe, M. Lowry, J.O. Karolin, C.D. Geddes, I.M. Warner, Anal. Chem., 88 (2016), 170–202.

[33] F. Teng, T.G. Xu, Y. Teng, S.H. Liang, B.G. Gauge, J. Lin, W.Q. Ya, R.L. Zong, Y.F. Zhu, Y.F. Zheng, 42 (2008), 3886–3892.

[34] L. Zhang, Y. Chen, N. He, C. Lu, Anal. Chem., 86 (2014), 870–875.

[35] L. Zhang, S. Wang, C. Lu, Anal. Chem., 87 (2015), 7313–7320.

[36] D. Baker, General Chemistry, 5th ed. (Ebbing, Darrell D.) Journal of Chemical Education 74 (1997), 1049.

[37] M.W. Chase Jr, NIST-JANAF Themochemical Tables. 4th Edition, J. Phys. Chem. Ref. Data, Monograph 9, 1–1951.

[38] W.F. Gale, T.C. Totemeier, Smithells metals reference book (8th ed.), Elsevier, Oxford (2004).

[39] J. Bartl, M. Baranek, Meas. Sci. Rev., 4 (2004), 31–36.

[40] C.H.F. Peden, D.N. Belton, S.J. Schmieg, J. Catal., 155 (1995), 204–218.

[41] J.R. Renzas, Rhodium catalysts in the oxidation of CO by O_2 and NO: Shape, composition, and hot electron generation, 2010.

[42] T.H. Fereja, A. Hymete, T. Gunasekaran, ISRN Spectrosc., 2013 (2013), 1–12.

[43] Z.P. Liu, P. Hu, Top. Catal., 28 (2004), 71–78.

Chapter 3

Development of Chemiluminescence Imaging Instrument for Rapid Catalysts Screening in Gas-Phase Reaction: A Case Study of Hydrocarbon Oxidation

Abstract.

Herein, I describe the development of a chemiluminescence (CL) imaging instrument to realize rapid catalysts screening for high-temperature gas-phase reactions. The CL instrument was designed by combining a reactor cell for gaseous catalysis and an electron multiplying CCD camera for single photon detection in the form of images. It was employed for imaging the CL emission over catalysts during the oxidation of C_3H_6, which is one of the major processes in catalytic converters for automotive emission control. Under steady-state conditions, the reaction rate was linearly correlated with the brightness of a catalyst (quantified as the CL intensity) from its continuously captured CL image, confirming the ability of the CL imaging method to detect the reaction. The feasibility of the CL imaging method in rapid catalysts screening was confirmed through a linear correlation between the reaction rate and the CL intensity over five different oxide-supported Rh catalysts. Finally, when the five catalysts were imaged at once in parallel CL imaging measurements, the obtained catalyst ranking based on the CL intensity was found consistent with their corresponding catalytic performance.

Keywords. Chemiluminescence imaging, parallel catalyst screening, high-temperature gas-phase reaction.

3.1. Introduction

The development of a performant heterogeneous catalyst relies on the exploration of a large parametric space of catalyst formulations and process conditions by repeated cycles of catalyst preparation and catalyst evaluation. Such a development is significantly aided by a variety of combinatorial preparation methods [1–5], while simple and straightforward techniques for rapid screening of heterogeneous catalysts are still limited by the product analysis [6–8]. It is known that several heterogeneously catalyzed gas-phase reactions accompany the emission of chemiluminescence (CL), which is attributed to the light emission due to the relaxation of excited molecular species produced in the course of exothermic reactions [9–12]. The detection of CL emitted from the surface of solid catalysts during chemical reactions is regarded as a potentially powerful technique for rapid screening of heterogeneous catalysts. Conceptually, the CL detection requires a reactor cell equipped with only a transparent window and a light detection unit. A variety of catalysts arranged in an array could be simultaneously and in-situ evaluated through imaging at typical time resolution of seconds. The application of the CL imaging technique for rapid screening of heterogenous catalysts was pioneered by the group of Zhang [13]. They deposited an array of five supported Au nanocatalysts on a ceramic chip, and applied the CL imaging during the oxidation of CO at 160 °C. They found that the CL intensity from the five catalysts well correlated with their activity, which was separately determined based on gas chromatography (GC). In a subsequent publication by the same group, the CL emission from 16 catalysts were successfully imaged [14]. Despite these promising results, the potential of the CL imaging technique has not been investigated for gas-phase catalysis other than the low-temperature CO oxidation. Especially, the feasibility of the technique in high-temperature reactions has to be evaluated, where the thermal

radiation from the reactor, as well as from catalysts is expected to overlap with the CL emission in terms of both the intensity and the wavelength. Examples of important high-temperature reactions include the reactions of the three-way catalytic converters, the oxidative coupling of methane, and dry reforming, which typically require a temperature above 350 °C for successful operation.

In Chapter 2, I attempted to understand the CL behavior of catalytic oxidation of CO and C_3H_6 in the presence of O_2 and/or NO in relation to the catalytic converters. Reactions were performed under both stoichiometric and non-stoichiometric conditions, typically at 400 °C. The CL emission was in-situ captured using a photon multiplier, and an on-line GC determined the composition of the effluent gas. At a constant temperature, a linear relationship between the CL intensity and the reaction rates was prevailed [12], which suggested that the CL emission was a direct product of these reactions. Moreover, a good correlation between the CL intensity and reactant conversion in C_3H_6 oxidation by O_2 with a series of oxide-supported Rh catalysts enabled the ranking of catalyst activity. Thus, Chapter 2 validates that the detection of CL emission is powerful to detect high-temperature reaction, and therefore it has the potential for rapid screening of heterogeneous catalysts. Accordingly, this chapter aims to develop a parallel catalyst screening instrument on the basis of CL-based array imaging. The CL imaging instrument was developed to capture the CL images of catalyst samples during a high-temperature reaction by an ultra-sensitive, low light electron multiplying charged-coupled device (EmCCD) camera. It can be connected to a gas mixer and a GC for continuously supplying the reactant gas mixture and analyzing the composition of the effluent gas. This chapter explains all the technological advancements in developing the CL imaging instrument using C_3H_6 oxidation as a case

study. The screening results of a series of oxide-supported Rh catalysts with the developed instrument are also discussed.

3.2. Experimental

3.2.1. Materials

Oxide-supported Rh catalysts were prepared by wet impregnation, in which five different oxide supports were employed: γ-Al_2O_3 (PURALOX SCFa100, SASOL, BET surface area of 106 m^2/g), CeO_2 (HSA-20, RODIA, BET surface area of 133 m^2/g), monoclinic ZrO_2 (RC-100, Daiichi Kigenso Kagaku Kogyo, BET surface area of 99 m^2/g), SiO_2 (Aerosil 50, EVONIK, BET surface area of 61 m^2/g), and TiO_2 (Aeroxide P25, EVONIK, BET surface area of 55 m^2/g). A specified amount of support powder was impregnated with an aqueous solution of $Rh(NO_3)_2$, followed by evaporation to remove the solvent. The solid was dried at 120 °C for 15 h and calcined in air at 500 °C for 2 h. The metal loading of these catalysts was fixed at 1.0 wt.%.

3.2.2. Catalyst characterization

The oxide-supported Rh catalysts were characterized by X-ray diffraction (XRD) and transmission electron microscopy (TEM). XRD patterns of the fresh catalysts were recorded on Rigaku SMARTLAB at a voltage of 40 kV and a current of 30 mA using Cu Kα (1.5418 Å) radiation. A step scan mode was employed in the 2θ range of 15–70° at the speed of 2°/min and the step size of 0.01°. TEM observation was performed on Hitachi H-7650 operating at an acceleration voltage of 100 kV.

3.2.3. Instrumental

The developed CL imaging instrument is illustrated in Figure 3.1, which consists of two major units: A detection unit and a reaction cell unit. In the detection unit, the

CL signal emitted during the reactions is continuously imaged by an EmCCD camera (iXon Ultra 888, Andor Technology Ltd.) that is capable of detecting single photon events without an image intensifier. The employed EmCCD camera exhibits superior sensitivity by maximizing quantum efficiency of > 95% (a measure of a camera's ability to capture valuable photons and to subsequently convert them to photoelectrons) and minimizing system noise. Moreover, the EmCCD camera has image resolution of as high as 13 μm. An UV/IR cut filter (cutoff wavelengths of 400 and 650 nm) is attached to the camera lens to cutoff infrared thermal radiation, which becomes evident when the measurement is carried out over 250 °C. The reaction cell unit is basically made of stainless steel and symmetrically equipped with gas ports (gas inlet/outlet). An Al block was placed inside the reactor to minimize the thermal radiation from the reactor substance. A catalyst is positioned in the center of the cell and closed with a transparent quartz viewport (inner diameter of 38 mm, outer diameter of 70 mm).

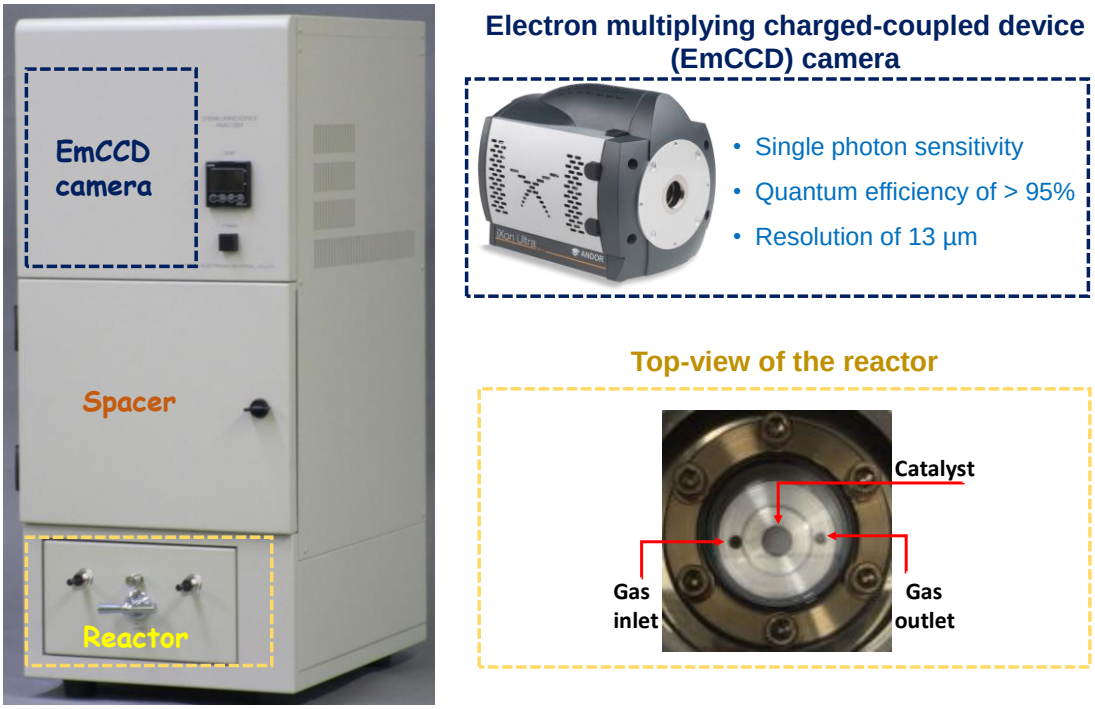

Figure 3.1. Developed chemiluminescence imaging instrument.

CL images were continuously captured for every 10 s, where the exposure time of the EmCCD camera (the period during which the EmCCD collects light prior to readout) was set as 5 s. The employed camera has a 1024 × 1024 sensor format and 13 μm pixel size. A catalyst bed of 10 mm in diameter occupies approximately 464 pixels in an image. A time series of CL images were analyzed by ImageJ software. Here, the time-resolved CL intensity is given by the analysis of an image at a certain moment, where the intensity is averaged over the pixels within the circular area of the catalyst sample. Then, the CL intensity at each condition is derived as the average of the time-resolved CL intensity for all the images captured during the corresponding condition.

3.2.4. Catalytic test

The catalytic oxidation of C_3H_6 in the presence of O_2 was implemented under different stoichiometric conditions (Table 3.1). A catalyst was first in-situ calcined at 400 °C under dry air in the reaction cell. Following this, steady-state measurements were performed at 350 °C, where the CL images and GC data were acquired at the individual conditions (Runs 1–4). When multiple catalysts were evaluated at the same time, both the total flow rate and the concentration of reactant gases were increased to acquire sufficient CL intensities during the reaction (Runs 5–8).

Table 3.1. Feed stream composition of C_3H_6 oxidation by O_2 under stoichiometric conditions.[a]

Run[b]	O_2 (%)	C_3H_6 (%)	Total flow rate (mL/min)
1	0	0	100
2	0.9	0.2	
3	1.8	0.4	
4	2.7	0.6	
5	0	0	400
6	4.5	1.0	
7	6.0	1.5	
8	9.0	2.0	

[a] *He was used as a balance gas and carrier gas.*

[b] *Runs 1–4 for single-catalyst measurements and Runs 5–8 for multiple-catalyst measurements.*

3.3. Results and discussion

The series of synthesized oxide-supported Rh catalysts were characterized with XRD and TEM. The XRD patterns of oxide-supported Rh catalysts are presented in Figure 3.2. Figure 3.2a shows the XRD pattern of Rh/CeO_2 catalyst, in which all the diffraction peaks are consistent with the characteristic peaks of well-crystallized fluorite-type phase of CeO_2 (JCPDS card 04-0593). The XRD pattern of Rh/ZrO_2 (Figure 3.2b) illustrates that the crystal structure of the catalyst is purely composed of the monoclinic phase (JCPDS card 36-0420). The XRD patterns of the Rh/TiO_2 are shown in Figure 3.2c, in which bicrystalline structure comprising of anatase (JCPDS card 21-1272) and rutile (JCPDS card 21-1276) phases was evident. In case of Rh/Al_2O_3 catalyst (Figure 3.2d), all the diffraction peaks can be indexed to the cubic structure of γ-Al_2O_3 (JCPDS card 29-0063). A broad diffraction peak at 2θ of 23° was evident in the XRD pattern of Rh/SiO_2 (Figure 3.2e), typically attributed to the amorphous SiO_2. The most important finding in Figure 3.2 is that Rh phases were not detected by XRD for any catalysts, indicating the fine dispersion, and very small metal particles due to the small amount of Rh loading (1 wt.%). This observation is in good agreement with the Rh-impregnated automotive catalysts in literature [15–19].

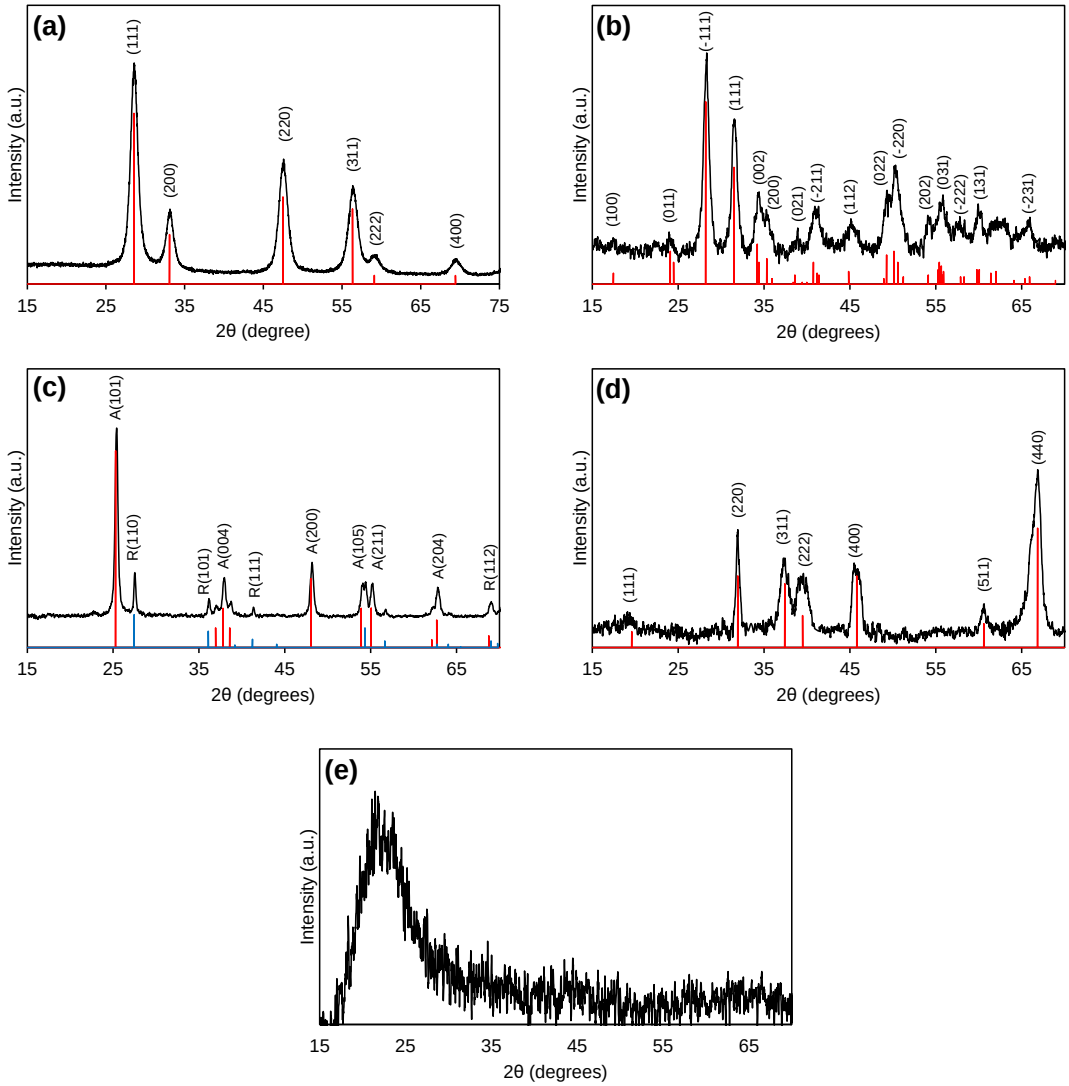

Figure 3.2. XRD patterns of oxide-supported Rh catalysts: (a) Rh/CeO_2, (b) Rh/ZrO_2, (c) Rh/TiO_2, (d) Rh/Al_2O_3, and (e) Rh/SiO_2.

TEM images of the Rh-based catalysts are shown in Figure 3.3. No explicit Rh can be visually identified on the TEM images of Rh/CeO_2 (Figure 3.3a), Rh/ZrO_2 (Figure 3.3b), and Rh/Al_2O_3 (Figure 3.3d) due to the low metal loading and the high dispersion on the surface of the supports, which is consistent with the XRD analysis results. In case of Rh/TiO_2 and Rh/SiO_2, small Rh nanoparticles of approximately 1–2

nm as well as their agglomeration were observed, which is probably attributed to the low surface area of the supports. To recall, the BET surface area of CeO_2, ZrO_2, TiO_2, Al_2O_3 and SiO_2 are 133, 99, 55, 106 and 61 m^2/g, respectively.

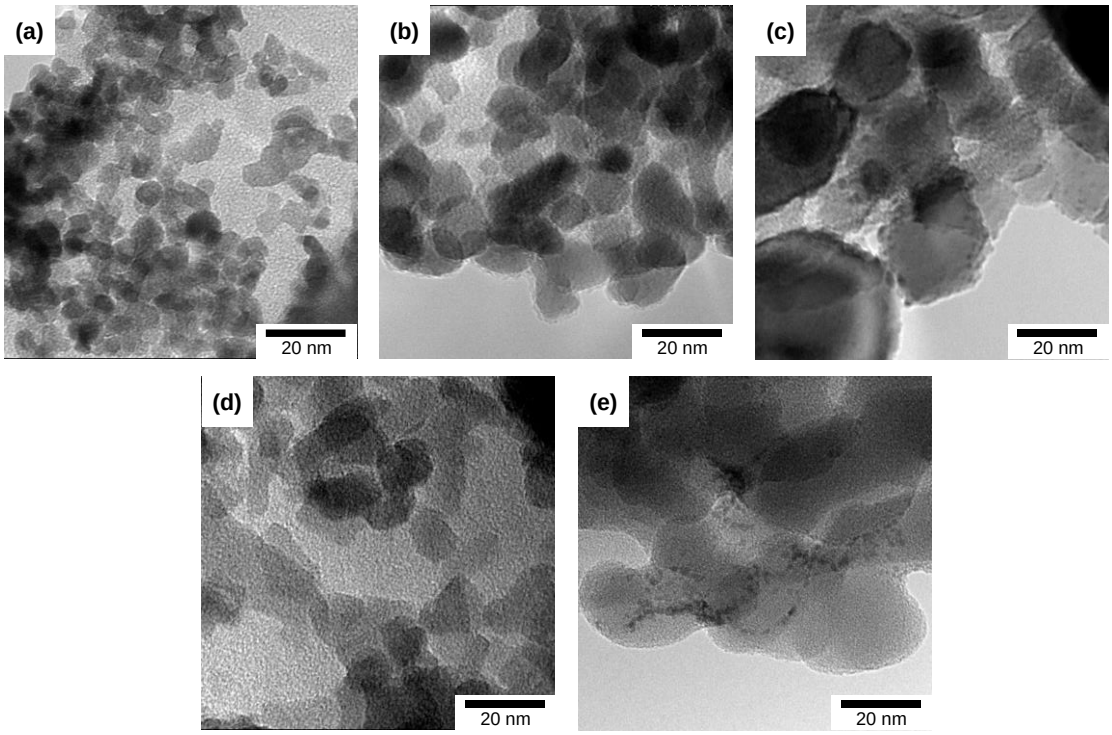

Figure 3.3. TEM images of oxide-supported Rh catalysts: (a) Rh/CeO_2, (b) Rh/ZrO_2, (c) Rh/TiO_2, (d) Rh/Al_2O_3, and (e) Rh/SiO_2.

In order to demonstrate the feasibility of the CL imaging technique in detecting the reaction, steady-state measurements were performed at 350 °C, where the concentration of reactants in the fixed feed volume were altered at individual stoichiometric conditions. To be comparable, a Rh/CeO_2 catalyst with a bed diameter of 10 mm (equivalent to 80 mg) was employed, as the same catalyst was used in Chapter 2 to understand the CL behaviour of the reaction using a photon multiplier. Figure 3.4a shows the representative images captured by the EmCCD camera during Runs 1–4 in

Table 3.1. It is evident that the catalyst surface could be clearly observed in the CL images at different reactant concentrations as a bright center spot. The brightness of the catalyst surface at 0 ppm and the two bright dots at the positions of the gas inlet and outlet are attributed to the thermal radiation from the catalyst surface and the stainless-steel substance of the reactor cell. The thermal radiation from these substances was higher than that from the aluminum block (emissivity of aluminum, CeO_2, and stainless steel are 0.032–0.15, 0.60–0.47, and 0.80–0.87, respectively) [12,20–22]. The brightness of the catalyst surface was found to increase from left to right (Figure 3.4a) along with the increase of the concentration of the reactants, suggesting that not only the thermal radiation from the catalyst but also the CL emission due to the catalysis could be imaged. The light intensity was extracted from the continuously captured images using the ImageJ software and plotted against the reaction time and the C_3H_6 concentration in Figure 3.4b. The extracted CL intensity from the images directly reflected the alternation in the feed concentrations, shown as the stepwise increase of the CL intensity. Figure 3.4c shows a quantitative relationship among the reactant concentration, the CL intensity, the C_3H_6 conversion, and the CO_2 yield. First of all, the conversion and yield were nearly constant and identical at different feed concentrations, indicating that the reaction rate increased proportionally to the reactant concentration at the full selectivity for CO_2. Importantly, a linear relationship was obtained between the CL intensity and the reactant concentration in Figure 3.4c. The correlation between the extracted CL intensity and the reaction rate suggests that the CL imaging measurement can be regarded as an effective tool for detecting the gas-phase rection.

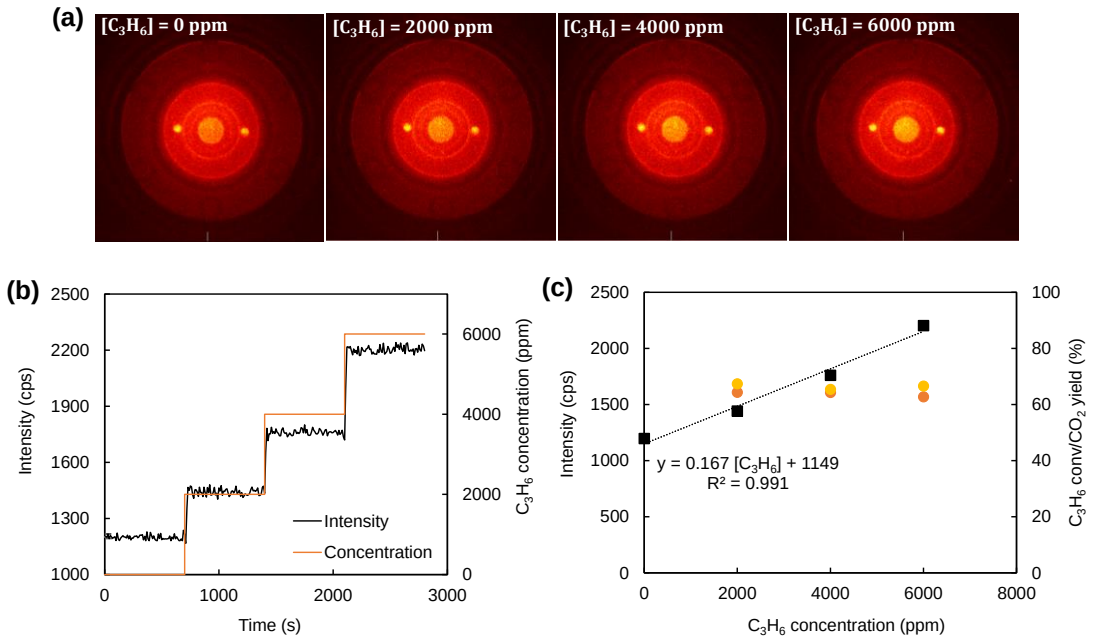

Figure 3.4. Results of chemiluminescence imaging in C_3H_6 oxidation over 80 mg of Rh/CeO_2 catalyst with a bed diameter of 10 mm at 350 °C: (a) Images captured at different concentration of C_3H_6, (b) plot of the raw intensity against the time and C_3H_6 concentration, and (c) development of chemiluminescence intensity (■), C_3H_6 conversion (●), and CO_2 yield (●) along with the C_3H_6 concentration.

From the results of the steady-state measurements, the detection limit of the CL imaging technique was determined. Since the CL emission is regarded as a production-based process, the CL efficiency of the C_3H_6 oxidation reaction was estimated based on the CL intensity (in cps) and the corresponding CO_2 yield rate (in molecule/s), which was $1.3 \times 10^{-15} \pm 14.0$ % photon per CO_2 molecule. On the other hand, the noise of the CL signal at 350 °C was around 70 cps (Figure 3.5). The amount of the reaction to overcome the noise level was then calculated to be approximately 90 nmol, which is comparable to the detection limit (19–72 nmol) of the photon multiplier employed in

the CL study in Chapter 2. Thus, high sensitivity of the CL imaging technique was assured.

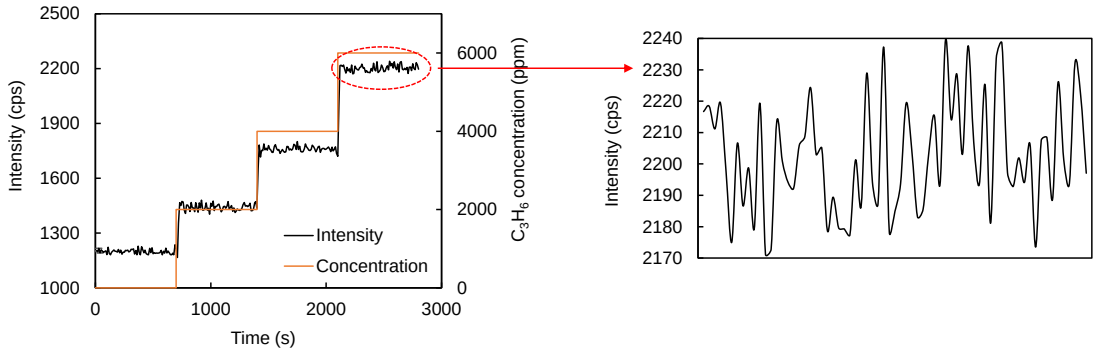

Figure 3.5. Noise level of steady-state CL imaging measurement at 350 °C.

Next, the impact of focal length adjustment on CL imaging was investigated. For the distance of 300 mm between the catalyst bed of 10 mm diameter, and the EmCCD camera having a 1024 × 1024 sensor format and 13 µm pixel size, the approximate focal length was calculated as 21 mm. Consequently, the camera lens (Xenon 0.95/17) with the focal length of 17 mm was replaced by a new lens (Xenon 0.95/25) with the focal length of 25 mm. Figure 3.6 shows the effect of focal length adjustment on the CL imaging in C_3H_6 oxidation at the highest reactant concentration (*i.e.* Run 4 in Table 3.1) over the Rh/CeO_2 catalyst at 350 °C. The distribution of CL intensity profiles obtained through the center of the catalyst became narrower within the catalyst area with the appearance of brighter edges when the new lens was used (Figure 3.6b vs. Figure 3.6a). The intensity error percentage within the catalyst area also decreased from *ca.* 13% to 9%. Moreover, the CL signal with improved intensity was acquired by the new lens (Figure 3.6c), which could be attributed to the less contribution from the substrate radiation when the image focus was enhanced. Therefore, the Xenon 0.95/25 lens was employed for all the subsequent measurements.

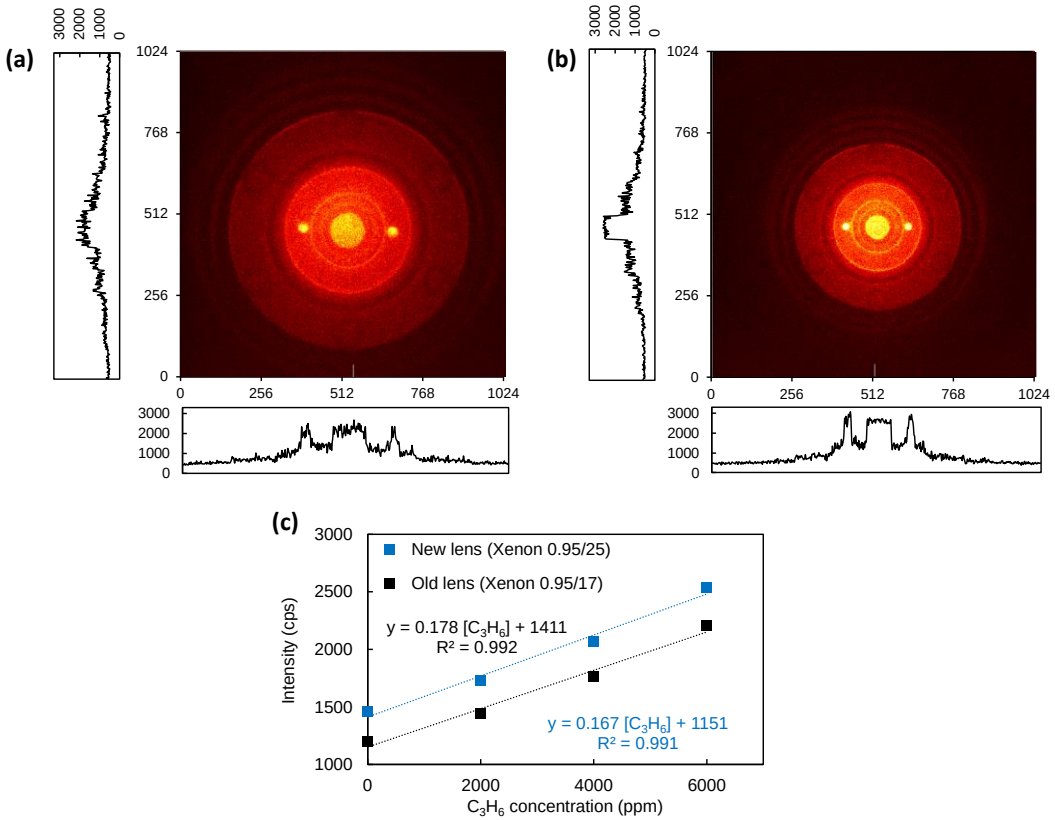

Figure 3.6. Effect of focal length adjustment on chemiluminescence imaging. The imaging was performed in C_3H_6 oxidation ([C_3H_6] = 6000 ppm) at 350 °C over a Rh/CeO_2 catalyst using (a) old lens (Xenon 0.95/17), (b) new lens (Xenon 0.95/25), and (c) comparison of chemiluminescence intensity development along with the C_3H_6 concentration at 350 °C over the Rh/CeO_2 catalyst using the two different lenses.

The CL imaging techniques was then utilized for catalyst screening. Employing a series of different oxide (SiO_2, CeO_2, ZrO_2, Al_2O_3, TiO_2)-supported Rh catalysts, CL imaging measurement was performed in C_3H_6 oxidation at the C_3H_6 concentration of 6000 ppm and 350 °C. The CL intensity after background subtraction was plotted against the C_3H_6 conversion for all catalysts (Figure 3.7). A one-to-one correspondence between the CL intensity and the conversion was obtained: The CL intensity increased according to the C_3H_6 conversion in the order of Rh/CeO_2 > Rh/SiO_2 ≈ Rh/ZrO_2 >

Rh/TiO_2 > Rh/Al_2O_3. The deviation from the linear correlation could be potentially explained by many factors, such as cataluminescence, surface plasmon resonance, diffusion length of reactants, and even errors. The former two factors were not likely as the same Rh nanoparticles were employed. The highest activity of Rh/CeO_2 compared to other oxide-supported Rh catalysts are in consistent with literature results, which can be explained via the reaction mechanism of C_3H_6 oxidation. In Rh/CeO_2 catalyst, the impregnated Rh interacts with CeO_2 and promotes the reduction of Ce^{4+} to Ce^{3+} to form oxygen vacancies in close vicinity to the Rh particles, which would improve both the lability and mobility of lattice oxygen of the support. The transfer of additional activated oxygen from the support to the adsorbed C_3H_6 would enhance the catalyst activity [15,23]. These results supported the CL imaging as a good technique for rapid catalysts screening.

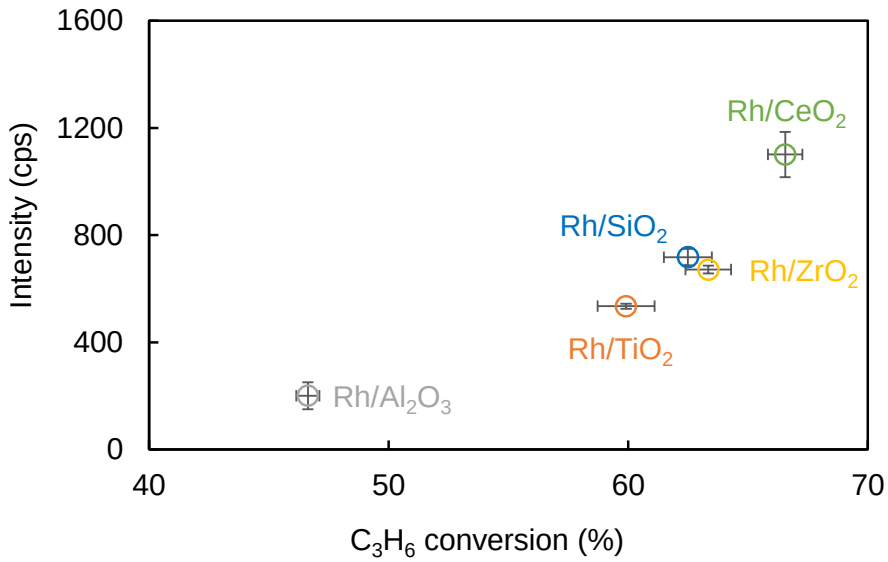

Figure 3.7. Correlation between the chemiluminescence intensity and the performance of different oxide-supported Rh catalysts in C_3H_6 oxidation ([C_3H_6] = 6000 ppm) at 350 °C.

Toward the rapid screening of multiple catalyst samples, the size of the catalyst bed was minimized to increase the number of catalysts to be simultaneously screened. The CL response upon decreasing the size of the catalyst bed was examined by conducting C_3H_6 oxidation at 350 °C using a catalyst bed of 1 mm in diameter. Figure 3.8a shows the CL image taken during the reaction as well as the vertical and horizontal intensity profiles crossing the catalyst. It can be seen that the 1 mm catalyst bed remained sufficient for the CL imaging. Figure 3.8b plots the CL intensity extracted from the continuously captured CL images over 1- and 10-mm catalyst beds along with the reactant concentration. It was observed that the catalyst background remained unchanged while the CL signal was enhanced by 9–20 % when the size of the catalyst bed was decreased from 10 to 1 mm. Considering the fact that the CL emission happened mainly on the topmost surface of the catalyst [24,25], the enhancement of the CL emission could be attributed to more chemiluminescent reaction per area when the size of the catalyst bed was decreased.

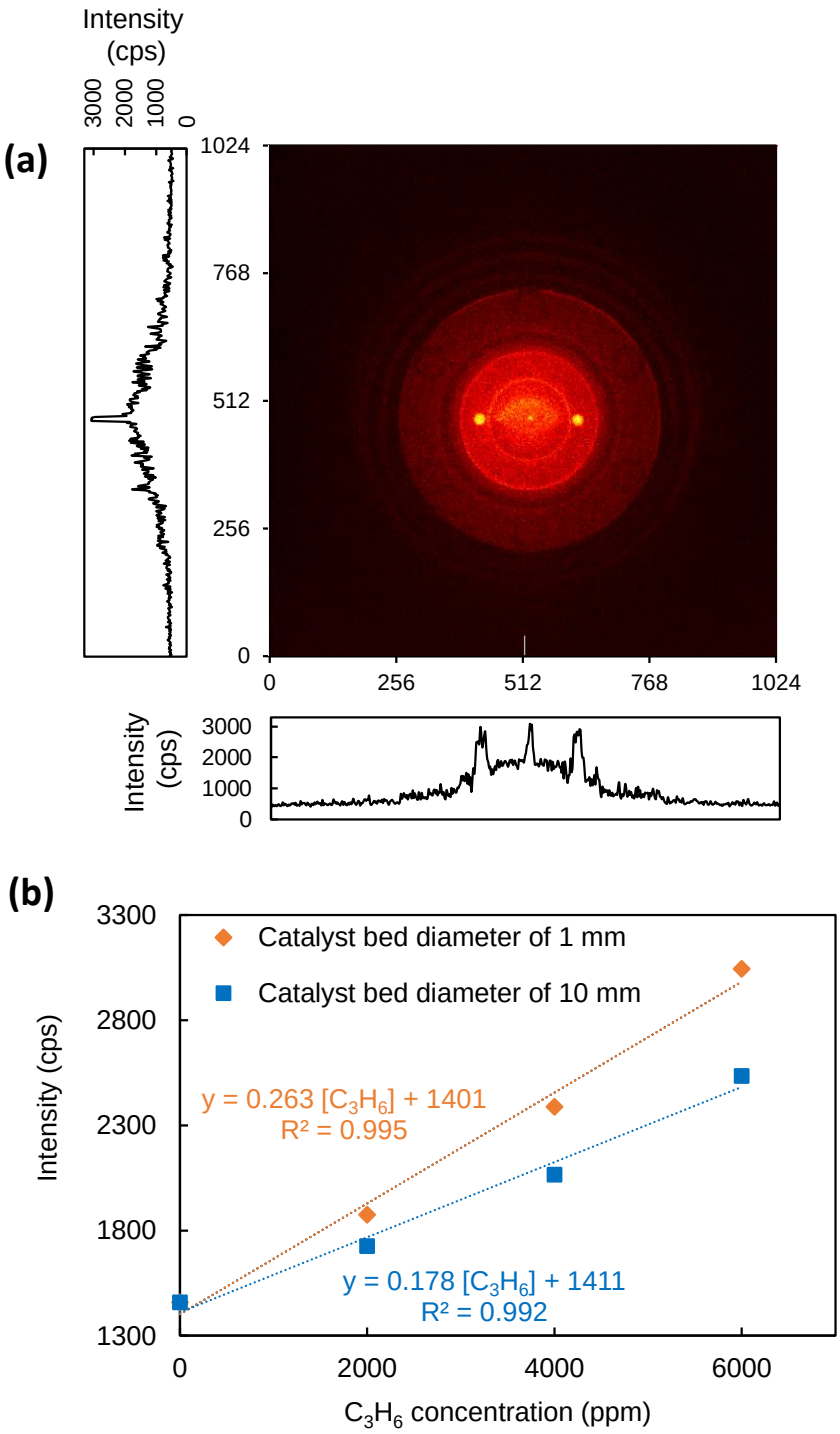

Figure 3.8. Effect of catalyst bed diameter on the chemiluminescence imaging. (a) The imaging was performed in C_3H_6 oxidation ([C_3H_6] = 6000 ppm) at 350 °C over a Rh/CeO_2 catalyst with the bed diameter of 1 mm and (b) comparison of chemiluminescence intensity development along with the C_3H_6 concentration at 350 °C over the Rh/CeO_2 catalyst with two different bed diameters.

To conduct parallel catalysts screening using the developed CL imaging instrument, an aluminum multicell having five identical wells (diameter of 1 mm, depth of 5 mm) was fabricated. It must be noted that the high flowrate was employed in the parallel CL imaging measurement to minimize the effect of concentration distribution in the reactor cell on the CL emission among five positions. As can be seen in Figure 3.9, at flow rate of 100 mL/min, the significant deviation in the CL emission can be clearly observed among five wells filled with same amount of catalyst. When the flow rate increased to 400 mL/min, such the deviation could be effectively suppressed. Furthermore, in considering the effect of contact time when increasing the flow rate, Table 3.2 summarizes the catalyst bed parameter and the corresponding calculated contact time in single and parallel CL imaging measurements. The difference in the contact time is not significant among two measurements and the values are within the typical contact time range for three-way catalytic tests (0.004–0.07 seconds [26]).

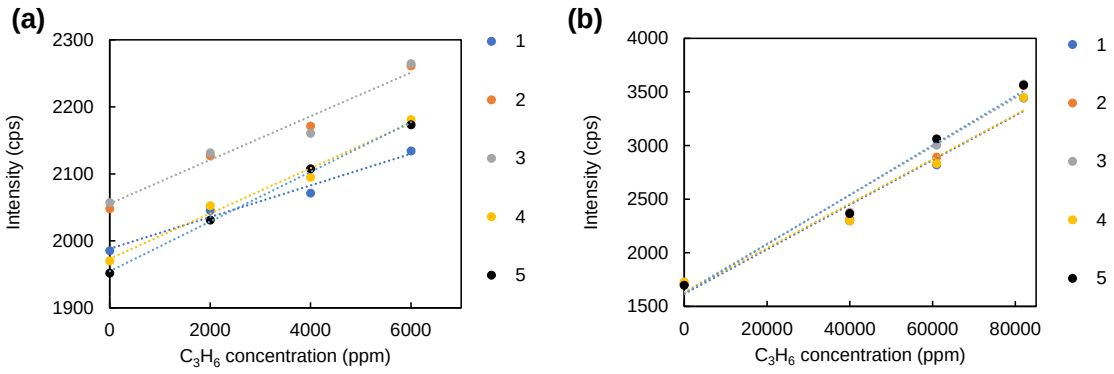

Figure 3.9. Effect of flow rate on the intensity distribution in the multiple cell: (a) 100 ml/min; (b) 400 ml/min. Five wells in the multiple cell were filled with same amount of Rh/CeO_2 catalyst and subjected to C_3H_6 oxidation at 350 °C.

Table 3.2. Catalyst parameters of single and parallel chemiluminescence imaging measurement

	Single measurement	Parallel measurement
Catalyst bed diameter (mm)	10	1
Catalyst bed height (mm)	0.1	5
Number of catalyst	1	5
Flow rate (mL/min)	100	400
Contact time (second)	0.047	0.029

Prior to the parallel CL imaging measurement over the fabricated multiple cell, it was essential to determine the dispersion of the CL intensity among the five wells, for which the following experiments were conducted: Two catalysts, namely Rh/SiO_2 and Rh/TiO_2, which, according to Figure 3.7, displayed a clear difference in performance, were chosen to fill the multicell separately. The five wells were filled with the same amount of a catalyst, and the multicell was placed at the center of the reactor as shown in Figure 3.10a. The CL imaging in C_3H_6 oxidation by O_2 was performed at four different C_3H_6 concentrations and 350 °C under a total gas flow rate of 400 mL/min (Runs 5–8, Table 3.1). The experiments were repeated four times for each catalyst, and the obtained CL imaging results are reported as the average of these four runs in Figures 3.10b,c. It was noticed that the five identical wells exhibited the dispersion of the CL intensity which was maximum 3.7% with respect to the average intensity for both catalysts. According to the heatmap visualization of CL intensity in Figure 3.10b, the dispersion patterns did not follow any general trend or regularity among different measurements for both of the catalysts, excluding the possibilities of instrumental errors, such as non-uniform gas flow, a temperature gradient, and so on [27]. On the other hand, all five wells gave good linearity between the CL intensity and C_3H_6 concentration irrespective of the catalyst (Figure 3.10c). This observation indicates that the dispersion of the intensity was originated from the unavoidable

internal heterogeneity when filling the wells with catalysts. When the same measurement was performed for a single cell, similar dispersion, as well as error percentage, were observed. Besides, considering the smallest deviation in the CL intensity emitted over different Rh catalysts in Figure 3.7 (*ca.* 7.0 % between Rh/SiO_2 and Rh/ZrO_2), the maximum dispersion of 3.7% in the intensity among the five wells obtained in this preliminary screening can be regarded as sufficiently small. Thus, it was believed that such a small deviation in the CL emission among the five wells could provide reliable screening results for different catalysts.

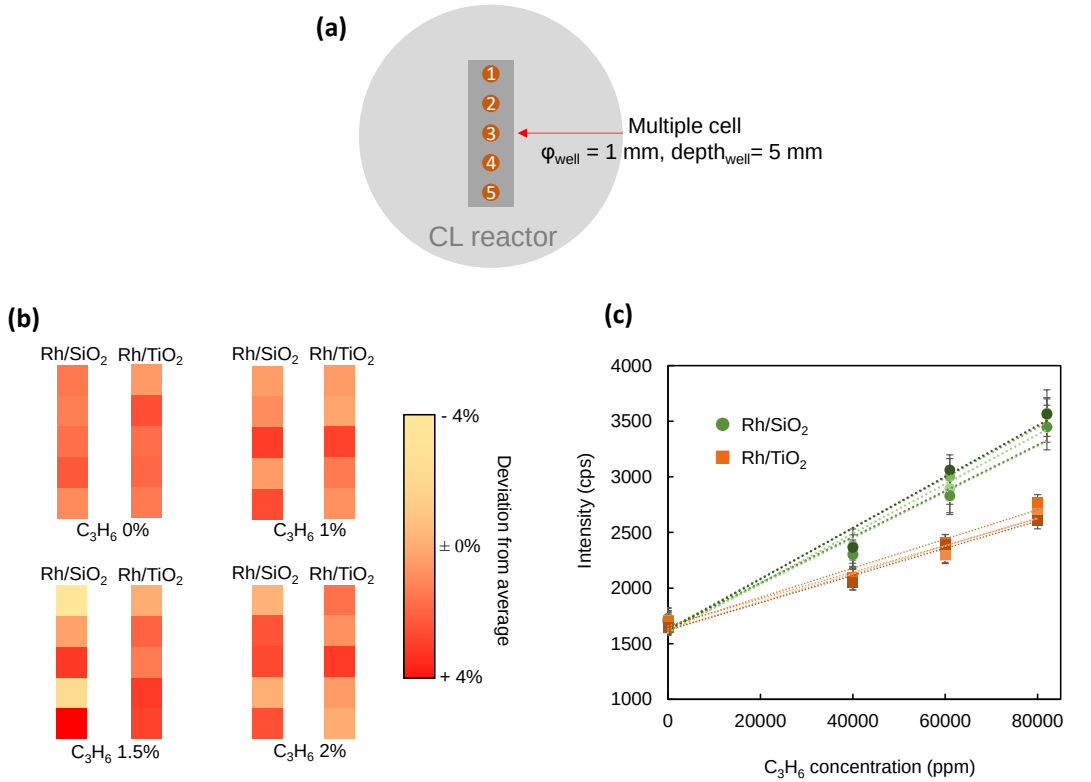

Figure 3.10. Results of parallel chemiluminescence imaging in C_3H_6 oxidation over Rh/SiO_2 and Rh/TiO_2 catalysts at 350 °C: (a) Illustration of the multiple cell and catalyst positions, (b) heatmap visualization of chemiluminescence intensity acquired at different C_3H_6 concentrations, and (c) development of chemiluminescence intensity along with the C_3H_6 concentration at different positions. For each catalyst, the

chemiluminescence intensity in Figure 3.10b,c was taken as the average value of four measurements to examine the reproducibility.

Lastly, the utilization of the CL imaging instrument was demonstrated for parallel catalyst screening. The multiple cell was randomly filled with oxide-supported Rh catalysts and subjected to the C_3H_6 oxidation by O_2 at 350 °C. The measurement was repeated several times over different multiple cells with randomized catalyst position to exclude the position-dependent behavior of the CL emission. The average CL intensity and the corresponding standard deviation of several CL imaging measurements for each catalyst was plotted against the C_3H_6 conversion in Figure 3.11. It was found that the catalyst ranking based on the CL intensity was in good agreement with those based on C_3H_6 conversion, following the order of Rh/CeO_2 > Rh/SiO_2 ≈ Rh/ZrO_2 > Rh/TiO_2 > Rh/Al_2O_3. These results confirmed the feasibility of the CL imaging instrument in parallel catalyst screening.

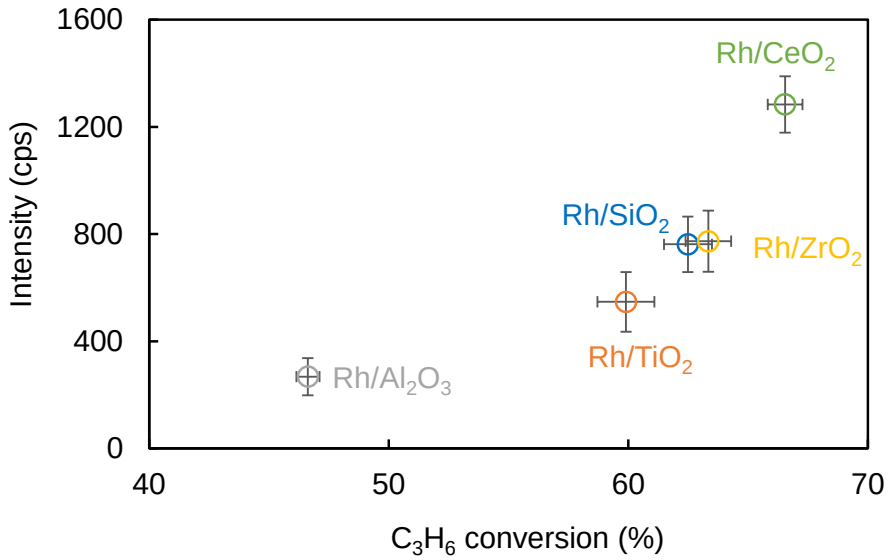

Figure 3.11. Correlation of C_3H_6 conversions with CL intensities in screening measurement for each Rh catalyst

3.4. Conclusions

In summary, to establish a parallel screening technique for high-temperature gas-phase catalysis, a chemiluminescence (CL) imaging instrument was designed and demonstrated in C_3H_6 oxidation reaction over Rh-based catalysts. Technical insight about the optical analytical system was provided via a thorough investigation on the effect of camera lens on the image quality and thus sensitivity of the method. From steady-state measurements, a linear correlation between the reactant concentration and the average intensity extracted from continuously captured CL images was obtained, suggesting the ability of the CL method to detect the high-temperature gas-phase reaction. The feasibility of the CL imaging instrument for rapid catalyst evaluation was successfully demonstrated based on a good correlation between the CL intensity and the C_3H_6 conversion. The one-to-one correspondence of the CL signal of Rh catalysts obtained from the parallel measurement and their corresponding catalytic activity signified the potential of the developed CL imaging instrument in high-throughput catalyst screening.

References

[1] S. Senkan, Angew. Chem. Int. Ed. 40 (2001) 312–329.

[2] S.M. Senkan, S. Ozturk, Angew. Chem. Int. Ed. 38 (1999) 791–795.

[3] R.J. Hendershot, C.M. Snively, J. Lauterbach, Chem. Eur. J. 11 (2005) 806–814.

[4] J. Scheidtmann, P.A. Weiß, W.F. Maier, Appl. Catal. 222 (2001) 79–89.

[5] R. Potyrailo, K. Rajan, K. Stoewe, I. Takeuchi, B. Chisholm, H. Lam, ACS Comb. Sci. 13 (2011) 579–633.

[6] Schunk, S.A., Demuth, D., Cross, A., Gerlach, O., Haas, A., Klein, J., Newsam, J.M., Sundermann, A., Stichert, W., Strehlau, W., Vietze, U. and Zech, T. (2005). Mastering the Challenges of Catalyst Screening in High-Throughput Experimentation for Heterogeneously Catalyzed Gas-Phase Reactions. In High-Throughput Screening in Heterogeneous Catalysis (eds A. Hagmeyer, P. Strasser and A.F. Volpe). doi:10.1002/3527604103.ch2

[7] H.W. Turner, A.F. Volpe, W.H. Weinberg, Surf. Sci. 603 (2009) 1763–1769.

[8] Weinberg, W. and Turner, H.W. (2005). Impact of High-Throughput Screening Technologies on Chemical Catalysis. In High-Throughput Screening in Heterogeneous Catalysis (eds A. Hagmeyer, P. Strasser and A.F. Volpe). doi:10.1002/3527604103.ch1

[9] M. Breysse, B. Claudel, L. Faure, M. Guenin, R.J.J. Williams, T. Wolkenstein, J. Catal. 45 (1976) 137–144.

[10] K. Nakao, S.-i. Ito, K. Tomishige, K. Kunimori, J. Phys. Chem. B 109 (2005) 17553–17559.

[11] T. Okabayashi, T. Fujimoto, I. Yamamoto, K. Utsunomiya, T. Wada, Y. Yamashita, N. Yamashita, M. Nakagawa, Sens. Actuators B Chem. 64 (2000) 54–58.

[12] T.P.N. Tran, A. Thakur, T.N. Nguyen, P. Mohan, T. Wada, P. Chammingkwan, T. Taniike, Catal. Today (2020).

[13] X. Wang, Na, S. Zhang, Y. Wu, X. Zhang, J. Am. Chem. Soc. 129 (2007) 6062–6063.

[14] N. Na, S. Zhang, X. Wang, X. Zhang, Anal. Chem. 81 (2009) 2092–2097.

[15] C. Wang, T. Zheng, J. Lu, X. Wu, H. Hochstadt, Y. Zhao, Appl. Catal. 544 (2017) 30–39.

[16] J. Yu, J. Yu, Z. Shi, Q. Guo, X. Xiao, H. Mao, D. Mao, Catal. Sci. Technol. 9 (2019) 3675–3685.

[17] H. Kusama, K.K. Bando, K. Okabe, H. Arakawa, Appl. Catal. 197 (2000) 255–268.

[18] Y. Cao, R. Ran, X. Wu, B. Zhao, D. Weng, J. Environ. Sci. 52 (2017) 197–203.

[19] Z. Zhan, L. Song, X. Liu, J. Jiao, J. Li, H. He, J. Environ. Sci. 26 (2014) 683–693.

[20] W.F. Gale, T.C. Totemeier, Smithells Metals Reference Book (8th ed.), Elsevier, Oxford (2004).

[21] J. Bartl, M. Baranek, Meas. Sci. Rev., 4 (2004) 31–36

[22] J. Huang, C. Fan, G. Song, Y. Li, X. He, X. Zhang, Y. Sun, S. Du, Y. Zhao, Appl. Surf. Sci. 280 (2013) 605–609.

[23] M.S. Avila, C.I. Vignatti, C.R. Apesteguía, T.F. Garetto, Chem. Eng. J. 241 (2014) 52–59.

[24] Z. Long, H. Ren, Y. Yang, J. Ouyang, N. Na, Anal. Bioanal. Chem 408 (2016) 2839–2859.

[25] S. Wang, Z. Yuan, L. Zhang, Y. Lin, C. Lu, Analyst 142 (2017) 1415–1428.

[26] V. Palma, D. Barba, Int. J. Hydrogen Energy 39 (2014) 21524–21530.

[27] N. Aratani, I. Katada, K. Nakayama, M. Terano, T. Taniike, Polym. Degrad. Stab. 121 (2015) 340–347.

Chapter 4

High-Throughput Screening of a Three-Way Catalyst Library for Automotive Applications

Abstract

The continuous development of more effective three-way catalysts (TWCs) to meet the global strict exhaust emission regulations enlightens the importance of efficient catalyst screening. Herein, a high-throughput (HTP) screening protocol for a library of the simulated lead TWCs was established with the aid of a previously developed HTP screening instrument. Three-way catalytic reactions were performed over 20 catalyst samples in 7 temperatures and 7 air/fuel equivalence ratios (λ), affording 980 data points in one fully automated operation. The obtained process-relevant and widely distributed dataset enabled a multi-aspect comparison study of the TWCs to extract knowledge for the catalyst design.

Keywords: High-throughput catalyst screening, three-way catalysts, multi-aspect comparison.

4.1. Introduction

The increasingly tighten regulation of the automotive exhaust emission has served as an impulse for the continuous development of more efficient three-way catalysts (TWCs). This goal has been pursued mainly *via* materials aspects, such as optimization of the washcoat formulation (catalyst supports [1–3], type and loading of noble metals [4–6], type and loading of promoters [7–10]); appropriate synthesis methods [11–14] (co-precipitation, impregnation, sol-gel, etc.); and optimization of process conditions (calcination temperature and aging condition [15–17]). It is likely that the research and development of the TWCs need to deal with a huge and diverse parametric materials space. On the other hand, the evaluation of newly generated TWCs has been implemented successively from one catalyst to another based on their light-off temperature (*i.e.* temperatures of 50% or 80% of individual reactant conversion) and the width of operation window [18–20]. The experiments to acquire this information need to be performed separately. Owning to the huge parametric materials space and time-consuming evaluation process, it is undoubtedly true that the automotive exhaust aftertreatment system market calls for an establishment of a high-throughput (HTP) screening protocol to accelerate the optimization and discovery of the TWCs.

To date, hte Aktiengesellschaft has been the only group who has successfully developed a HTP screening technique for automotive catalyst screening [21–23]. According to the authors, the scarcity of the study on the application of HTP screening techniques for the TWCs might be due to: i) costs; ii) the requirement of online and time-resolved analytical techniques for all reactants and products; and iii) the lack of data acquisition in an automated sequence of process conditions. The testing unit of their HTP screening instrument consisted of a reactor block bearing identical 48 channels and operated at isothermal conditions with the temperature range from 100 to

575 °C. The reactor operates in a fast-switch fashion, in which reactant gas mixture is supplied to one channel selected at a time, and then the gas effluent is switched to a line for product analysis by mass spectrometry. The same protocol is applied for other channels in a sequential mode. As a consequence of the sequential operation, it takes time for each single channel to reach a steady state. Thus, the HTP screening instrument in hte Aktiengesellschaft is rather proprietary and mostly used for catalyst screening at a few fixed conditions.

In a previous publication, our group has successfully developed a HTP catalyst screening instrument for heterogeneously catalyzed gas-phase reactions [24]. This instrument realizes automatic evaluation of 20 catalysts at a series of predefined conditions in a parallelized fixed-bed reactor configuration with the aid of an auto-sampler and a high-speed quadruple mass spectrometer (QMS). QMS is particularly advantageous for product analysis of a complex gas mixture with great ability to provide time-on-stream data. Herein, a HTP screening protocol for a library of the simulated lead TWCs was established with the aid of the previously developed HTP screening instrument. A library of 18 simulated lead TWCs comprising of three noble metals as active species (Rh, Pd, Pt) and six metal oxides as catalyst supports (SiO_2, Al_2O_3, TiO_2, ZrO_2, CeO_2-ZrO_2, and CeO_2) were prepared and evaluated for their performance in 49 different conditions, resulting in 980 process-relevant data points in one fully automated operation. Multi-aspect comparison of the simulated lead TWCs was carried out to deduce the common features of good/poor catalysts and thus enable knowledge extraction for the catalyst design.

4.2. Experimental

4.2.1. Establishment of the simulated lead TWC library

Simulated model TWCs generally composed of two main components: noble metals as the main active component and metal oxide supports to disperse and carry the noble metals. Platinum group metals (PGM) have been well-known to be excellent oxidation catalysts; however, the utilization of Ru, Ir, and Os is rarely reported due to their formation to volatile oxides [20,25]. Rh, Pd and Pt were left as clear choices and have long been employed in the TWCs since their introduction. Rh is the most active, yet the most expensive among the three PGMs, and approximately 80% of global Rh demand is for TWCs. Therefore, Rh is usually specified to promote NO reduction, while Pt and Pd are considered as metal of choice to promote the oxidation of CO and C_3H_6.

The catalyst supports employed in TWCs must at least meet the following criteria: high accessible specific surface area, good thermal and chemical stabilities, and high mechanical strength. Based on these criteria and surveying from literature [26–30], six metal oxide supports were employed, which are γ-Al_2O_3 (PURALOX SCFa100, SASOL), SiO_2 (Aerosil 50, EVONIK), TiO_2 (Aeroxide P25, EVONIK), monoclinic ZrO_2 (RC-100, Daiichi Kigenso Kagaku Kogyo), CeO_2 (HSA-20, RODIA), and CeO_2-ZrO_2 (Toyota Corp.).

γ-Al_2O_3 is the first and the most popular support for the TWCs due to its high surface area (BET surface area of 106 m^2/g) compared to other transitional Al_2O_3 and relatively good thermal stability [19,28]. SiO_2 (BET surface area of 61 m^2/g) can also be used in the TWCs owning to its advantage of high tolerance towards sulfur poisoning [31,32]. TiO_2 is just as SiO_2 also has excellent inhibiting effect to the potential sulfur deposits on the catalyst surface. This study employed Evonik Aeroxide P25, which is a

flame-made multiphasic TiO_2 containing anatase, rutile and a small amount of amorphous TiO_2 [33], as it mostly used for high-temperature catalytic applications due to its higher surface area (BET surface area of 55 m^2/g) and greater thermal stability compared to the other types of TiO_2 [32]. ZrO_2 is more chemically inert than the classical supports (*e.g.* Al_2O_3 and SiO_2), and monoclinic ZrO_2 is widely employed in TWCs [30,34,35] due to its great thermal stability at up to 1170 °C. Commercially available high-surface-area monoclinic ZrO_2 RC 100 (BET surface area of 99 m^2/g) was selected as a catalyst support. The major advantage of CeO_2 in the TWCs lies on its excellent oxygen storage capacity, which is due to its ability to switch between Ce^{4+} under oxidizing conditions and Ce^{3+} under reducing conditions. Also, CeO_2 can promote the dispersion and reduction of noble metals. Herein commercial HAS CeO_2 (BET surface area of 133 m^2/g) was selected as it exhibits significantly highest level of thermal stability among other type of CeO_2 [36,37]. Zirconia is usually added to CeO_2, generating mixed oxide CeO_2–ZrO_2 to improve the thermal stability, reducibility and sulfur tolerance of CeO_2 [19,28]. CeO_2–ZrO_2 (BET surface area of 56 m^2/g) with 50–60 wt% of CeO_2 has been used extensively as support for the TWCs.

4.2.2. Catalyst preparation

Catalyst samples were prepared by a wet impregnation method. A specified amount of support powder was impregnated with an aqueous solution of a metal salt ($Rh(NO_3)_2$, $PdCl_2$ or $PtCl_2$-Sigma Aldrich). The solid was dried at 120 °C for 15 h, followed by the calcination at 500 °C in air for 2 h. The metal loading of these catalysts was 1.0 wt.%.

4.2.2. High-throughput screening system

A schematic layout of the previously developed HTP screening instrument [24] is shown in Figure 4.1. The instrument consists of a gas mixer, a flow distributor, reaction tubes, an electric furnace, an autosampler, and a quadrupole mass spectrometer (QMS).

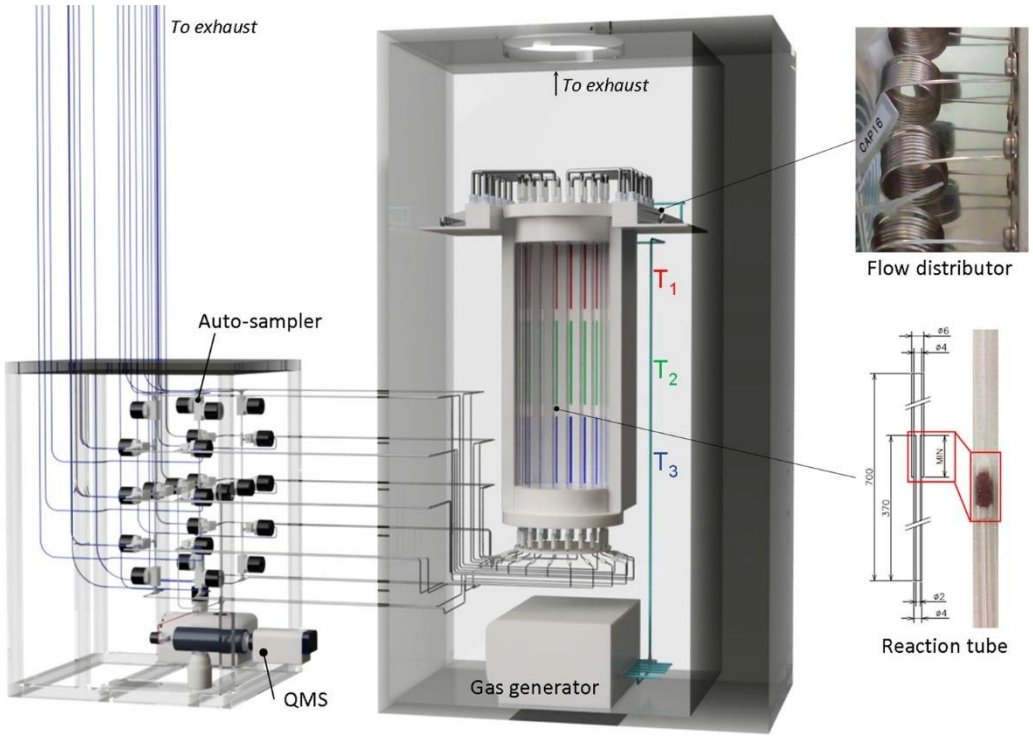

Figure 4.1. Schematic representation of the HTP screening instrument for gas-phase reactions. The figure is reprinted with the permission from Ref. [24].

The composition of the reaction gas and its flow rate are adjusted by the gas mixer (MU-3200, HORIBA, Ltd.). The specific flow volume of each gas is regulated by setting its volume percentage over the whole flow volume of the gas mixture. Ar was used as the balance and carrier gas. The testing unit comprises 20 reaction channels placed in an electric furnace. The equal flow distribution into the 20 reaction channels is constantly acquired with the aid of capillary tubes (inner diameter of 0.2 mm, length of 1000 mm) as a flow distributor. The validation test of uniform gas distribution was

performed by supplying 200 mL/min of Ar gas through all 20 reaction channels, then the flow rate at the outlet of each channel was recorded several times. The results in Figure 4.2a indicate that the average flow rate of the effluent gas was 10 mL/min/channel for all the 20 reaction channels with negligible deviation, confirming the equal flow distribution. Similar experiments were performed in the presence of a catalyst bed (Rh/CeO_2) at different amounts (Figure 4.2b). It was confirmed that the usage of the capillary tubes provided persistently uniform flow distribution regardless of the supplied flow rate, presence of catalyst, and catalyst amount.

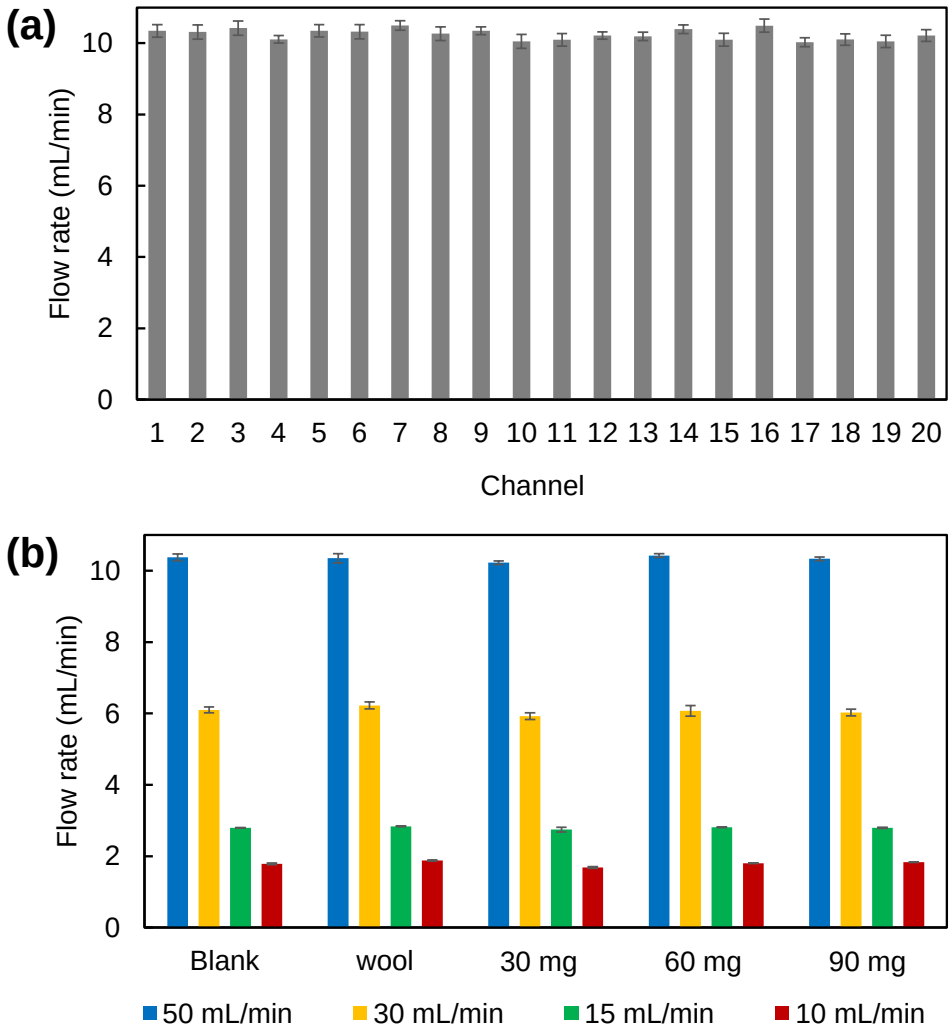

Figure 4.2. Validation of gas distribution in the HTP screening system. (a) Without catalysts; (b) with different amounts of catalysts and quartz wool.

The temperature of the electric furnace could be programable up to 1000 °C. The uniform temperature distribution is achieved by a symmetric and circular design with radiant heating: The heating is uniformly done by three-zone proportional-integral-derivative temperature controllers. The catalyst beds are placed in the middle of the center zone with the aid of inert quartz wool. When the same temperature is applied for the three zones, the other two zones will buffer the temperature perturbation of the catalyst beds. A reaction tube is made of inert quartz. Its internal diameter for inlet and outlet parts are 4 mm and 2 mm, respectively. A catalyst bed is fixed at the middle of the tube.

The autosampler contains 20 fully automated sampling lines. Each sampling line is individually connected with the outlet of each reactor channel by a solenoid valve, allowing rapid switch between different reactor channels for sequential analysis. Gas from the sampling line is then transferred to QMS for analysis. The sampling time for the effluent gas of one channel was set at 1.6 s, and the evacuation time to clean the sampling line was 7.0 s, resulting in 172 s for one running round. The full automation of the HTP system is realized by synchronizing the gas mixer, temperature program of the reactor, and the QMS measurement.

The uniformity of the sampling was examined by a blank measurement of a feed containing C_3H_6 and carrier gas Ar at the volume ratio of C_3H_6/Ar = 3/7 and flow rate of 10 mL/min/channel. The average relative pressure of C_3H_6 over Ar among 20 channels was obtained as 0.426 ± 0.0172 (Figure 4.3), confirming the uniform sampling of the HTP instrument.

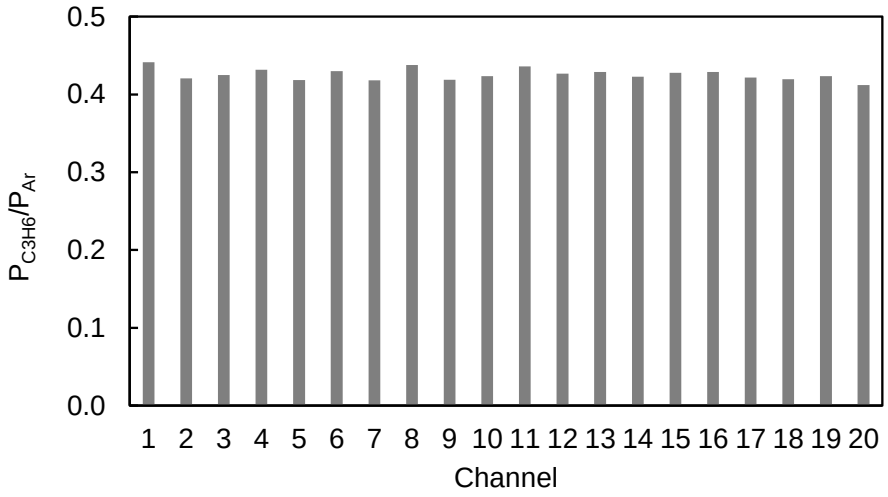

Figure 4.3. Validation of uniform sampling in the HTP screening instrument.

4.2.3. Catalytic test

The three-way catalytic test was performed with a simulated exhaust gas containing CO (13000 ppm), C_3H_6 (2000 ppm), NO (3000 ppm), CO_2 (20000 ppm), O_2 (7000–18000 ppm), and Ar (balance). 18 channels were assigned to the above-mentioned 18 catalysts. The remaining 2 channels were used for blank and a reproduction test with a Rh/CeO_2 catalyst. The height of the catalyst bed was unified at 10 mm. The flow volume was fixed at 10 mL/min/channel, corresponding to the volume-based contact time of 0.75 s. The programmed sequence of the reaction conditions is shown in Figure 4.4. First, catalysts were activated at 600 °C under a continuous flow of pure O_2 for 1 h. Then, the temperature was stepwise decreased from 600 °C to 400, 350, 300, 250, 200, 150 and 100 °C (Figure 4.4a). At each temperature step, the O_2 concentration was stepwise varied from 18000 to 7000 ppm, corresponding to the variation in the λ value from 1.3 to 0.5 (Figure 4.4b). Each condition was held for 30 min, corresponding to 10 rounds of QMS evaluation for the 20 channels. The

data of the first 2 rounds were not taken into account due to potential instability of the flow system. The data reported was the average of 8 rounds. The combined variations in the temperature and the O_2 concentration led to 49 conditions per catalyst and 980 data points for 20 catalysts in a single automated operation.

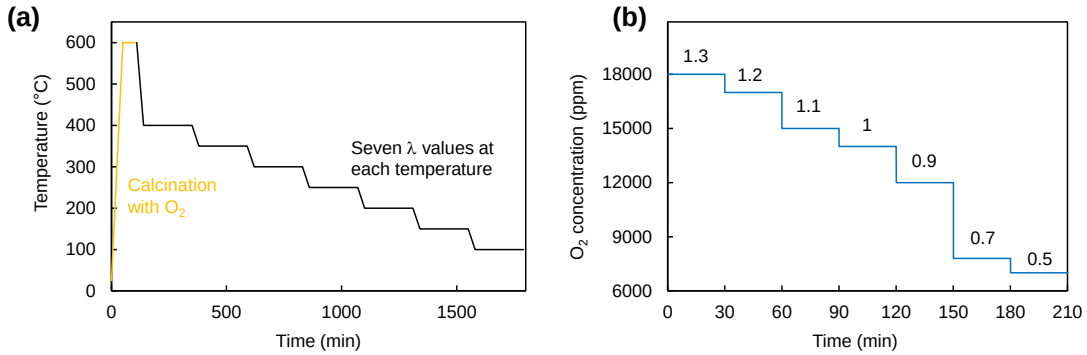

Figure 4.4. (a) Temperature program and (b) O_2 concentration program for the catalytic tests. The data labels in Figure 4.4b are the corresponding λ values.

4.3. Results and discussion

The reproducibility of the HTP screening instrument was assessed by mounting two reactor channels with the same Rh/CeO_2 catalyst for the catalytic test. Figure 4.5 depicts the reproduction results in terms of temperature- and λ-dependent behaviors of CO, C_3H_6 and NO conversion obtained from these two channels. In the region of interest (*i.e.* > 80% conversion), negligible deviation (< 2%) among two channels was obtained, confirming good reproducibility of the evaluation with the HTP screening instrument.

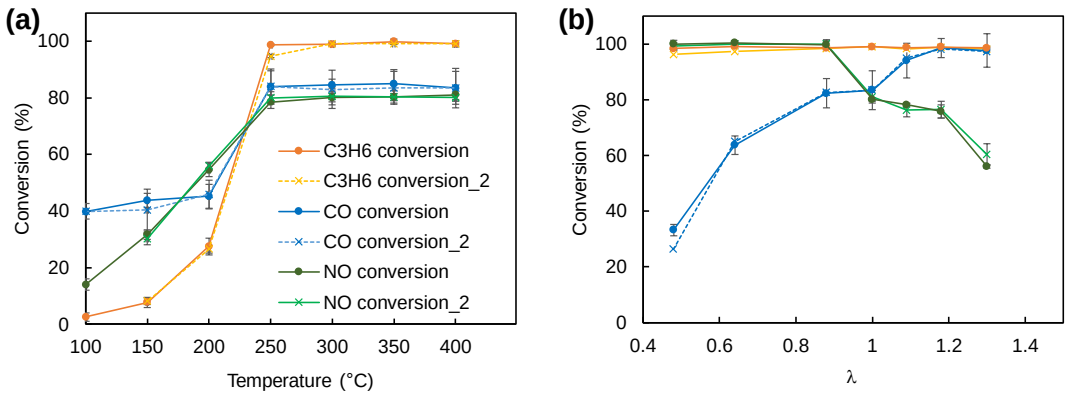

Figure 4.5. Reproduction test for two reactor channels mounted with the same amount of Rh/CeO_2 catalyst. (a) Effect of temperature at λ = 1 and (b) effect of λ at 400 °C.

To deduce qualitative tendencies within the obtained dataset, the visualization of the whole data was conducted by means of scatter plots, where the behaviors of CO, C_3H_6, and NO conversion were illustrated with respects to temperature and λ (Figure 4.6). One can see that CO conversion is regarded as the simplest process since datapoints of 0 conversion are rarely observed (Figure 4.6a). However, the complete removal of CO remained the most challenging as evidenced by the lowest density of 100% conversion datapoints. Contrarily, C_3H_6 conversion showed the best performance

in this regard (Figure 4.6b) based on its highest density of 100% conversion among three processes. In addition, the heavy concentration of 0% and 100% datapoints in the scatter plot for C_3H_6 conversion demonstrated that the process is the most sensitive to the temperature. In Figure 4.6c, the datapoints of NO conversion is the most scattered and widely distributed along the value from 0–100%, indicating that the process exhibited the most apparent catalysts- and condition-dependent behaviors.

The scatter plots also allow quick determination of two important parameters in three-way catalysis, including light-off temperature (T_{80}-lowest temperature at which 80% conversion is achieved) and the effect of λ values. For example, CO oxidation generally started to light-off at around 200 °C under stoichiometric and fuel-lean conditions ($\lambda \geq 1$) as 80% of CO conversion started to be observed at this temperature. C_3H_6 oxidation and NO reduction exhibited 50 °C slower light-off compared to CO oxidation. In term of the response to the variation in λ, more than 80% of CO and C_3H_6 conversion mainly came from $\lambda > 1$, indicating that these two processes are favorable in the fuel-lean conditions. In case of NO removal, more than 80% conversion was obtained mainly at $\lambda < 1$, signifying its preference for working under fuel-rich atmosphere.

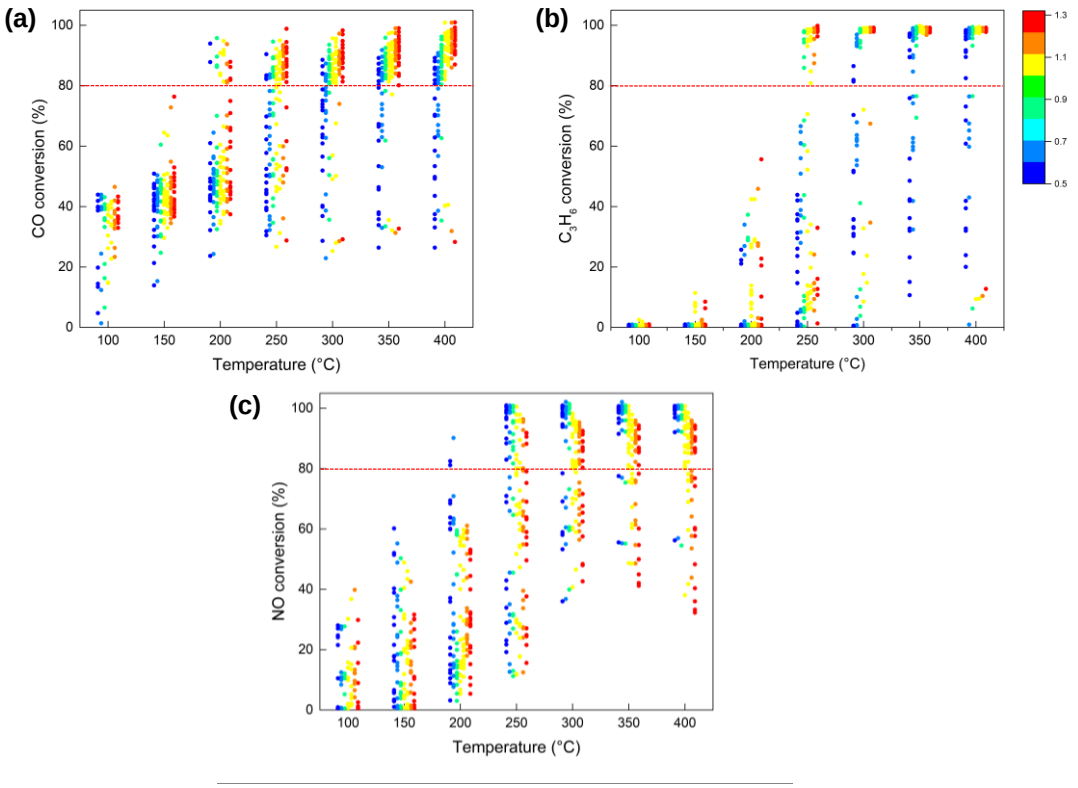

Figure 4.6. Visualization of all data by scatter plots for (a) CO conversion; (b) C_3H_6 conversion; and (c) NO conversion. The color bar indicates the λ value.

In literature, the evaluation of the light-off performances has been mostly limited at one specific value of λ (mostly at stoichiometric condition [14,18,38–43]), mainly due to the high cost and long time frame of the experiments. However, in the real operation, the engine is usually operated in a slightly flue-rich mode for enhanced power [44]. Under this condition, the removal of CO and C_3H_6 becomes more difficult due to the lack of the oxidants, which would result in the slower light-off. For example, Figure 4.7 compares the light-off curves for CO conversion over Pd/SiO_2 catalyst obtained under fuel-rich (λ = 0.9) and stoichiometric (λ = 1.0) conditions. It can be seen that the T_{80} increased from 340 to over 400 °C in response to the switching of the exhaust environment from stoichiometric to reducing condition. In addition, the

technologies for lean-burn gasoline targeting at removing NO in the presence of O_2 exceeding the concentration of reductants have been regarded as immature and still required significant efforts. On the basis of the above discussions, it is true that a study on the light-off behavior of the TWCs should be conducted not only under stoichiometric but also under fuel-rich/lean conditions.

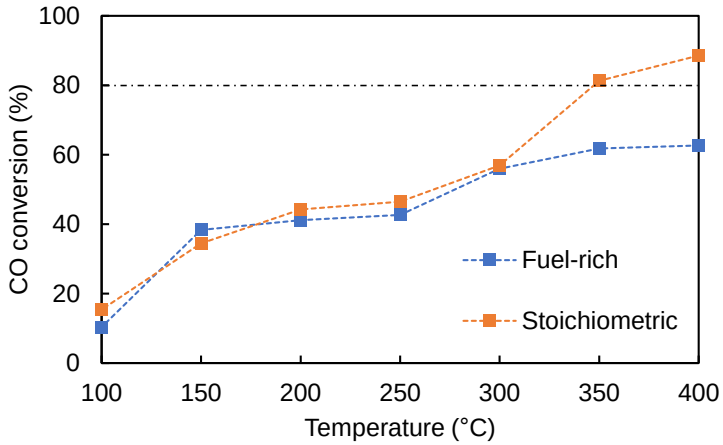

Figure 4.7. Light-off behavior of Pd/SiO_2 catalyst for CO oxidation with respect to stoichiometric and fuel-rich conditions.

Herein, the implementation of HTP screening for a library of TWCs over a wide range of reaction conditions allows the catalyst evaluation and comparison in various aspects, which include the light-off behavior for CO, C_3H_6 conversion under stoichiometric and fuel-rich conditions, light-off behavior for NO conversion under stoichiometric and fuel-lean conditions, and the width of operation window at typical working temperature of the TWCs (*i.e.* 400 °C), resulting in total seven aspects (Figure 4.8). It is worthy to emphasize that the multi-aspect comparison study of a TWCs library was done for the first time.

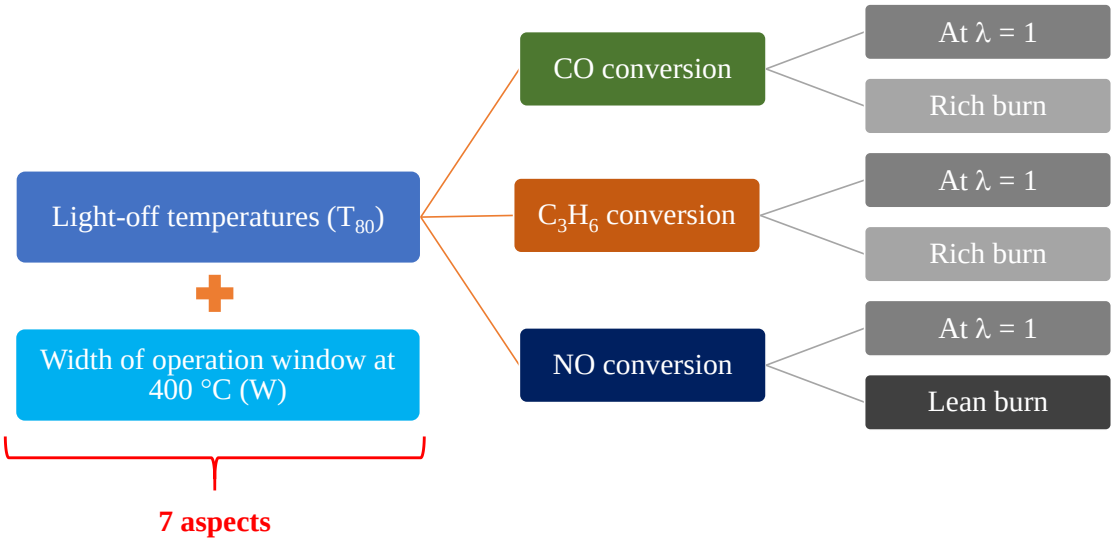

Figure 4.8. List of 7 aspects for catalyst comparison employed in this study.

The results of catalyst evaluation in 7 aspects are summarized in Figure 4.9. The red dashed line in each figure represents the upper limit in the typical range of each aspect based on literature. Particularly, TWCs are generally characterized by T_{80} at around 250–350 °C [19], meaning that those having T_{80} within this range are regarded as performant/good catalysts in term of light-off performance. Following this definition, most of the employed TWCs in this study are good catalysts as their T_{80} are mostly less than 350 °C (Figure 4.9a-f). In term of W, TWCs are featured by W values in the range of 0.1–0.2 [2,45–50]; therefore, except Pd/SiO_2, all the TWCs are performant catalysts in this regard (Figure 4.9g). Based on the above observations, herein the good/poor catalysts were preferentially selected based on their relative ranking rather than their absolute performance.

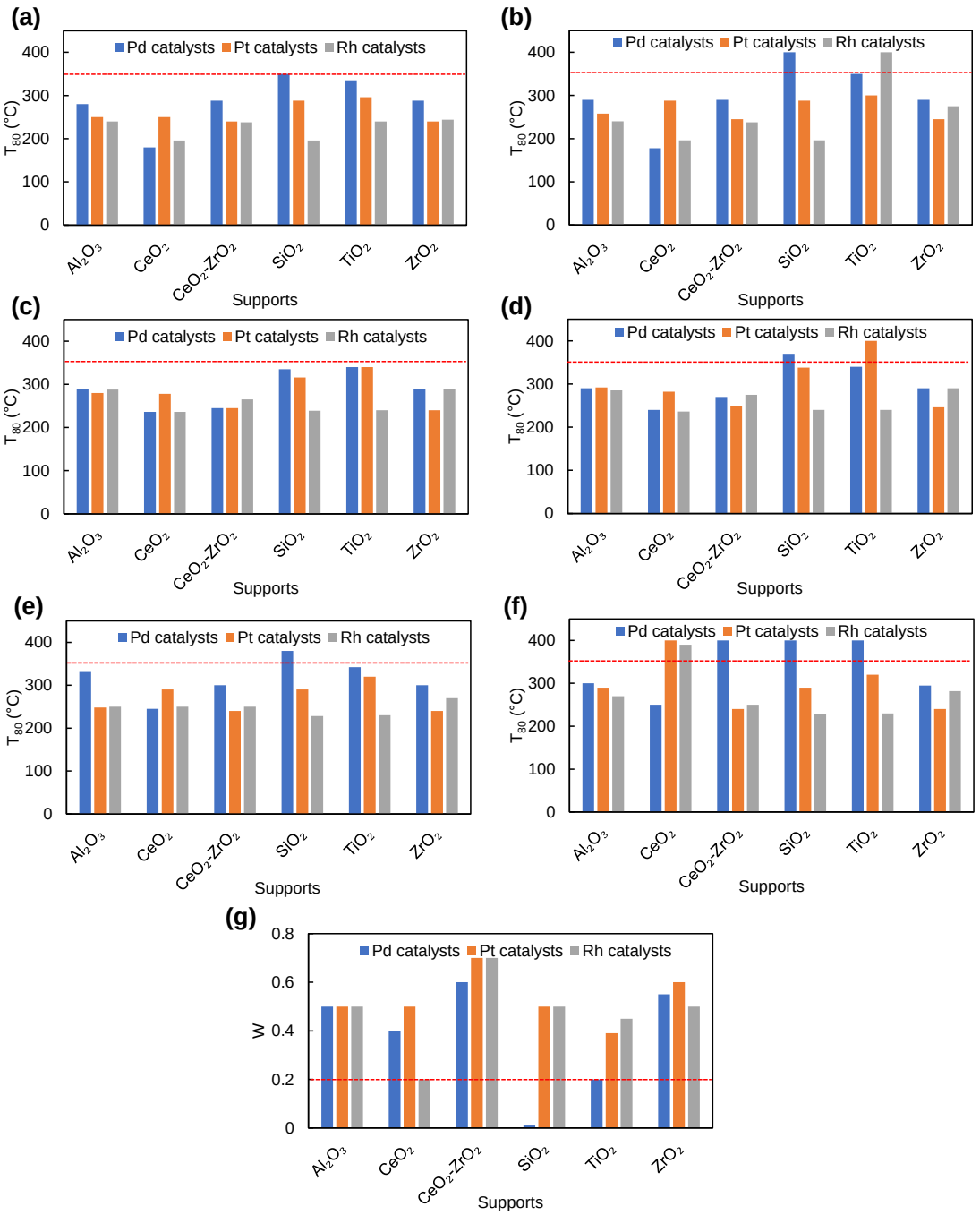

Figure 4.9. Catalyst evaluation results in 7 aspects. Light-off temperature (T_{80}) at: (a) CO oxidation at stoichiometric condition; (b) CO oxidation at fuel-rich conditions, (c) C_3H_6 oxidation at stoichiometric condition, (d) C_3H_6 oxidation at fuel-rich conditions, (e) NO oxidation at stoichiometric condition; (f) NO oxidation at fuel-lean conditions, and (g) Width of operation window (W) at 400 °C.

Table 4.1 summarizes the performance ranking of 18 TWCs with respect to the 7 aspects listed in Figure 4.8. Therein the four best and worst catalyst in each aspect were labeled as orange and blue color, respectively. In general, the group of good catalysts varied among aspects; however, we can observe clearly that Pd/SiO_2 and Pd/TiO_2 always exhibited poor performance in all seven aspects. The table provides a significant insight into the choice of catalysts for a specific purpose. For example, when one seeks for good catalysts to efficiently remove CO in the exhaust, Pd/CeO_2, Rh/CeO_2, Rh/CeO_2-ZrO_2 and Rh/SiO_2 are the choices. When NO removal become the point of focus, one can consider the usage of Pt/CeO_2-ZrO_2, Pt/ZrO_2, Rh/SiO_2 and Rh/TiO_2. The performant catalysts with respect to the exhaust environment can also be acquired from Table 4.1. For example, the catalysts that can work efficiently under fuel-rich condition are Pd/CeO_2, Rh/CeO_2 and Rh/SiO_2 as they can effectively remove CO and C_3H_6 even when the O_2 is deficient. On the other hand, Pt/CeO_2-ZrO_2 and Pt/ZrO_2 are good catalysts under fuel-lean conditions due to their good activity to remove NO when O_2 become excess.

Table 4.1. Comparison of 18 TWCs in seven aspects. In each aspect, the best and worst four catalysts are highlighted as orange and blue colors, respectively.

Catalyst	C_3H_6 conversion (%)		CO conversion (%)		NO conversion (%)		W
	λ = 1.0	λ = 0.9	λ = 1.0	λ = 0.9	λ = 1.0	λ = 1.2	
Pd/Al_2O_3					×		
Pd/CeO_2	○	○	○	○			
Pd/CeO_2-ZrO_2						×	○
Pd/SiO_2	×	×	×	×	×	×	×
Pd/TiO_2	×	×	×	×	×	×	×
Pd/ZrO_2							
Pt/Al_2O_3							
Pt/CeO_2						×	
Pt/CeO_2-ZrO_2					○	○	○
Pt/SiO_2	×	×	×				
Pt/TiO_2	×	×	×	×	×		×
Pt/ZrO_2					○	○	○
Rh/Al_2O_3							
Rh/CeO_2	○	○	○	○			×
Rh/CeO_2-ZrO_2			○	○			○
Rh/SiO_2	○	○	○	○	○	○	
Rh/TiO_2	○	○		×	○	○	
Rh/ZrO_2							

In order to demonstrate how to extract knowledge for the catalyst design from the multi-aspect comparison of the TWCs library, the aspects of C_3H_6 oxidation under fuel-rich condition and W at 400 °C were randomly picked as examples. In the catalyst ranking based on W given in Figure 4.10, one can see that M/CeO_2-ZrO_2 catalysts exhibited great W while all M/TiO_2 tended to give small W. In general, the explanation for the catalyst performance of TWCs was done mainly via the effect of noble metal,

effect of supports and/or synergy effect generated from the metal-support interaction [26]. From the selection of best/worst catalysts in Figure 4.10, it seems that the support is the most impactful factor for W. As a result, the comparison among six supports was performed, where the W of each support was obtained by taking the average of the W from three TWCs containing that support. In Figure 4.11, the catalysts supported on CeO_2-ZrO_2 exhibited the best performance, which could be explained by the great oxygen storage capacity (OSC) as well as the great thermal stability of the support. The low W values obtained from M/TiO_2 is plausibly due to the intrinsically low OSC and the open structure of the support which lead to the migration of the surface metal to the bulk of TiO_2 during high temperature reduction [51,52]. Consequently, the metals are buried inside the bulk of the support, resulting in a loss of the adsorptive and catalytic properties.

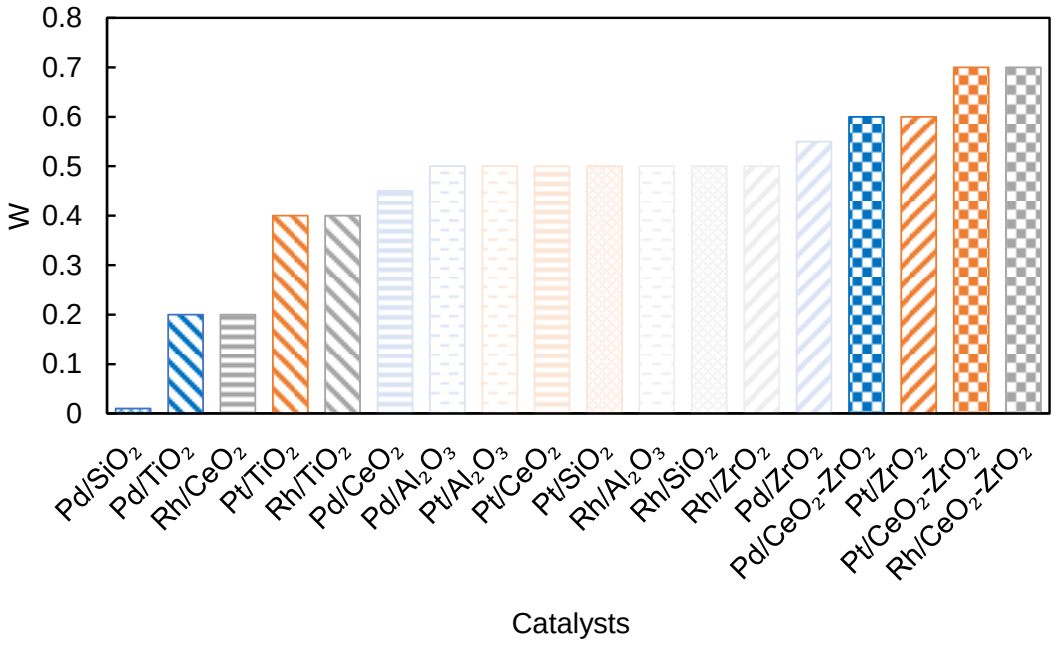

Figure 4.10. Catalyst ranking based on W at 400 °C.

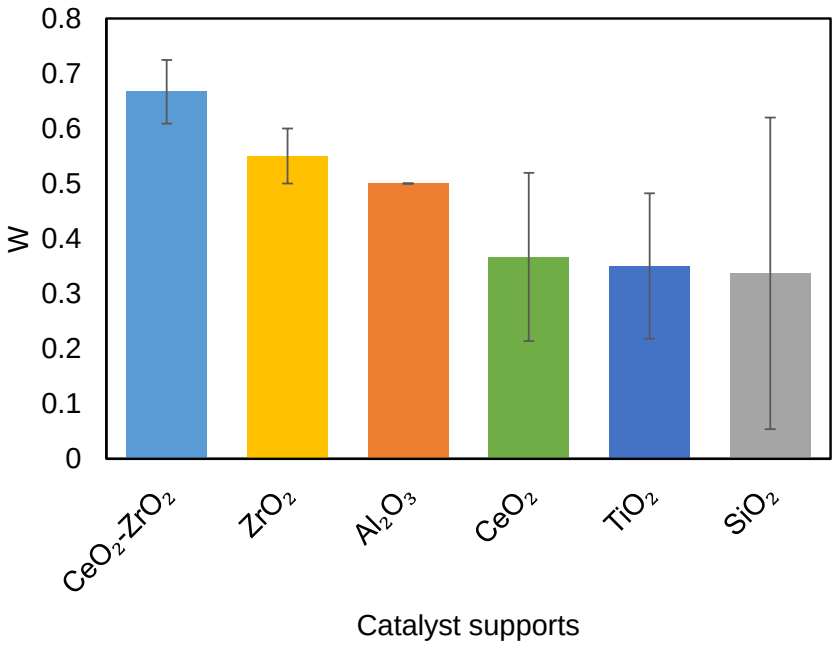

Figure 4.11. Comparison of W at 400 °C among different catalyst supports.

Another example of the knowledge extraction from the multi-aspect comparison in Table 4.1 is the removal of C_3H_6 under fuel-rich conditions. Figure 4.12 provides the catalyst ranking based on T_{80} for C_3H_6 conversion at $\lambda = 0.9$. One can observe that the group of best four catalysts with outstanding light-off performance ($T_{80} \leq 240$ °C) are dominated by Rh-catalysts, which includes Rh/CeO_2, Rh/SiO_2 and Rh/TiO_2. Meanwhile, Pt- and Pd-catalysts dominated the group of worst catalysts. Therefore, the classification of best/worst catalysts in this aspect was mainly based on the noble metals. As a consequence, the average T_{80} of each noble metal was obtained from the T_{80} of six catalysts containing that metal loaded on six different supports and then compared in Figure 4.13. The light-off performance order of Rh > Pd > Pt was observed, which consistently followed the level of C_3H_6 poisoning effect on metal surface. It has been approved that C_3H_6 has strong adsorption property, and the poisoning by C_3H_6 adsorption is one of the main cause for the catalyst deterioration under C_3H_6-rich

atmosphere [4]. Among three noble metals, Rh exhibited great tolerance for C_3H_6 poisoning, while this phenomenon frequently occurs on the Pd and Pt surface when C_3H_6 become excess.

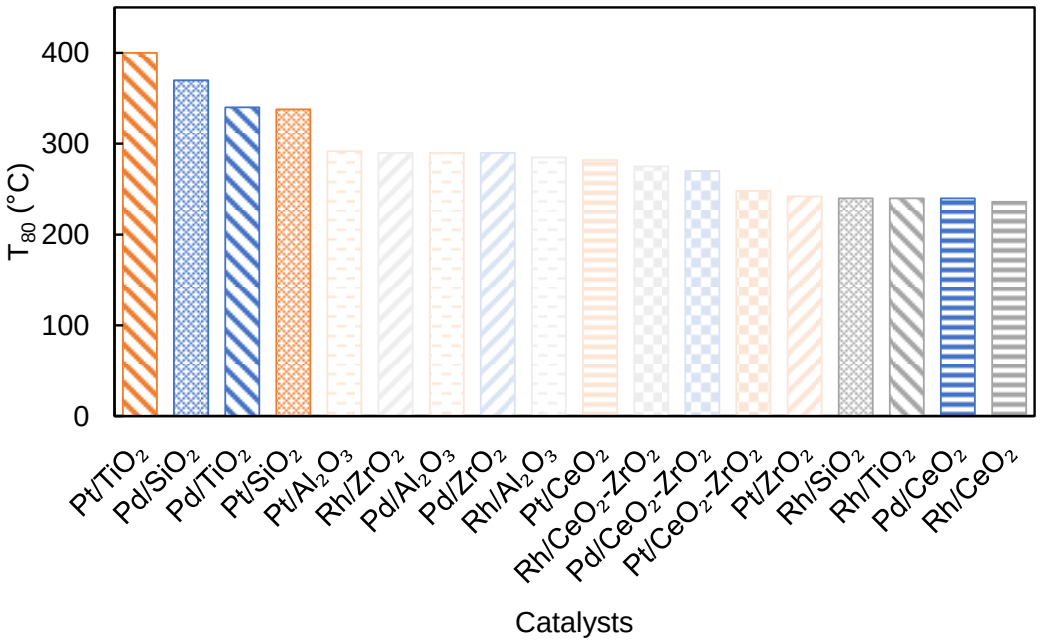

Figure 4.12. Catalyst ranking based on T_{80} for C_3H_6 conversion under fuel-rich condition ($\lambda = 0.9$).

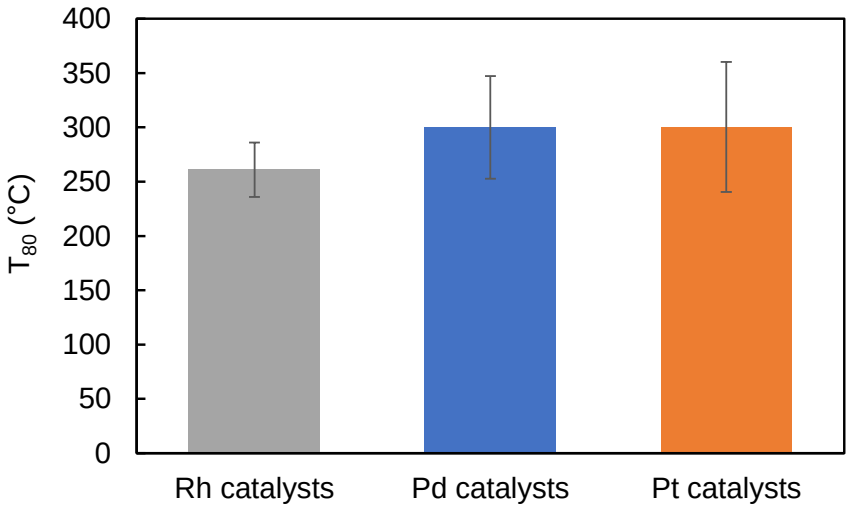

Figure 4.13. Comparison of T_{80} for C_3H_6 conversion under fuel-rich condition ($\lambda = 0.9$) among different noble metal.

Lastly, an attempt to extract knowledge on the synergy effect of metals-supports interaction on the catalyst performance of the TWCs, which is normally demonstrated as the strong metal-support interaction (SMSI), was made. SMSI plays an important role in catalytic performance of the TWCs: The supports can enhance the dispersion of metals and suppress their sintering/agglomeration during high-temperature thermal aging (typically ≥ 800 °C) [26,27] [53] , whereas metals can improve the redox performance and OSC of the supports [54,55]. However, the negative effects of the SMSI are also evidenced via the inward diffusion and encapsulation of metals into the supports at high temperature (> 900 °C) [55,56]. The SMSI in TWCs are mostly observed between platinum-group metals (Rh, Pt, Pd) and γ-Al_2O_3, CeO_2 supports [26]. Theoretically, Pt/Al_2O_3 and Rh/Al_2O_3 are prone to rapid sintering during heat treatment at ≥ 700 ºC [57-59]. At such the high temperature, Rh also reacts with γ-Al_2O_3 to form an irreducible oxide phase [60]. In case of Pd/Al_2O_3, Pd are generally covered by a thin layer of an aluminate phase, leading to the formation of a core-shell structure during the calcination at ≥ 550 °C [61]. Herein the heat treatment of the catalyst was done at 600 ºC, thus the SMSI in M/Al_2O_3 catalyst system are not expected to be observed, which is evidenced by the insignificant variation in catalyst performance between these three catalysts in all 7 aspects according to Table 4.1. On the other hand, the SMSI effect can be clearly demonstrated in the M/CeO_2 system: Rh/CeO_2 and Pd/CeO_2 appear as the performant catalyst under fuel-rich conditions, whereas Pt/CeO_2 is not present in top best catalysts in any aspects. It has been well-approved that the noble metals interact with CeO_2 via the strong M-O-Ce bonds, and the order of the affinity of the noble metals with CeO_2 was investigated by Hosokawa *et al.* and reported as Rh ≈ Pd > Pt: Rh and Pd could retain their M-O-Ce bonds even after calcination at 800 °C, while Pt can keep the Pt-O-Ce bond at below 500 °C [62]. In addition, the impregnated Rh and Pd can

promote the reduction of Ce^{4+} to Ce^{3+} to form oxygen vacancies in close vicinity to the metal particles, which would improve both the lability and mobility of lattice oxygen of the support [63,64].

4.4. Conclusions

The previously developed high-throughput (HTP) instrument was proven to be a good tool for rapid screening of various three-way catalysts (TWCs). The catalytic tests were performed over 20 catalyst samples, including 18 simulated lead TWCs, 1 blank and 1 repeated catalyst for reproduction test, at 7 temperatures and 7 values of air/fuel equivalence ratio (λ), resulting the acquisition of 980 datapoints in fully automated fashion. The obtained dataset is of high reproducibility, and the catalyst performance (in terms of light-off temperature and width of operation window) were found consistent with literature data The reaction conditions covered a wide range of temperature and λ, allowing the catalysts comparison in many aspects for the first time. Knowledge extraction from the HTP data was demonstrated for the width of operation window at 400 °C and rich burn C_3H_6, in which M/CeO_2-ZrO_2 was found as a good choice to increase the W value, while Rh-containing TWC is performant for rich burn C_3H_6. The HTP screening instrument yields process-relevant dataset, which can drive a rational approach to the development and optimization of the TWCs.

References

[1] C. Ya-Juan, F. Rui-Mei, S. Hong-Yan, S. Zhong-Hua, G. Mao-Chu, C. Yao-Qiang, Chinese J. Inorg. Chem. 31 (2015) 989–1002.

[2] B. Zhao, G. Li, C. Ge, Q. Wang, R. Zhou, Appl. Catal. B 96 (2010) 338–349.

[3] G. Kim, Ind. Eng. Chem. Prod. Res. Dev. 21 (1982) 267–274.

[4] T. Sekiba, S. Kimura, H. Yamamoto, A. Okada, Catal. Today 22 (1994) 113–126.

[5] J. Cooper, J. Beecham, Platinum Metals Rev 57 (2013) 281–288.

[6] J. Wang, H. Chen, Z. Hu, M. Yao, Y. Li, Catal. Rev. 57 (2015) 79–144.

[7] T. Kobayashi, T. Yamada, K. Kayano, Appl. Catal. B 30 (2001) 287–292.

[8] Q. Wang, G. Li, B. Zhao, R. Zhou, J. Hazard. Mater. 189 (2011) 150–157.

[9] b. Zhao, Q. Wang, G. Li, R. Zhou, J. Environ. Chem. Eng. 1 (2013) 534–543.

[10] M. Haneda, Y. Tomida, T. Takahashi, Y. Azuma, T. Fujimoto, Catal. Commun. 90 (2017) 1–4.

[11] Z. Zhan, L. Song, X. Liu, J. Jiao, J. Li, H. He, J. Environ. Sci. 26 (2014) 683–693.

[12] L. Lan, S. Chen, M. Zhao, M. Gong, Y. Chen, J. Mol. Catal. A: Chem. 394 (2014) 10–21.

[13] Q. Wang, Z. Li, B. Zhao, G. Li, R. Zhou, J. Mol. Catal. A: Chem. 344 (2011) 132–137.

[14] L. Lan, S. Chen, H. Li, J. Wang, D. Li, Y. Chen, Mater. Des. 147 (2018) 191–199.

[15] J.H. Baik, H.J. Kwon, Y.T. Kwon, I.-S. Nam, S.H. Oh, Top. Catal. 42 (2007) 337–340.

[16] C.E. Hori, K.Y.S. Ng, A. Brenner, K.M. Rahmoeller, D. Belton, Braz. J. Chem. Eng. 18 (2001) 23–33.

[17] M. Giuliano, G. Ricchiardi, A. Damin, M. Sgroi, G. Nicol, F. Parussa, Int. J. Automot. Technol. 21 (2020) 329–337.

[18] H.S. Gandhi, A.G. Piken, M. Shelef, R.G. Delosh, Laboratory Evaluation of Three–Way Catalysts, SAE International, 1976.

[19] J. Kašpar, P. Fornasiero, N. Hickey, Catal. Today 77 (2003) 419–449.

[20] H.S. Gandhi, G.W. Graham, R.W. McCabe, J. Catal. 216 (2003) 433–442.

[21] A. Sundermann, M. Kögel, O. Gerlach, Catalysts 9 (2019) 776.

[22] A. Sundermann, O. Gerlach, Chem. Ing. Tech. 86 (2014) 1941–1947.

[23] A. Sundermann, O. Gerlach, Catalysts 6 (2016) 23.

[24] T.N. Nguyen, T.T.P. Nhat, K. Takimoto, A. Thakur, S. Nishimura, J. Ohyama, I. Miyazato, L. Takahashi, J. Fujima, K. Takahashi, T. Taniike, ACS Catal. 10 (2020) 921–932.

[25] N. Guillén-Hurtado, V. Rico-Pérez, A. Garcia-Garcia, D. Lozano-Castelló, A. Bueno-López, Dyna 79 (2012) 114–121.

[26] T. Zheng, J. He, Y. Zhao, W. Xia, J. He, J. Rare Earths 32 (2014) 97–107.

[27] Y. Nagai, T. Hirabayashi, K. Dohmae, N. Takagi, T. Minami, H. Shinjoh, S.i. Matsumoto, J. Catal. 242 (2006) 103–109.

[28] X. Karatzas, K. Jansson, A. González, J. Dawody, L.J. Pettersson, Appl. Catal. B 106 (2011) 476–487.

[29] V.G. Papadakis, C.A. Pliangos, I.V. Yentekakis, X.E. Verykios, C.G. Vayenas, Nonlinear Anal.Theo. Methods & Appl. 30 (1997) 2353–2361.

[30] T. Yoshida, A. Sato, H. Suzuki, T. Tanabe, N. Takahashi, Development of High Performance Three-Way-Catalyst, SAE International, 2006.

[31] R.M. Heck, R.J. Farrauto, S.T. Gulati, Catalytic air pollution control: commercial technology, John Wiley & Sons, 2016.

[32] A.B. Stiles, (1987).

[33] X. Jiang, M. Manawan, T. Feng, R. Qian, T. Zhao, G. Zhou, F. Kong, Q. Wang, S. Dai, J.H. Pan, Catal. Today 300 (2018) 12–17.

[34] T. Nakatsuji, V. Komppa, Top. Catal. 16 (2001) 217–223.

[35] X. Meng, H. Huang, H. Weng, L. Shi, Bull. Korean Chem. Soc. 33 (2012) 3213–3217.

[36] N. Ohtake, M. Katoh, S. Sugiyama, J. Ceram. Soc. Jpn. 125 (2017) 57–61.

[37] H.R. Marchbank, A.H. Clark, T.I. Hyde, H.Y. Playford, M.G. Tucker, D. Thompsett, J.M. Fisher, K.W. Chapman, K.A. Beyer, M. Monte, A. Longo, G. Sankar, ChemPhysChem 17 (2016) 3494–3503.

[38] H.J. Kwon, J.H. Baik, S.B. Kang, I.-S. Nam, B.J. Yoon, S.H. Oh, Ind. Eng. Chem. Res. 49 (2010) 7039–7051.

[39] I. Heo, D.Y. Yoon, B.K. Cho, I.-S. Nam, J.W. Choung, S. Yoo, Appl. Catal. B 121–122 (2012) 75–87.

[40] S.B. Kang, S.J. Han, S.B. Nam, I.-S. Nam, B.K. Cho, C.H. Kim, S.H. Oh, Chem. Eng. J. 207–208 (2012) 117–121.

[41] Q. Wang, B. Zhao, G. Li, R. Zhou, Environ. Sci. Technol. 44 (2010) 3870–3875.

[42] S.B. Kang, S.B. Nam, B.K. Cho, I.-S. Nam, C.H. Kim, S.H. Oh, Catal. Today 231 (2014) 3–14.

[43] D. Crolla, Encyclopedia of automotive engineering, John Wiley & Sons, 2015.

[44] R.J. Farrauto, M. Deeba, S. Alerasool, Nat. Catal. 2 (2019) 603–613.

[45] G. Li, B. Zhao, Q. Wang, R. Zhou, Appl. Catal. B 97 (2010) 41–48.

[46] G. Li, Q. Wang, B. Zhao, R. Zhou, Catal. Today 158 (2010) 385–392.

[47] J. Wang, M. Shen, Y. An, J. Wang, Catal. Commun. 10 (2008) 103–107.

[48] J. Wang, M. Shen, J. Wang, J. Gao, J. Ma, S. Liu, J. Rare Earths 30 (2012) 878–883.

[49] J. Wang, M. Shen, J. Wang, J. Gao, J. Ma, S. Liu, J. Rare Earths 30 (2012) 748–752.

[50] G. Li, Q. Wang, B. Zhao, R. Zhou, Appl. Catal. B 105 (2011) 151–162.

[51] M. Braja Gopal, Bull. Catal. Soc. Ind., 2 (2003) 122–134.

[52] S. Bernal, J.J. Calvino, M.A. Cauqui, G.A. Cifredo, A. Jobacho, J.M. Rodríguez-Izquierdo, Appl. Catal. 99 (1993) 1–8.

[53] Y. Nagai, R&D Review of Toyota CRDL 41 (2006) 32.

[54] P. Fornasiero, J. Kašpar, V. Sergo, M. Graziani, J. Catal. 182 (1999) 56–69.

[55] L. Liotta, A. Longo, A. Macaluso, A. Martorana, G. Pantaleo, A. Venezia, G. Deganello, Appl. Catal. B 48 (2004) 133–149.

[56] K. Kenevey, F. Valdivieso, M. Soustelle, M. Pijolat, Appl. Catal. B 29 (2001) 93–101.

[57] P. Harris, J. Catal. 97 (1986) 527–542.

[58] C. Linsmeier, E. Taglauer, Appl. Catal. 391 (2011) 175–186.

[59] C. Van, J. Dettling, Studies in Surface Science and Catalysis, Elsevier, 1987, pp. 369–386.

[60] S. Suhonen, M. Valden, M. Hietikko, R. Laitinen, A. Savimäki, M. Härkönen, Appl. Catal. 218 (2001) 151–160.

[61] A.S. Ivanova, E.M. Slavinskaya, R.V. Gulyaev, V.I. Zaikovskii, O.A. Stonkus, I.G. Danilova, L.M. Plyasova, I.A. Polukhina, A.I. Boronin, Appl. Catal. B 97 (2010) 57–71.

[62] S. Hosokawa, M. Taniguchi, K. Utani, H. Kanai, S. Imamura, Appl. Catal. 289 (2005) 115–120.

[63] M.S. Avila, C.I. Vignatti, C.R. Apesteguía, T.F. Garetto, Chem. Eng. J. 241 (2014) 52–59.

[64] C. Wang, T. Zheng, J. Lu, X. Wu, H. Hochstadt, Y. Zhao, Appl. Catal. 544 (2017) 30–39.

Chapter 5

General summary and conclusions

Chapter 5

5.1. Summary of the thesis

Three-way catalysts (TWCs) have been one of the most satisfactory and effective techniques to control automotive exhaust emissions due to their capability of simultaneously catalyzing the conversion of pollutants into less harmful compounds. The development of more efficient TWCs has long remained a hot topic in environmental catalysis as a result of the increasingly stringent legislation on automotive emissions. Tremendous efforts have been devoted to achieving this target mainly via materials aspects, while the methodology for the evaluation of the newly generated catalysts are not sufficiently devised. As the TWCs are multi-component systems and their performance needs to be evaluated in a variety of potential conditions, it is obvious that the research and development of the TWCs need to be supported by high-throughput (HTP) experiments. In this dissertation, HTP techniques and protocols for primary and secondary screening were designed and implemented for the TWCs.

For the primary screening, non-invasive and truly parallel optical methods are regarded ideal. Herein, a chemiluminescence (CL) method was proposed and developed to realize rapid catalyst evaluation in high-temperature gaseous catalysis. Chapter 2 provided a fundamental study on the principle and potential of the CL method in detecting redox reactions in a catalytic converter. The proof of concept of the CL method was established by thoroughly examining the CL behaviors of catalytic oxidation of CO and C_3H_6 by O_2/NO as well as their combinations towards three-way catalysis. All the reactions were found to be CL-active and exhibited linear relationships between the CL intensity and the reactions rate regardless of air/fuel stoichiometry. The CL method is also recognized as a straightforward technique since the CL emission was found as a direct and production-based process. The development of a CL imaging

instrument towards HTP catalyst screening was then realized in Chapter 3. The potential of the CL imaging instrument for rapid catalyst screening was successfully established based on a good correlation between the brightness of spots in the CL image and the corresponding catalytic activity of Rh-based catalysts in C_3H_6 oxidation. Moreover, the one-to-one correspondence of the CL signal obtained from the single and parallel measurements signified the great applicability of the CL imaging instrument in HTP catalyst screening. After the successful establishment of the CL imaging method as a promising and powerful optical technique for HTP primary catalyst screening, in Chapter 4, the HTP secondary screening of the TWCs was described using another HTP screening instrument which enables automatic catalyst evaluation in a predefined set of conditions and had been separately developed. The three-way catalytic tests were performed for 20 catalysts samples over a wide range of temperatures and air/fuel equivalence ratios, resulting in total 980 data points in one fully automated operation. The high quality of the obtained dataset was verified based on their consistency in catalytic performances with the literature results.

5.2. General conclusions and perspectives

I believe that the research conducted in this dissertation would make a considerable contribution on the research and development of automotive exhaust aftertreatment systems, in particular in methodological aspects. To the best of my knowledge, this is regarded the first integrated HTP screening catalyst screening methodology designed for the TWCs. Furthermore, the developed novel instrument and technique in this research can hold a great promise not only for the automotive catalyst application but also for research and development of many analogous catalytic systems.

In the future, the research will be driven toward completing the HTP primary screening by the CL imaging method. Specifically, a more sophisticated reactor design is desired with central emphasis on uniform flow and heat distribution to scale up the screening up to 100 or even more catalysts per one operation. Afterwards, 20 leads obtained from the HTP-CL imaging measurement will be subjected to secondary screening. In addition, the TWCs library will be extended to bimetallic system contain nanoalloying of Rh, Pd, and Pt at different compositions supported on various oxide supports. With the aid of the developed HTP screening techniques, it is expected that novel and more efficient catalyst formulations will be generated.

List of Publications and Other Achievements

Tran Phuong Nhat Thuy

A) PUBLICATIONS

1. Dai Xuan Trinh, **Thuy Phuong Nhat Tran**, Toshiaki Taniike, Fabrication of new composite membrane filled with UiO-66 nanoparticles and its application to nanofiltration, *Separation and Purification Technology*, 2017, 177, 249–256.

2. Linh Hoang Le, Dai Xuan Trinh, Nguyen Ba Trung, **Thuy Phuong Nhat Tran**, Toshiaki Taniike, Fabrication of assembled membrane from malonate-functionalized graphene and evaluation of its permeation performance, *Carbon*, 2017, 114, 519–525.

3. **Thuy Phuong Nhat Tran**, Ashutosh Thakur, Dai Xuan Trinh, Anh T.N. Dao, Toshiaki Taniike, Design of Pd@Graphene Oxide Framework nanocatalyst with improved activity and recyclability in Suzuki-Miyaura cross-coupling reaction, *Applied Catalysis A: General*, 2018, 549, 60–67.

4. Thanh Nhat Nguyen, **Thuy Tran Phuong Nhat**, Ken Takimoto, Ashutosh Thakur, Shun Nishimura, Junya Ohyama, Itsuki Miyazato, Lauren Takahashi, Jun Fujima, Keisuke Takahashi, Toshiaki Taniike, High-throughput experimentation and catalyst informatics for oxidative coupling of methane, *ACS Catalysis*, 2020, 10, 921–932.

5. **Thuy Phuong Nhat Tran,** Ashutosh Thakur, Thanh Nhat Nguyen, Priyank Mohan, Toru Wada, Patchanee Chammingkwan, Toshiaki Taniike, Understanding chemiluminescence in catalytic oxidation of CO and hydrocarbons, *Catalysis Today*, 2020, doi.org/10.1016/j.cattod.2020.02.034

6. **Thuy Phuong Nhat Tran,** Toshiaki Taniike, Shun Nishimura, Tailoring graphene oxide framework for the confinement of Pd nanoparticles towards a recycling-free catalyst system, *Catalysis Letters*, 2020, doi.org/10.1007/s10562-020-03284-y

B) DOMESTIC CONFERENCES

1. **Thuy Phuong Nhat Tran**, Ashutosh Thakur, Toshiaki Taniike, Design of Pd@Graphene Oxide Framework nanocatalyst and its application in Suzuki-Miyaura

cross-coupling reaction, The 97th Annual Meeting of the Chemical Society of Japan, Yokohama, March 16-19, 2017, oral presentation.

2. **Thuy Phuong Nhat Tran**, Ashutosh Thakur, Toshiaki Taniike, Stabilizing nanoparticles in graphene oxide framework: A case study of Pd nanocatalyst, The 8th JACI/GSC Symposium, Tokyo, 24-25 June 2019, poster presentation.

C) INTERNATIONAL CONFERENCES

1. **Thuy Phuong Nhat Tran**, Ashutosh Thakur, Toshiaki Taniike, Pd nanoparticles confined in graphene oxide framework: An efficient and reusable nanocatalyst in Suzuki-Miyaura cross-coupling reaction, JAIST Japan-India Symposium on Materials Science 2017, Nomi, Japan, Mar. 6-7, 2017, poster presentation.

2. **Thuy Phuong Nhat Tran**, Ashutosh Thakur, Toshiaki Taniike, Synthesis of Pd nanoparticles confined in graphene oxide framework as nano catalyst with improved activity and recyclability in Suzuki-Miyaura cross-coupling reaction, The 20th International Conference on Heterogeneous Catalysis, Osaka, Japan, Oct. 11-12, 2018, oral presentation.

3. **Thuy Phuong Nhat Tran**, Ashutosh Thakur, Thanh Nhat Nguyen, Toshiaki Taniike, Operando chemiluminescence method for automotive catalytic converter, The 8th Asia Pacific Congress on Catalysis, Bangkok, Thailand, Aug. 4-7, 2019, poster presentation.

4. **Thuy Phuong Nhat Tran**, Thanh Nhat Nguyen, Toshiaki Taniike, Application of chemiluminescence method for rapid catalyst evaluation in catalytic oxidation of co and hydrocarbons, Chemistry Conference for Young Scientists 2020 (CHEMCYS2020), Blankenberge, Belgium, Feb. 19-21, 2020, oral presentation.

5. **Thuy Phuong Nhat Tran**, Shun Nishimura, Toshiaki Taniike, Confinement of Pd nanoparticles in graphene oxide framework: recyclable nanocatalyst for Suzuki-Miyaura Cross-Coupling, Chemistry Conference for Young Scientists 2020 (CHEMCYS2020), Blankenberge, Belgium, Feb. 19-21, 2020, poster presentation.

D) AWARDS

1. **Best Presentation Award**, The 20th International Conference on Heterogeneous Catalysis 2018, Osaka, Japan, 10/2018.

2. **Best Poster Presentation Award**, The 8th Asia-Pacific Congress on Catalysis 2019 (APCAT-8), Bangkok, Thailand, 8/2019.